UCRL 9388

UNIVERSITY OF CALIFORNIA

Ernest O. Lawrence Radiation Laboratory

THERMAL PROPERTIES OF SOLID HYDROGEN UNDER PRESSURE

TWO-WEEK LOAN COPY

This is a Library Circulating Copy
which may be borrowed for two weeks.
For a personal retention copy, call
Tech. Info. Division, Ext. 5545

DISCLAIMER

This document was prepared as an account of work sponsored by the United States Government. While this document is believed to contain correct information, neither the United States Government nor any agency thereof, nor the Regents of the University of California, nor any of their employees, makes any warranty, express or implied, or assumes any legal responsibility for the accuracy, completeness, or usefulness of any information, apparatus, product, or process disclosed, or represents that its use would not infringe privately owned rights. Reference herein to any specific commercial product, process, or service by its trade name, trademark, manufacturer, or otherwise, does not necessarily constitute or imply its endorsement, recommendation, or favoring by the United States Government or any agency thereof, or the Regents of the University of California. The views and opinions of authors expressed herein do not necessarily state or reflect those of the United States Government or any agency thereof or the Regents of the University of California.

UCRL-9388
Chemistry General Distribution
TID-4500 (16th Ed.)

UNIVERSITY OF CALIFORNIA

Lawrence Radiation Laboratory
Berkeley, California

Contract No. W-7405-eng-48

THERMAL PROPERTIES OF SOLID HYDROGEN UNDER PRESSURE

William Herbert Orttung

(Thesis)

February 1, 1961

Printed in USA. Price $2.75. Available from the
Office of Technical Services
U. S. Department of Commerce
Washington 25, D.C.

THERMAL PROPERTIES OF SOLID HYDROGEN UNDER PRESSURE

Contents

Abstract 5

I. Introduction 7

II. Calorimeter 17

General Description 17

Properties and Operation of the Calorimeter Baths 26

Description of the Cell and Environment 29

Calorimetry Circuits 31

III. Pressure System 40

General Description 40

Low-Pressure System 43

Mercury-Depth Indicator 46

Shielding 49

Medium-Pressure System 51

High-Pressure System 56

High-Pressure Cells 59

IV. Sample Preparation and Analysis 72

Para Hydrogen Converters 72

Ortho Hydrogen Separators 75

Hydrogen Purifier 75

Ortho-Para Analyzer 75

V. Thermal Measurements 80

Thermometer Calibration 80

Treatment of the Calibration Data 82

Estimate of Thermal Properties of the Isothermal Shield and Cell 89

Effect of Stainless Steel Capillaries on Heat-Capacity Measurements 92

Heat-Capacity Measurements 103

Measurements Below $2^{o}K$. 104

VI. Experimental Aspects of High-Pressure Measurements 105
Errors Due to Uncertainties in the Volumes of the Pressure System 105
Volumes in the Pressure System 106
Uncertainties From Other Sources 109
The Equation of State of Hydrogen 110
Extrusion of Hydrogen Through Capillaries 112
VII. Theoretical Considerations 114
Introduction 114
Interaction Between Two Hydrogen Molecules 116
Application of Perturbation Theory to Pairwise Interaction. 120
Linear Arrangement of Three Ortho Molecules 126
Calculations of Heat Capacities From the Splittings 133
Statistical Considerations at Low Ortho Concentrations. . . 137
Analysis of Available One-Atmosphere Data 142
VIII. Comment on London's Theory 153
Acknowledgments. 154
Appendices
A. Assembly and Disassembly of the Calorimeter 155
B. Summary of Useful Formulas for Thick-walled Cylinders . 156
References 159

THERMAL PROPERTIES OF SOLID HYDROGEN UNDER PRESSURE

William Herbert Orttung

Lawrence Radiation Laboratory
University of California
Berkeley, California

February 1, 1961

ABSTRACT

A calorimeter was designed and constructed for use in the temperature interval 1 to 25°K. with samples of solid hydrogen under pressures up to 12,000 kg./cm^2. Unusual features of the calorimeter include the use of two baths for liquid hydrogen or helium, a jaw-type thermal contact capable of high contact pressure, and a set of flanges at the cell level for ready access. The associated high-pressure-generating apparatus was also designed and constructed. Pressures were generated with oil pumps and an intensifier. The oil was separated from the hydrogen by steel U-tubes half full of mercury, three of which were required for different pressure ranges. The highest-pressure U-tube was isolated from the rest of the system by mercury frozen in a steel capillary. The hydrogen entered the calorimeter through high-pressure capillary tubing, in which it was then frozen to isolate the sample in the cell. Catalyst chambers were constructed for the conversion of normal hydrogen to para hydrogen, and a three-stage system utilizing alumina catalyst at liquid-hydrogen temperature was constructed for the separation of ortho hydrogen from para hydrogen.

Because the calorimeter was of unconventional design, various modifications and procedures had to be worked out. A dummy cell was used for these developments. The high-pressure apparatus was tested to 6000 kg/cm^2 with hydrogen at room temperature. Satisfactory high-pressure seals for the low-temperature cell were not developed soon enough to enable data to be taken.

The theory of the anomalous heat capacity for low concentrations of ortho hydrogen or para deuterium has been extended by a calculation based on the angular potential energy between adjacent molecules. At 1 atm it was found that only electrostatic quadrupole-quadrupole interactions had to be considered, but at higher pressures, the valence forces became important. The

case of three ortho molecules in a row was also treated in the quadrupole approximation. The heat capacity predicted by this model is somewhat different from that predicted for isolated ortho-ortho pairs. The theory was compared with the available 1-atm data, taking into consideration the relation between the total ortho concentration and the relative amounts of isolated ortho molecules, isolated pairs of ortho molecules, and more complicated configurations. The suggestion of T. Nakamura that an additional term in the anomalous heat capacity proportional to the ortho concentration is needed to explain the data seems to be supported by the analysis, although comparison with a larger amount of data would be desirable.

THERMAL PROPERTIES OF SOLID HYDROGEN UNDER PRESSURE

I. INTRODUCTION

The simplest system exhibiting molecular rotation in the solid state is hydrogen. Examples of more complicated molecules that are known to rotate in the solid phase are fairly numerous. Methane and ammonium ions in some salts are the most commonly known. Although solid hydrogen would appear to be the simplest of this series, the number of unsolved problems and unanswered questions relating to it is still quite large, as will be seen from the following discussion.

As is well known, the idea of a proton spin, combined with the Pauli principle, led to the discovery of the ortho and para modifications of the hydrogen molecule. Since the conversion of the symmetric nuclear state (ortho) to the antisymmetric nuclear state (para) is forbidden in the absence of an inhomogeneous magnetic field, the two species are not in thermal equilibrium with each other during experiments of relatively short duration. The significance of this fact for the present discussion is readily seen. In liquid (20 to 14°K) and solid (below 14°K) hydrogen, the ortho molecules are in the lowest antisymmetric rotational state ($J = 1$) and the para molecules are in the lowest symmetric state ($J = 0$), even though the thermal equilibrium at 20°K has only about 0.2% of the ortho species. For this reason, it is possible to study the rotating species in the solid state. The high temperature or statistical equilibrium is three-fourths ortho hydrogen, and until very recently, this was the highest fraction of ortho hydrogen available for experiments. The situation in the deuterium molecule is somewhat different because the nuclei have different spin and statistics. The highest fraction of the rotating species (para)* obtainable thermally is only one-third in this case.

An over-all discussion of the nature of solid hydrogen and deuterium must cover crystal structure, lattice vibrations, interactions between neighboring ortho molecules, the cooperative phenomenon at about 1.5°K,

---

* By convention, the most abundant high-temperature species is ortho, and the other para.

the kinetics of the ortho-para conversion in the solid phase, the nature of the nuclear magnetic resonance (NMR) spectra, and the effect of pressure on lattice and rotational properties.

Keesom, DeSmedt, and Mooy determined the structure of pure para hydrogen at liquid-helium temperature in 1930,[1] and concluded that the structure was hexagonal close-packed with a = 3.75A and c/a = 1.633. Recent work by Kogan, Lazarev, and Bulatova on the crystal structure of solid deuterium indicated that it is tetragonal with c/a = 0.94 and a = 5.4A.[2] These values gave a density of 0.18 g/cm^3, within 10% of the experimental value. These authors reexamined the analysis of Keesom et al. and decided that their data could also have been interpreted in terms of a tetragonal lattice. Evidence was found for double refraction in both hydrogen and deuterium. In a later communication on the phase diagram of the hydrogen-deuterium system,[3] the same authors discovered a solid-phase separation below 16.4°K. An X-ray study of the mixtures at 4°K revealed that the hydrogen-rich and deuterium-rich phases had different crystal structures that differed only slightly from those of pure hydrogen and deuterium. In this paper, the authors did not think it possible to accurately determine the structure of either hydrogen or deuterium. They conclude only that the structures of hydrogen and deuterium are different and the Leiden assignment was incorrect. No mention of the ortho-para composition was given in the Russian work,[2,3] leading one to suspect that high-temperature equilibrium mixtures were used. Since this would be 75% rotating hydrogen and 33% rotating deuterium in the Russian work, and no rotating hydrogen in the Leiden work, the possibility that the structure is a function of ortho concentration may not have been ruled out.

The first measurements of the heat capacity of solid hydrogen in the liquid-helium temperature range were published in 1931 by Mendelssohn, Ruhemann, and Simon.[4] Mixtures containing 75, 50, and 0% ortho hydrogen were studied over the temperature range 2 to 11°K. However, the data below 5°K were affected by the adsorption of the helium exchange gas. The data on para hydrogen were fitted to a T^3 law corresponding to a Debye Θ of 91°K. The samples containing ortho hydrogen gave an additional contribution to the heat capacity below 12°K which was greater for 75% than for 50% ortho hydrogen. Since a phase separation or a phase separation combined with a rotational anomaly proportional to the orhto concentration would predict the reverse, these possibilities seem to have been ruled out. This point is of interest

in connection with diffusion in the solid, which is discussed below.

In 1930 Pauling published a theoretical paper dealing with the rotational motion of molecules in crystals.[5] The limiting cases of oscillation and rotation were considered, and it was shown that in solid hydrogen just below the melting point, a state of almost free rotation existed for the ortho molecules. At lower temperatures, it was postulated that the rotation would be frozen out. Pauling proposed that "the solid solution becomes unstable relative to phases of definite composition", or that both the triple degeneracy of the J = 1 ortho state and the entropy of mixing of the ortho and para hydrogen would be lost in the freezing-out process in order to explain the observed zero-point entropy of R ln 3 per mole of ortho hydrogen. In the same year, Simon[6] pointed out that the zero-point entropy of n-H_2 (for values of kT large compared to nuclear-interaction energies) is R ln 4 (entropy of mixing of ortho and para plus ortho nuclear degeneracy) and that only R ln 3 per mole of ortho hydrogen is involved in the rotational anomaly.

In an attempt to explain the vapor-pressure difference or ortho and para hydrogen, Schaefer[7] found that the least complicated angular potential pertaining to a hydrogen molecule in a hexagonal close-packed crystal was the spherical harmonic, Y_4^0. A second-order perturbation calculation indicated that a 1000-cal potential barrier was necessary to explain the data on this basis. The use of a potential based on the spherical harmonic, Y_2^0, gave the more reasonable value of 28.2 cal, corresponding to an energy difference between ortho and para hydrogen of 7.5 cal/mole at 0°K in the solid state. The above comparison was made by using a Schottky-type anomaly for the heat capacity. In order to obtain a good fit, it was necessary to assume that the potential increased slightly as the temperature decreased.

In 1954, Hill and Ricketson measured the heat capacity of solid hydrogen in the range 1.15°K to the triple point (14°K) and discovered a λ-type anomaly at 1.6°K in normal hydrogen.[8] The temperature of the λ anomaly was found to decrease with decreasing ortho hydrogen concentration, and no anomaly was found at 56% ortho hydrogen above 1.15°K. The total anomalous entropy was found to be within a few tenths of an entropy unit of R ln 3. A year later, the measurements were extended to 0.2°K.[9] The lowest concentration at which the anomaly occurred was about 63% at a temperature of 1.1°K.

In a theoretical paper in 1955, Tomita attributed the crystal-field splitting in ortho hydrogen to electric-quadrupole interaction between adjacent ortho molecules and treated the heat-capacity anomaly as a cooperative

phenomenon.[10] A treatment corresponding to the Bragg-Williams approximation was given first. This approach was unsatisfactory because (a) it did not predict an ortho concentration below which the anomaly would be absent, and (b) it did not predict a residual heat capacity above the anomaly. A calculation corresponding to the Bethe-Peierls approximation was then carried out. The effect of ortho concentration on the critical temperature was predicted fairly well by this theory, but the lower limit in ortho concentration for which a critical temperature can exist was predicted to be only 16.7%. No comparison was made with the residual heat capacity above the anomaly.

Translational effects in the lattice of solid hydrogen, aside from their intrinsic interest, are also of importance in the considerations of the splitting of the rotational degeneracy and in the ortho-para conversion kinetics. The first heat-capacity measurements on para hydrogen[4] and normal deuterium[11] (above the region of the anomaly) gave Debye Θ values of $91^{\circ}K$ and $89^{\circ}K$, respectively. These values were obtained by fitting the Debye theory to C_p data. The direct calorimetric determination of C_v for hydrogen and deuterium was then carried out for the 1-atm molar volumes at 11.20 and $11.60^{\circ}K$, respectively.[12] The data were fitted by Debye Θ's of 105° and $97^{\circ}K$, respectively. Megaw corrected the above values for the volume at $0^{\circ}K$ and found $\Theta_D = 111$ and $108^{\circ}K$ for hydrogen and deuterium, respectively.[13] Recent more-accurate data on hydrogen[8] and deuterium[14] below $14^{\circ}K$ indicate that C_p does not follow a T^3 law in this region, and that the original data of Mendelssohn, Ruhemann, and Simon[4] were appreciably too large.

The zero-point energy of the lattice predicted by the Debye theory is given by $E_0 = (9/8)(Nk\Theta_D)$. Using $\Theta_D = 111$ and $108^{\circ}K$, one obtains 249 and 242 cal/mole, respectively. Comparison with the potential energy of the crystal (predicted from gas imperfections) at the known molar volume indicates that the Debye theory gives too large zero-point energies. Since the hydrogen molecules in the solid do not move in a harmonic potential well, this deviation is not surprising. By combining the expression for the zero-point energy of a particle in a spherical box with that for a quantized mean free path, London succeeded in describing the properties of liquid helium near absolute zero.[15] Hobbs applied the same treatment to solid hydrogen and deuterium, obtaining zero-point energies of 162 and 123 cal/mole, which, when combined with the potential energies, gave excellent agreement with experiment.[16]

The first study of the kinetics of the ortho-para conversion in the solid and liquid phases was made by Cremer and Polanyi in 1933.[17] The conversion velocity was found to be independent of temperature in both the liquid (14 to 20°K) and solid (4 to 12°K) regions. The reaction was second order in the ortho concentration, and the rate constants were 17.5×10^{-5} and 11.2×10^{-5} per hour per percentage unit of ortho concentration in the solid and liquid phases, respectively.[18] The higher rate in the solid phase reflects the higher density of the solid. It was observed that the rate of reaction in the solid phase decreased as the ortho concentration became smaller, and approached a limiting concentration. A later study was made by Cremer to investigate this phenomenon.[19] It was found that the decrease in rate did not occur in the liquid phase or in the solid phase just after being frozen (regardless of the initial concentration of ortho). Cremer concluded that self-diffusion was very limited in solid hydrogen and that the residual ortho molecules were isolated from each other. Experiments gave $19 \pm 5\%$ as the residual ortho concentration. Since this value is greater than would be predicted statistically, it was suggested that some neighboring ortho molecules were in unfavorable positions for reaction. In a third paper in the same series, Cremer made a theoretical estimate of the course of the reaction, assuming the ortho molecules fixed.[19] Comparison with the data allowed him to make the following estimates of the self-diffusion coefficients in solid hydrogen: $D_{11.3^\circ K} \leq 1.5 \times 10^{-17}$; $D_{11.8^\circ K} = 3 \pm 3 \times 10^{-17}$; $D_{13.2^\circ K} = 1 \pm 0.2 \times 10^{-15}$; $D_{13.6^\circ K} \geq 1.7 \times 10^{-15}$ cm^2/day. From the temperature dependence of the self-diffusion, a heat of activation of 790 ± 130 cal/mole was obtained.

For comparison, recent NMR work by Rollin and Watson[20] and Bloom[21] on the 10°K self-diffusion transition has given values of 350 and 380 ± 20 cal/mole, respectively, for the activation energy of self-diffusion. Smith and Squire studied the effect of pressure on the self-diffusion transition and obtained 350 ± 50 cal/mole for the activation energy at 1 atm.[22] They estimated the correlation time (the average time an ortho molecule spends on a lattice site during the self-diffusion process) to be 2×10^{-6} sec at 10°K and 230 atm.

Cremer's method of calculating the final ortho concentration[19] is of interest and is summarized here.[19] The reaction mechanism is assumed to be o + o = p + o, where o denotes ortho and p denotes para. The crystal structure

is assumed to be cubic close-packed, so that the twelve neighbors of any molecule fall on six straight lines intersecting the molecule. For hexagonal close packing, zig-zag lines must be drawn. The problem is first treated for the linear case, and the final ortho concentration is calculated as a function of the initial concentration. The three-dimensional case is treated by assuming that the reaction first proceeds along one direction. The resulting concentration is then used as the initial concentration for reaction along another direction, until all six direction have been used. The calculation predicts a final concentration of about 12% for an initial concentration of 75%. When the mechanism o + o = p + p was considered, lower final concentrations resulted.

A quantum-mechanical treatment of the ortho-para conversion kinetics in solid hydrogen has been carried out by Motizuki and Nagamiya.[23] The interaction between two adjacent ortho molecules leading to conversion of one of them is taken to be the magnetic interaction between nuclear spins on adjacent molecules and between the rotational moment of one molecule with the nuclear spins of the other. Perturbation theory is used, and the matrix elements are expanded in powers of the mean distance of the neighboring molecules in the crystal. The lattice modes are assumed to be expressed by the Debye theory, and the probability of ortho-para transition with the simultaneous emission of phonons is calculated. In solid hydrogen, the rotational energy is larger than the largest lattice-mode energy, so that a one-phonon emission is not possible. Two-phonon emission is found to be the dominant process, with a contribution from three-phonon emission. The calculation is in very good agreement with experiment.

Motizuki carried out an analogous calculation for the case of solid deuterium.[24] There were several important differences between the cases of solid hydrogen and deuterium that had to be considered. First, the spin of the deuterium nucleus is 1 and Bose statistics are followed. In the lowest rotational state ($J = 0$), nuclear states $I = 0$ and $I = 2$ are found. In the first rotational state ($J = 1$), the nuclear state $I = 1$ occurs. Second, the deuterium nucleus has an electric-quadrupole moment which interacts with the quadrupole moment of adjacent para ($J = 1$) molecules. In the case of the para-para interaction, both the nuclear-magnetic and electric-quadrupole effects contribute to the conversion rate, and the kinetics are second order as with hydrogen. The magnetic interaction between para nuclei and ortho nuclei with $I = 2$ has a concentration dependence of the type $c(100 - c)$,

where c is the percentage of para deuterium. The net reaction rate is

$$\frac{dc}{dt} = -k\,c^2 - k'\,c(100 - c). \qquad (1)$$

The calculation gave the result that k and k' were both about 1×10^{-6} per hour per percentage unit. Hence the quadratic terms approximately cancel, and the net reaction rate is proportional to c.

The fact that the Debye Θ for deuterium is almost the same as that for hydrogen, while the rotational energy is one-half that of hydrogen, indicates that one-phonon emission is possible in the case of deuterium. Motizuki did not look up the experimental value of Θ_D for deuterium (108°K), but guessed a value of 64.4°K on the basis of the harmonic-oscillator approximation, and so missed this point. Accurate data on the para-ortho conversion in solid deuterium do not seem to have been reported in the literature as yet.

Of the many recent NMR studies made on solid hydrogen, the work of Reif and Purcell seems most pertinent to the present experiments.[25] These authors studied the change in line shape as a function of temperature below 4°K. At 4°K, a simple line of 18 kc/sec width was observed. Below 1.5°K, the line was flanked by two side peaks which grew in intensity at the expense of the central line as the temperature was lowered still further. At 1.16°K, there was still a vestige of the central line. Upon warming to 1.35°K, the line underwent a rather rapid change of shape which did not reverse itself when the sample was again cooled to 1.16°K and held there for several hours. The cause of this hysteresis could not be explained. The shape of the resonance line below 1.5°K was explained in terms of a general crystal field of spherical harmonics of second order. The resulting splitting of the three sublevels was large enough to quench the rotational magnetic moment of the ortho molecules. The high-frequency transitions between the split rotational levels could be neglected in the NMR so that each of the three rotational sublevels gave rise to two resonance lines. A rough calculation of the rate of transition between the rotational sublevels indicated that it was greater than the nuclear dipole-dipole splitting in an ortho molecule (expressed in kc/sec). In this case the dipole-dipole interaction should be averaged over all of the rotational sublevels, with each weighted according to its Boltzmann factor, rather than over the probability distribution of a single sublevel.

The authors carried out both calculations, and found that both gave essentially the same line shape. The remnant central line at low temperatures was explained by the presence of some ortho molecules with a small number of ortho-molecule neighbors. The line shape also indicated that the sublevels of a large number of ortho molecules were split by amounts larger than $E/k = 4^{o}K$.

Studies of pressure effects in solid hydrogen have become of interest in recent years, although some earlier work is important. Megaw measured the compressibility of solid hydrogen and deuterium from 1 to 100 kg/cm^2 at $4.2^{o}K$.[13] The molar volumes of hydrogen and deuterium at 1 atm were found to be 22.65 ± 0.1 and 19.56 ± 0.1 cm^3, respectively. The volumes at $4^{o}K$ were assumed to be the same as those at $0^{o}K$. The compressibilities were $6.8 \pm 1.5 \times 10^{-4}$ and $4.5 \pm 2 \times 10^{-4}$ cm^2/kg at 1 kg/cm^2 and about 3.2×10^{-4} and 2.1×10^{-4} cm^2/kg at 100 kg/cm^2, respectively. Simon obtained for the pressure and compressibility due to zero-point energy predicted by Debye theory[26]

$$P_0 = \frac{9}{8} R \gamma \frac{\theta}{v} \qquad (2)$$

and

$$\beta_0 = \frac{v}{\frac{9}{8} R\theta \gamma(\gamma + 1)} , \qquad (3)$$

where θ is the Debye temperature, v is the molar volume, and $\gamma = d \log \theta / d \log v$ is Grueneisen's constant. These results were applied to the data, and it was shown that the experimental compressibilities were predicted very well by the above expression.

Stewart[27,28] measured the compressibility of solid hydrogen and deuterium at $4.2^{o}K$ up to 20,000 kg/cm^2.[27,28] The molar volume and compressibility of hydrogen (based on Megaw's 1-atm value[13]) were found to be greater up to the highest pressures, indicating to Stewart that the zero-point energies were still of importance. No phase changes seem to have been discovered by these measurements.

The effect of pressure on the rotational levels of hydrogen molecules in the solid has been considered by London.[29] A summary of the effect of a hindering potential on the rotational states of a diatomic molecule in a crystal was given earlier by Pitzer.[30] With a small potential barrier, the rotational states are the same as in the gas phase, while with a high barrier, the rotation becomes a torsional oscillation. The gas-phase rotational states

J = 0 and J = 1, M = 0 converge and become degenerate for a homonuclear diatomic molecule when the potential barrier to rotation becomes infinite. Since solid hydrogen has a large compressibility, London proposed that it might be possible to increase the rotational barrier sufficiently to bring the above-mentioned states very close in energy. He pointed out that if one started with para hydrogen and compressed the solid to the point where the para and m = 0 ortho levels were essentially degenerate, a large increase in entropy (R ln4) would be obtained if the para hydrogen could convert to the statistical mixture of nuclear states. The above mechanism would constitute a powerful, but hardly practical, cooling mechanism in the vicinity of $1^{o}K$.

London interpreted the large compressibility of solid hydrogen by assuming that the initial work of compression was used to reduce space for the molecules by confining their rotational motion to a smaller angle. Since the crystal potential barrier may be thought of as being erected at the node of the J = 1, m = 0 wave function, most of the compression energy should go into increasing the energy of the para molecules. On this basis, London made a rough estimate of the pressure required to raise the J = 0 level to the J = 1, m = 0 level by assuming that all of the compression energy went into raising the J = 0 level. Since the J = 1 level would also be raised somewhat in compression, he doubled his estimate and obtained a pressure of the order of magnitude of 10,000 kg/cm^2. An objection might be raised to London's calculation on the grounds that between 1 and 5000 kg/cm^2, most of the compression energy probably goes into increasing the zero-point energy of the crystal, rather than changing the relative energies of the ortho and para species. Above 5000 kg/cm^2, however, one might expect steric hindrance to become important, so that the pressure estimate of 10,000 kg/cm^2 may still be reasonable. In a theoretical calculation of the non-spherical potential field between two hydrogen molecules, deBoer used the Heitler-London-Wang wave functions for the hydrogen molecules, and calculated the inter-molecular potential curve for various relative orientations of the molecules.[31] Consideration of these results also indicates that the hindering potential becomes appreciable in the pressure range between 5000 and 10,000 atm.

The effect of pressure on the NMR down to $1.2^{o}K$ was studied by Smith and Squire.[22] They did not detect any change in line shape or shift in the $1.5^{o}K$ rotational transition temperature at pressures up to 337 atm. McCormick and

Fairbank, in an attempt to obtain some data relating to London's theory, studied the nuclear resonance to a pressure of 5000 atm.[32] The shape and amplitude of the line at 4.2°K remained constant to this pressure, but the transition temperature was observed to increase. The ortho-para conversion rate remained small to 5000 atm, as indicated by the rate of change of the amplitude of the resonance line.

The present experiments were undertaken with the hope of studying the properties of solid hydrogen in the interesting region above 5000 atm. The two methods of measurement considered for this study were NMR and heat capacity. Results from these methods would give the same information in some ways (such as the temperature of the anomaly as a function of pressure) and complimentary information in others. Since work on the nuclear resonance seemed well advanced in other laboratories[22] and since the heat-capacity data would be extremely interesting in any case, it was decided to attempt the thermal measurements.

The plan of the experiments was to measure the heat capacity in the region 1.1 to 20°K. as a function of pressure and ortho concentration. The change in the interaction between neighboring molecules with pressure was the phenomenon to be studied. In more specific terms, the effect of pressure on the splitting of the rotational sublevels, the shape of the anomalous heat capacity, and the lattice heat capacity was of interest. The same apparatus could be used to study the rate of conversion of ortho to para hydrogen as a function of density.

The first part of this report is essentially a description of the apparatus necessary to carry out the above experiments. The basic problem was to compress a sample of hydrogen into a cell in which its heat capacity could be measured. The solution of the problem involved the construction of special apparatus and the development of the techniques necessary to obtain the data.

II. CALORIMETER

General Description

The general layout and main features of the calorimeter are shown in the schematic diagram in Fig. 1. The outer vacuum can, A, was aluminum, and the top flanges, B and C, were stainless steel. There was also a flange, D, near the bottom for access to the cell. The pumping system was connected to the main vacuum can through the pipe, E, and consisted of a Temescal 4-in. gate valve, F, a water-cooled baffle, G, a Consolidated Electrodynamics MCF-300 oil-diffusion pump, H, and a KC-6 Kinney forepump. A High Voltage Engineering ion gauge was attached at EE. The liquid nitrogen reservoir, J, was suspended from the flange, B, by six tubes. A copper radiation shield was attached to the bottom of the reservoir and was detachable at K. A copper shield arrangement, L, was connected to the top of the reservoir to keep room-temperature radiation out of the top. Four concentric cylindrical dimpled stainless steel sheets were loosely attached to the inside of the reservoir above K to act as radiation shields. Ten sheets of a similar nature were placed below K and across the bottom of the shield. The vacuum can, pumping system, and liquid-nitrogen reservoir were adapted from a standard accelerator target design in use at the Lawrence Radiation Laboratory. The liquid-nitrogen bath was arranged so that it could be pumped down in order to reduce the heat leak to the inner parts of the apparatus for certain experiments.

Two baths were necessary for the liquid hydrogen or helium. The purpose of the outer bath, M, was to absorb the heat leak from higher temperature, so that the inner bath, N, could be pumped to the vicinity of $1^{\circ}K$ with a pump of moderate capacity. Although the outer bath made the calorimeter a good bit more complicated, the shortness of the apparatus and the unavailability of high pumping speed made it a necessity. The outer bath surrounded the pumping tube of the inner bath, P, and had a copper radiation shield attached to the bottom of it which was detachable at Q. Additional protection for the outer bath was provided by a pile of four disc-shaped dimpled stainless steel discs, R, loosely connected to the pumping tube, P, at a point about half-way to the liquid-nitrogen shield. The pumping tube for the outer bath was located at S, and was connected to a KS-13 Kinney pump. The transfer tube, T, was permanently fixed in the calorimeter because of the low ceiling. The other part of the

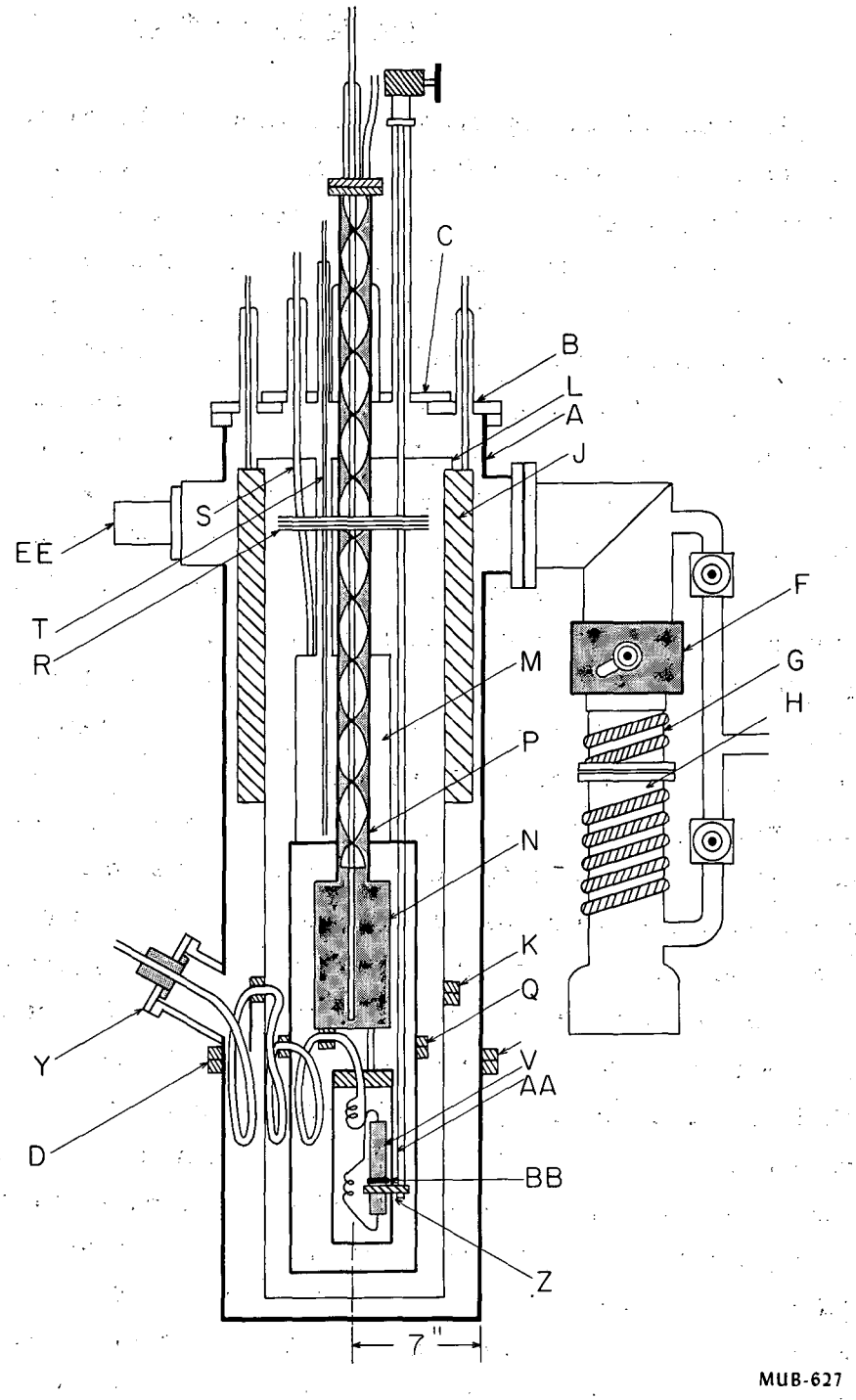

Fig. 1. Schematic drawing of calorimeter.

transfer tube could be disconnected at the top of the calorimeter. The mechanism of coupling of the two parts of the transfer tube is illustrated in Fig. 2. The jacket of the outer-bath transfer tube was part of the main vacuum system, while a separate vacuum had to be provided for the jacket of the inner-bath transfer tube, U. Two well-baffled holes were put in the copper shield below Q for the purpose of evacuating the inner part (see Fig. 3). The baffles and the inside of the shield were painted black in order to minimize the amount of radiation reflecting in toward the cell.*

The inner bath was supported by its pumping tube. The transfer tube was permanently positioned in the pumping tube, and a spiral stainless steel radiation shield, painted black at the bottom, was suspended in the pumping tube. A KD-30 Kinney pump was connected to the top of the pumping tube through a 3-in. copper line (see Fig. 4). The isothermal shield consisted of a block of copper and lead at the top and of a copper shield surrounding the cell, W. The shield was mechanically connected to the inner-bath bottom by two stainless steel rods. The cell was supported in the shield by the stainless steel pressure capillaries, X, as shown in Fig. 5. The capillaries were in thermal contact with the isothermal shield, inner bath, and outer bath, but not with the liquid-nitrogen shield. The capillaries passed out of the calorimeter to the pressure system at the flange, Y. They were sealed to the flange with Armstrong Products Co. epoxy resin.

A double-jaw-type thermal clamp, Z, was used for cooling the cell. It contacted the cell on two flat 1/4-in.-thick copper faces. It was connected thermally to the inner bath with a flexible copper connection of about 1 cm^2 cross section. The clamp was operated mechanically by two stainless steel tubes, AA, passing out the top of the calorimeter, and externally connected together by means of gears. An auxiliary clamp was connected to the tubes for cooling the shield. A worm-gear arrangement was used to open and close the clamp. Rotary vacuum seals enabled the clamp to be opened and closed without disturbing the vacuum. The section of the clamp tubes between the outer bath and liquid-nitrogen bath was made from several different diameter tubes to increase the path length and reduce the

---

* Suggested by Professor N. E. Phillips, Department of Chemistry, University of California, Berkeley.

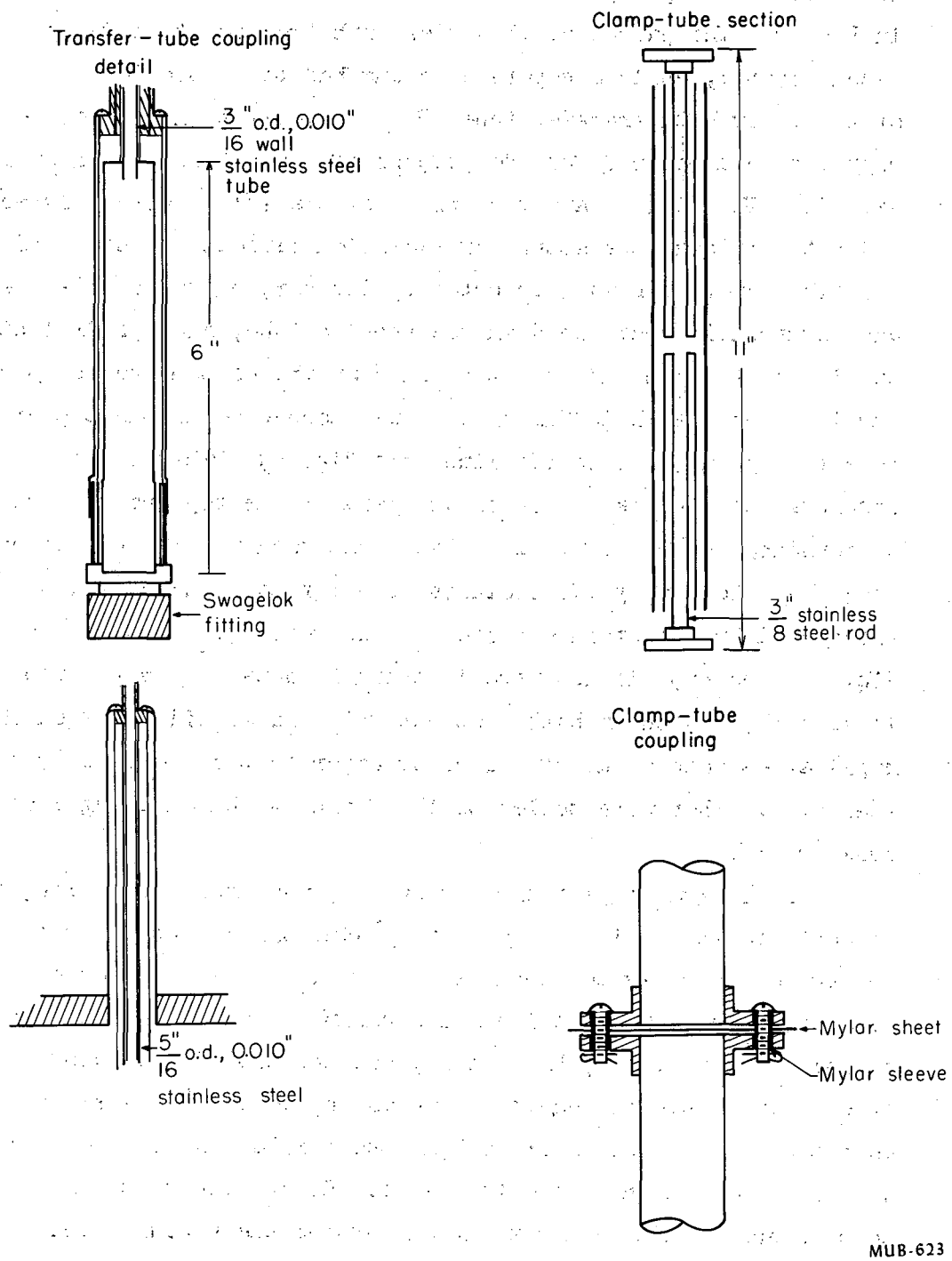

Fig. 2. (a) Transfer-tube coupling; (b) clamp-tube section; (c) clamp-tube coupling.

ZN-2729

Fig. 3. Thermal shields and vacuum can at bottom of calorimeter.

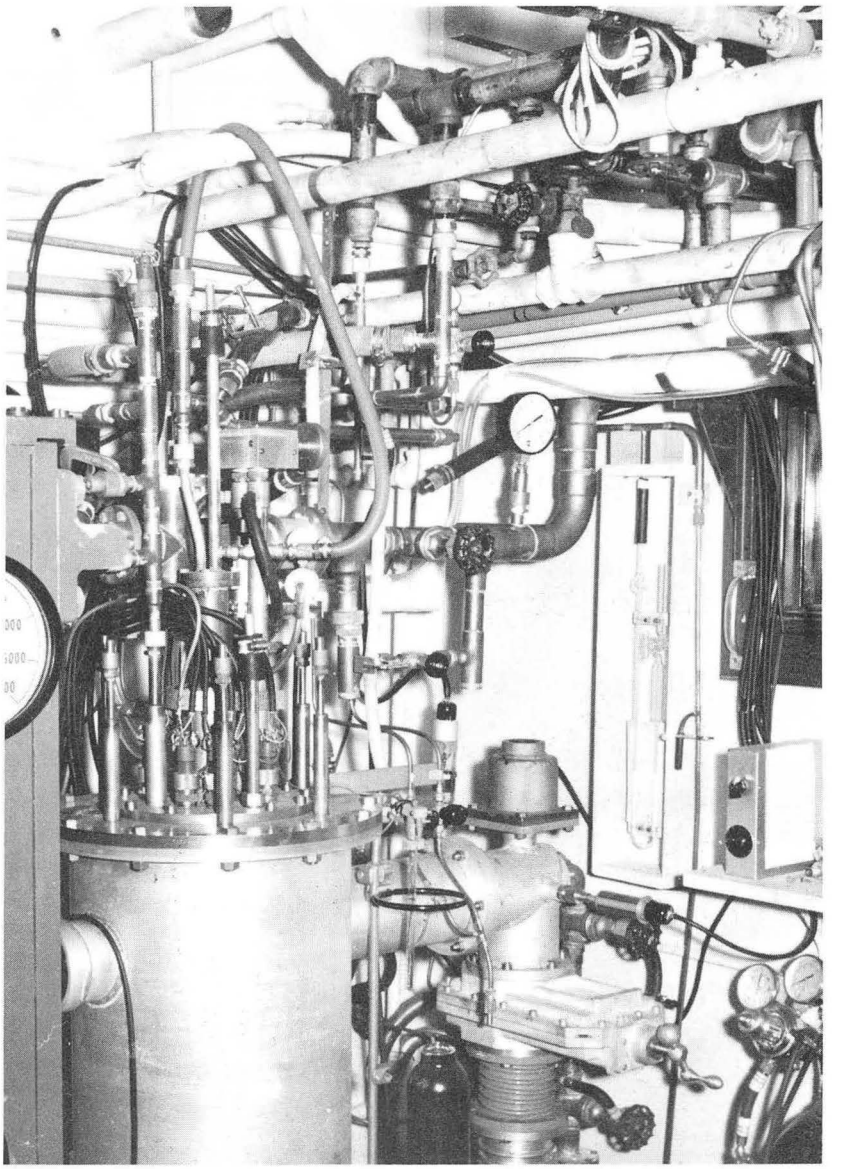

ZN-2730

Fig. 4. Connections at top of calorimeter.

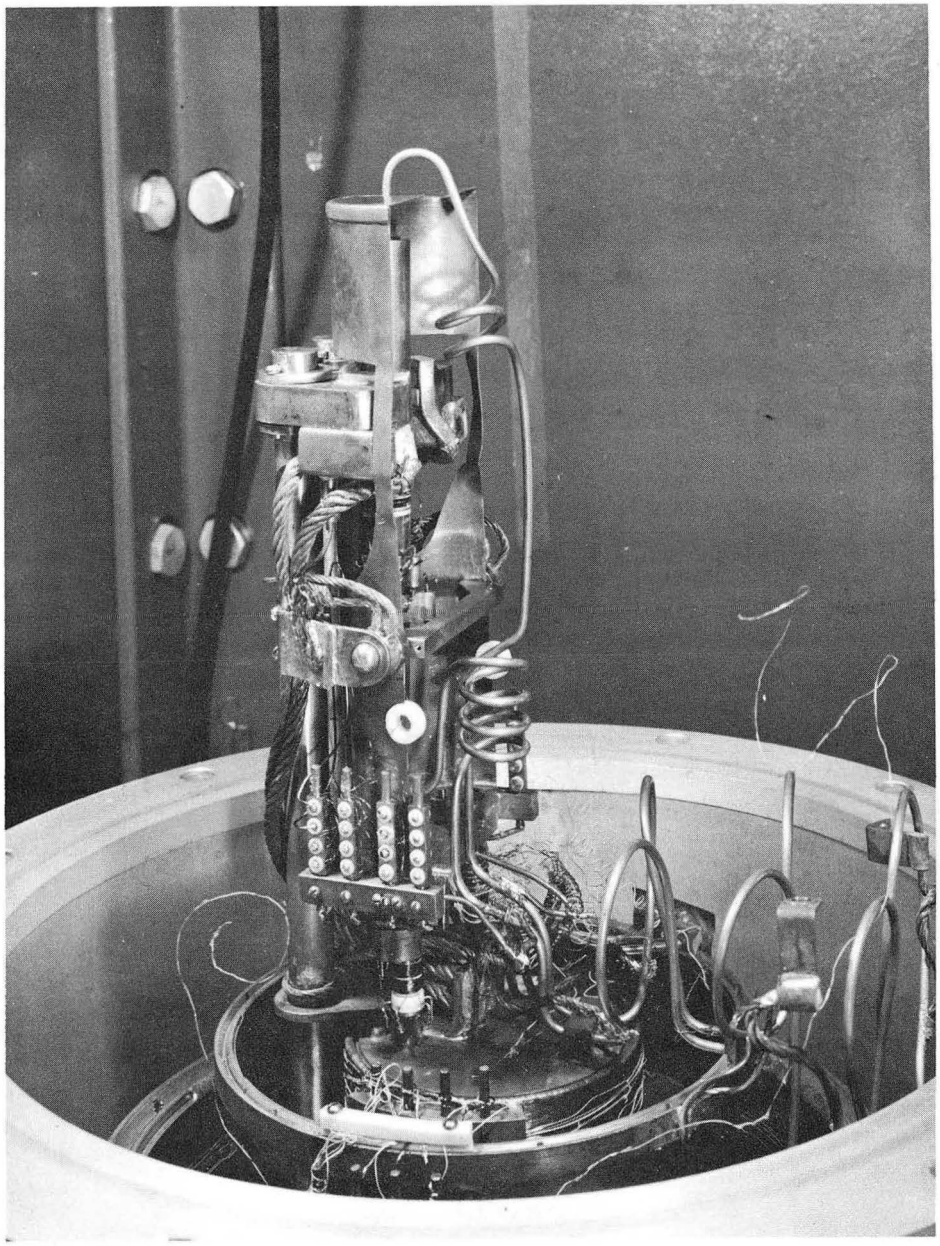

ZN-2734

Fig. 5. Closeup of cell, shield, and clamp.

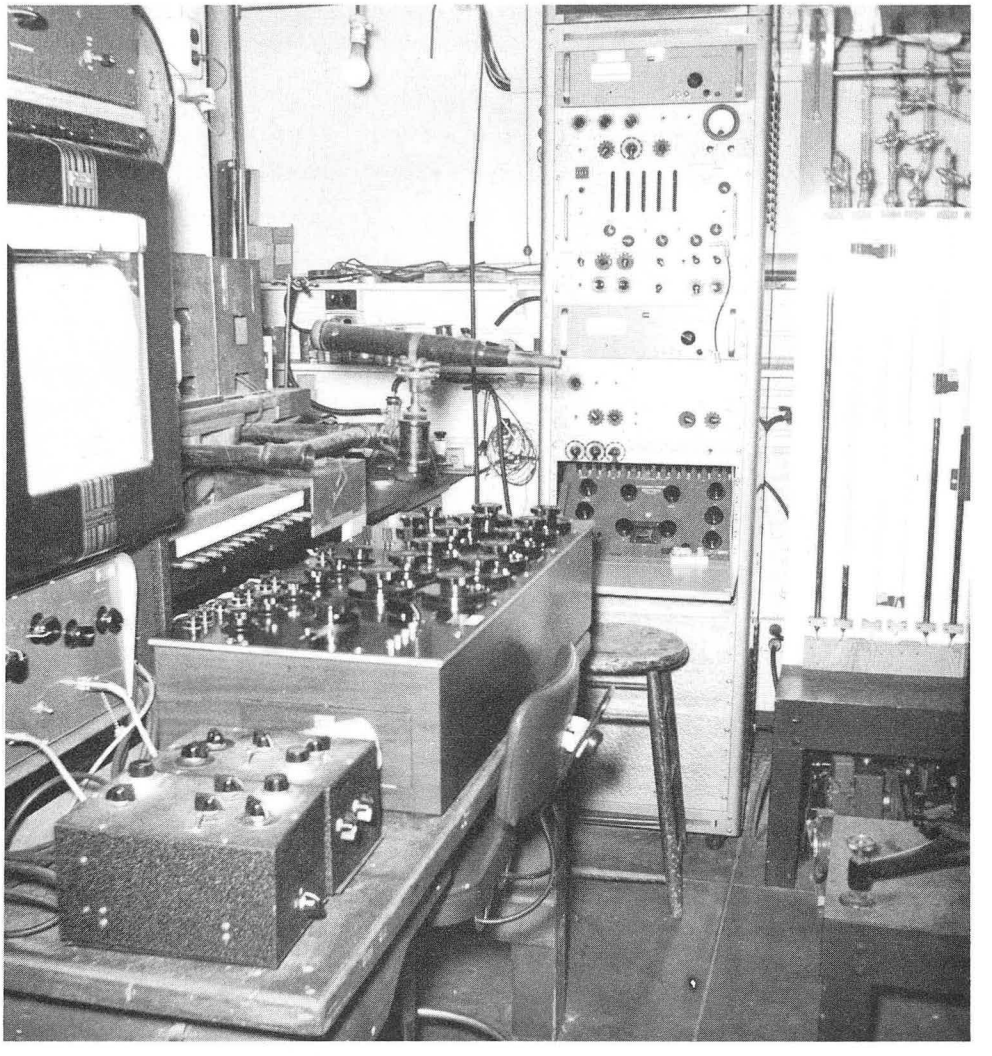

ZN-2731

Fig. 6. Some of the measuring equipment.

heat leak (see Fig. 2). An extension above the main flange was also made for this purpose. The sections of the clamp tubes were insulated from each other by thin mylar sheets to reduce the heat leak further when the jaws were open.

A vapor-pressure bulb, BB, was soldered to the top of each jaw so that it would be in good thermal contact with the cell when the clamp was closed. Each bulb was made from a single piece of 1/16-in. copper hard-soldered into a rectangular shape having a volume of about 4 cm^3. A 1/4-in. stainless steel tube was hard-soldered into the top surface for adapting to the smaller stainless-steel tubing. The bulbs were soft-soldered directly to the copper faces of the main clamps. Since the vapor pressure bulbs moved with the jaws, a flexible connection was required between the bulbs and the inner bath. For this purpose, 1/16-in. stainless steel tubing was used. It was connected to 1/8-in. tubing at the inner bath and then run out the top of the calorimeter. It was essential for the vapor-pressure tubes leading to the bulbs to slope downward at every point within the calorimeter.

The electrical leads were brought into the calorimeter through five 3/4-in. Lawrence Radiation Laboratory fittings in the top flange, C. The wires were cast into epon plugs in the shape of the fittings. Thermal contact of the wires at the liquid-nitrogen temperature was achieved by wrapping them around a copper tube at the top of the liquid-nitrogen shield and attaching them with G.E. 7031 cement. Contact at the two inner baths was made by wrapping the wires around the baths twice and gluing them. A lug post was provided on the isothermal shield for terminating the current and potential leads from the top of the calorimeter and for connecting the leads from the cell.

There were several general reasons for designing the calorimeter in the above fashion. By making the vacuum can and shields removable at the cell level, it was possible to open up the calorimeter to the cell very rapidly without disturbing any of the electrical, thermal, or pressure connections. In addition, it was possible to remove the cell and pressure capillaries without touching the thermal apparatus, and, conversely, to hoist out the thermal parts without disconnecting the cell from the pressure system.

Properties and Operation of the Calorimeter Baths

Liquid-Nitrogen Reservoir

The capacity of the reservoir was about 13 liters. A Styrofoam-insulated tube was run from a 50-liter dewar to one of the inlet tubes, and the nitrogen level in the reservoir was regulated with an automatic device.* The level was kept near the top and did not vary more than an inch during runs. For the initial cooldown, it was found that a 50-liter dewar was adequate for bringing the reservoir to liquid-nitrogen temperature and for keeping it full several hours. After the apparatus was fully cooled to liquid-nitrogen temperature, one 50-liter dewar was required every 24 hr, and the automatic bath filler transferred regularly at about 1-hr intervals. For the initial cooldown, the two inner baths were also filled with liquid nitrogen. It took about 3 hr for the thermocouples on the copper parts to indicate liquid-nitrogen temperature, but since there were several long lengths of stainless steel tubing with a considerable heat capacity, the apparatus took at least 8 hr to cool completely to liquid-nitrogen temperature. The initial cooldown was usually carried out over night. The reservoir was also connected to a vacuum manifold so that its pressure could be reduced to the triple point ($63.2^{\circ}K$) or lower in order to reduce the heat leak to the outer liquid-helium bath.

Outer Liquid-Helium Bath

A rough estimate of the heat leak to the outer liquid-helium bath for the nitrogen reservoir at $77^{\circ}K$ is given in Table I. In this estimate, we assume that all radiation hitting the outer bath is absorbed. If the liquid-nitrogen reservoir is pumped down to $63.2^{\circ}K$, the heat leak is reduced by 30%. For comparison, the heat of vaporization of liquid hydrogen is 32,400 joules per liter, and of liquid helium is 2750 joules per liter. With the nitrogen reservoir at $77^{\circ}K$, liquid helium should last about 1 hr per liter and liquid hydrogen about 13 hr per liter. The capacity of the bath is 2.7 liters. In practice the bath was usually filled with liquid hydrogen every 12 hr

---

* Constructed by Jack Harvey, Maintenance Machinist Group, Lawrence Radiation Laboratory.

Table I. Heat leaks to outer liquid-helium bath

Path of heat leak	Heat flow (mw)
Clamp tubes	207
Large pumping tube	108
Small pumping tube	45
Fill tube	13
High-pressure capillaries	80
Electrical leads	75
Radiation (with four baffles)	250
Total	778

without letting it get empty. Since a cell temperature of 1.2°K could be reached with hydrogen in the outer bath pumped down to a few mm, it was not necessary to use liquid helium except to reach the lowest temperatures. By pumping the nitrogen reservoir well below the triple point, it should be possible to keep liquid helium in the outer bath about 5 hr. The amount of liquid helium required to cool the outer bath and its shield from liquid-hydrogen temperatures should be less than 100 cm^3. Liquid helium has not yet been tried in the outer bath.

One shortcoming of the present design is that the gas heat capacity of the evaporating liquid is not used. A fairly simple modification could be made by putting a heat exchanger in the pump or exhaust tube at some point between helium and nitrogen temperatures with the heat leaks attached to it. A substantial reduction in the amount of heat reaching the bath itself should be effected by this means. It would also be more desirable to make the sides and top of the bath stainless steel rather than copper so that the gas would be exposed to a temperature gradient right above the bath. This improvement could not be incorporated without completely rebuilding the calorimeter.

Inner Liquid-Helium Bath

A rough estimate of the heat leak between the inner and outer baths is given in Table II for the upper bath at 11°K. At its theoretical pumping

Table II. Heat leak to inner liquid-helium bath

Path of heat leak	Heat flow (mw)
Clamp tubes	3.3
Inner pump tube	7.3
High-pressure capillaries	0.3
Copper wires	5.0
Radiation down tube	0.1
Total	16.0

speed, the KD-30 Kinney pump should pump the bath down to 0.3 mm (1.1°K) with the above heat leak. In practice, a temperature of 1.23°K was reached (0.8 mm). With liquid helium in the outer bath, it should be possible to reduce the heat leak another factor of three or four and to reach 1.1°K, the value hoped for in the initial design. The capacity of the bath was 1.5 liters.

Filling of the Baths

In a glass apparatus, there is no problem associated with filling the baths, but when it is not possible to see how the transfer is proceding and when the bath is full, some special precautions are necessary. For the first liquid-hydrogen tests, a string of three resistors was suspended in each bath so that the depth of liquid could be determined from the measurement of the resistance. This technique failed because the resistors had to be too close together. During filling the rush of cold gas made all three read the same, and even after the filling, there was very little difference between them. With liquid hydrogen, the lack of an indicator was not a serious problem. When the outer bath had filled to the level of the pump tube, the soft rubber safety valve at the top started bumping violently. Experience indicated how long it was safe to use the bath without refilling it (12 hr). Since the heat leak to the inner bath was so small, it was never completely filled with liquid hydrogen, and did not have to be re-filled for much more than a day.

With liquid helium, however, the problem of transferring was more

serious. The safety valve did not bump when the bath was full, so that a large amount of liquid could easily be blown out the vent. An oil-manometer flow gauge was connected to the vent to give an indication of the rate of evaporation of the liquid, and a thermocouple attached to the outside of the bath was monitored during the transfer. Initially, the flow out the vent was large because of the cooling of the transfer tube. There was then a lull, followed by a second large flow. At first the second flow was interpreted as indicating that the bath was full; however, it turned out that this was just the beginning of the filling of the bath. The amount of liquid helium lost during each transfer was about 1 liter or less.

Description of the Cell and Environment

Isothermal Shield

The top of the shield was a 3-in.-diam. by 5/8-in.-thick copper disc. A cylindrical 0.022-in. copper shield 8-1/2-in. long was soft-soldered to the bottom of the copper disc. The shield was sliced in half vertically and held together with two copper screws through the disc. The back half was permanently attached to the inner bath by two stainless rods. The front half was removable for access to the cell. Two half-circles of lead, each 1-3/8-in. diam. and 1/4-in. thick, were soldered to the underside of the copper disc on the removable part of the shield. About 30 cm of the electrical leads were coiled up between the inner bath and the shield and glued to a copper rod screwed into the top of the back half of the shield with G.E. 7031 cement. The wires then went to soldering lugs on the sides of the shield. These were simply brass screws insulated with Teflon washers from copper strips soldered to the shield. Manganin wires went from the lugs through the shield to the cell. They were wrapped around the end of the lug posts and glued before going to the cell. It is thought that the largest thermal emf's in the measuring circuits occurred at the copper-to-manganin joints. The heater-regulator components (two 2000-ohm heaters and a 10-ohm thermometer) were mounted on a copper rod screwed into the top of the back half of the shield.

Cells

The cells were made from beryllium copper. The outside dimensions of the first design were 6-1/4-in. long by 11/16-in. diam. The inside dimensions were

4-in. long and 1/4-in. diam. The design considerations for the cell are discussed in Section III and the heat capacities are discussed in Section V. About 1000 ohms of Driver Harris 0.00175-in.- diam. Formvar-insulated manganin wire (92.30 ohms/ft) were bifilarly wound on the cell. It was found necessary to put a layer of cigarette paper under the windings to keep the leakage resistance to the cell large enough. The windings were glued to the cell with G.E. 7031 cement. Solder lugs on the cell were provided by two heavier copper loops glued to the cell. The potential leads were No. 40 manganin, the current leads No. 30. The current leads were 48 $\pm$ 2 mm long. The use of short lengths of manganin was necessary to obtain small enough heat leak and electrical resistance. Two radio resistors were used as thermometers. These were 1/2-w Allen-Bradley 10- and 56-ohm types with the covers ground off. They were glued in dead soft-copper clips which were shaped around them and glued to the cell. The leads on the resistors served as solder lugs. The manganin wires were wrapped around the cell once and glued before going to the shield.

Thermal Clamps

As mentioned in the general description, heavy stainless steel tubes rotated from the top of the calorimeter were used to open and close the jaws of the clamps. The clamps consisted of a heavy stainless steel body, with copper faces for contacting the cell. A large force was desirable on the main clamp so that the heat of conversion of ortho to para hydrogen could be conducted away rapidly enough that the lowest temperatures could be reached. It is estimated that several hundred pounds could be exerted on the cell with the clamp. The data of Berman on the thermal conductivity of copper-to-copper contacts at low temperatures were used in designing the clamps.[33] In the initial design, the jaws made contact with the cell at four spots at an angle of 30 deg to the direction of closing. Although this method gave very good contact, it was found that the heat of friction on opening the clamp at 1.2°K gave more than an 0.5°K temperature rise. In order to remedy this situation, a 1/4-in-thick piece of copper was screwed into each jaw so that its surface was 90 deg. to the direction of motion. The copper faces of the clamps were connected to the inner bath through four flexible copper wires of about 1 cm^2 total cross section. A second set

of clamps of a lighter design was attached to the tubes at a higher point to contact the shield. These clamps made contact before the main jaws, but did not exert as much force. About 1.5 hr were required to cool the shield from liquid-nitrogen to liquid-hydrogen temperature. The limiting process in this respect, however, was the cooling of the stainless steel capillaries between the cell and shield, which required 4 hr.

Vapor-Pressure Bulbs

The mechanical arrangement of the bulbs is given in the general description. The front bulb was usually used with hydrogen and the rear one with helium. The sample used was placed in a 2-liter bulb at room temperature and slightly less than 1 atm. and then condensed into the bulb. The manometers were made from 20-mm. tubing, and the mercury or oil (Octoil) levels were read with a Gaertner cathetometer accurate to about ± 0.1 mm. The copper-iron—versus—copper thermocouple used as an auxiliary calibration thermometer and a copper-constantan thermocouple were glued to the rear vapor-pressure bulb.

Calorimetry Circuits

Thermometer, heater, temperature control, and thermocouple circuits used in the calorimeter are shown in Figs. 7, 8, 9, 10, and 11.

Thermometer Circuit

Two 1/2-w Allen-Bradley carbon-composition resistors of the nominal 10-ohm and 56-ohm values were used as thermometers. The first was used from 1 to 3°K and the second from 3° to the highest temperature (about 25°K). The properties of these resistors have been discussed in the literature.[34,35] The information in Table III is useful in understanding the circuit requirements.

Table III. Approximate thermometer characteristics

10 ohm			56 ohm		
T	R	-dR/dT	T	R	-dR/dT
1.13	2000	4610	1.62	10000	13900
2.72	162	76	3.96	1000	294
4.21	80	18	11.0	270	15
			18.4	180	4.3

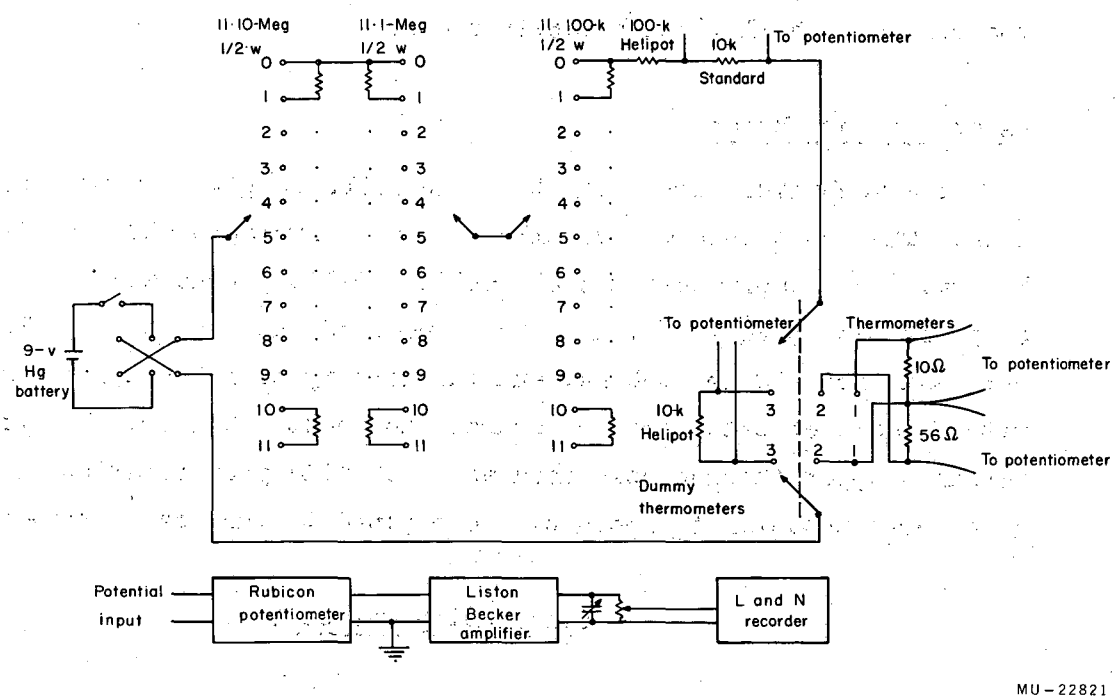

Fig. 7. Thermometer circuit.

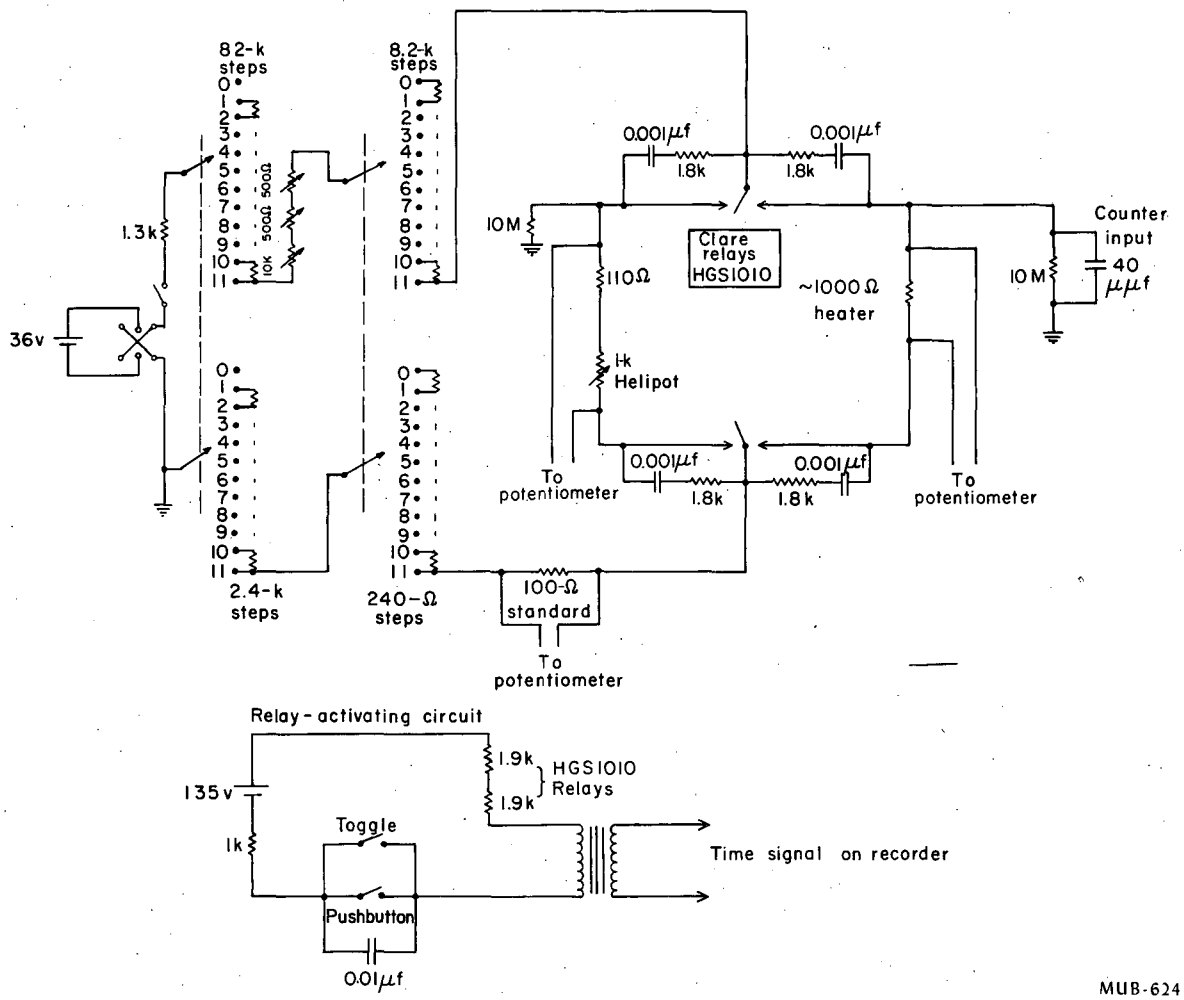

Fig. 8. Heater circuit.

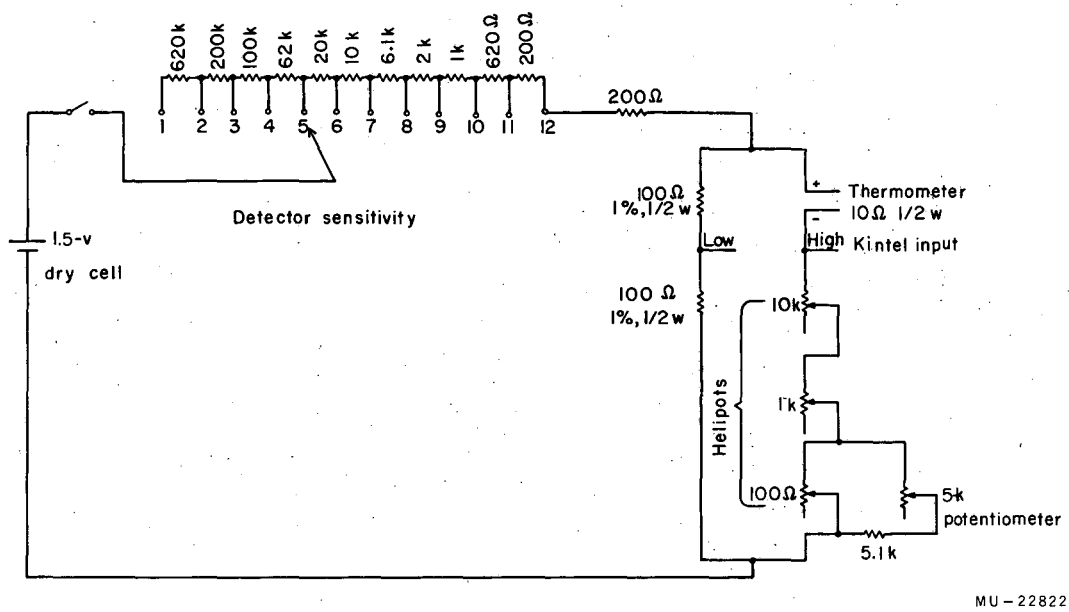

Fig. 9. Detector bridge for temperature-control circuit.

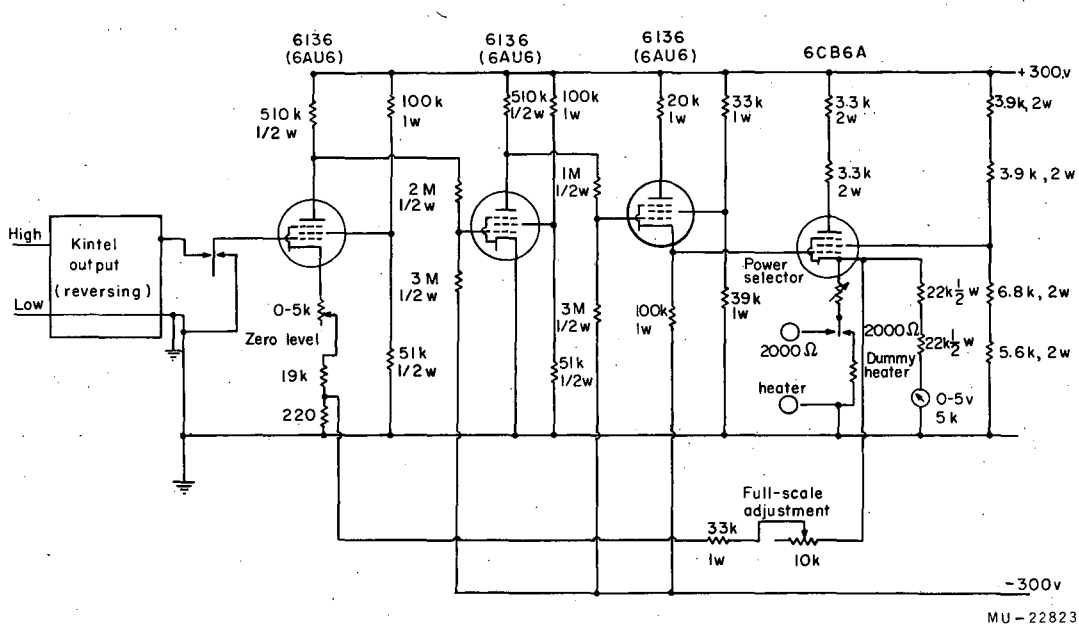

Fig. 10. Power amplifier for temperature-control circuit.

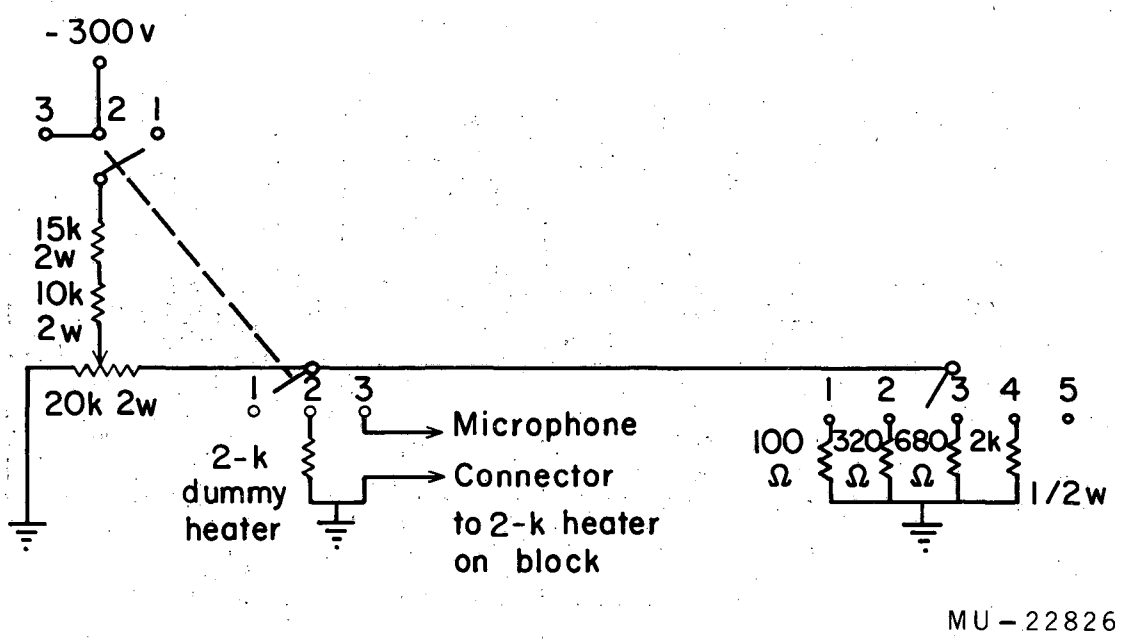

Fig. 11. Auxiliary heater for temperature-control circuit.

A current range of 0.07 to 150 μa was used to obtain adequate precision of temperature measurement (somewhat better than 10^{-3} °K). The currents were small enough that the power dissipation in the thermometer and temperature difference from the cell were negligible.[36]

A single 9-v mercury battery (Mallory TR-146R) was used. During runs the potential was constant to better than 0.01% per hour if the windows in the room were kept closed. The 1000-ohm standard resistor was obtained from Leeds and Northrup Co. (Cat. No. 4040-B; Serial No. 1530456). The resistance was 10,000.2 ± .005% at 25°C. and the temperature coefficient was 0.0005% per °C. Multiconductor shielded copper cable was used to connect the various parts of the circuit. All potential leads were connected with copper lugs or knife switches. Ordinary rosin-core electrical solder was used. The major thermals appeared to be caused by manganin wires very near the cell. Leakage to ground of the thermometer circuit was always unreadable on a Weston meter (i.e., greater than 10 meg).

The potentials were measured with a Rubicon Double Six-Dial Thermofree Potentiometer (Cat. No. 2773-S; Serial No. 108030). A Beckman Instruments (formerly Liston Becker) Model 14 D.C. Breaking Amplifier was used as a galvanometer. Its input impedance was 10,000 ohms and the noise level was about 0.05 μv. A Leeds and Northrup Speedomax Type G Model S 60000 Series Recorder was used to display the output of the Liston Becker amplifier. Its full scale sensitivity was 10 mv.

An attenuation of 200 was found necessary in the output of the Liston Becker amplifier because of the nonlinearity of the output circuit at low signals. A higher attenuation was not used because of saturation of the output circuit at higher voltages and because of the limited amplification available. The nonlinearity of the output appears to be a property of the amplifier circuit and not of the particular amplifier being used, since the same phenomenon occurred with two other available models. An over-all linearity of about 1% of the recorder scale was obtained with the galvanometer system. When the potentials on the standard resistor were large, they were read on the K-3 potentiometer, which is described in the following section.

Heater Circuit

The heater circuit was independent of the thermometer circuit. The heat capacities to be measured ranged from 4 to 10,000 mjoules/°K.

A 1000-ohm heater was used with an available current range of 50 μa to 10 ma. Four 9-v mercury batteries (Mallory TR-146R) were connected in series. These batteries have a life of 400ma hr, and a maximum drain of 40 ma. In use, the drain was usually less than 3 ma. The heater was made from 0.00175-in. diam. Formvar-insulated Driver-Harris manganin. The leakage to ground was unreadable on the Weston meter (greater than 10 meg). The dummy was a helipot set to the same resistance as the heater.

In a measurement, the current was stabilized on the dummy and measured across the standard resistor, a Leeds and Northrup 100,000-ohm standard resistor (Cat. No. 4030-B; Serial No. 1534139). The current was then switched to the heater with two Clare Type HGS 1010 Mercury-Wetted Contact Relays. According to the sales literature, the operating time of the relays is about 1.3 msec. The contact action of the relays is make-before-break, and the bridging time is 0.5 msec. maximum. The time during which the relays were in contact with the heater was measured with a Model 7250CR Time Interval Meter (Berkeley Division, Beckman Instruments, Inc.), which was good to about one part in 10^5, with a minimum measurable time interval of 10 μ sec. The input impedance was 10 meg shunted by 40 μμf. The current adjustment switches in the heater circuit were set up so that the counter always had an adequate triggering voltage (0.3-1.0 v). The counter also required that the circuit be grounded at the point indicated in the schematic. The input impedance of the counter was matched to the dummy, so that the current through the standard resistor did not change on switching.

The heater potential was measured on a Leeds and Northrup Type K-3 Universal Potentiometer. The heater current was set so that it could be read on the Auxiliary EMF setting of the K-3. A Kintel Model 204A Electronic Galvanometer was used as a null detector. Its noise level was about 0.5 μv, and the over-all accuracy of the potential measurements was about ± 1 μv, or one part in 10^4.

Bath and Shield Temperature Regulator

The temperature regulator was needed for controlling the bath temperature during a thermometer calibration and for controlling the temperature of the isothermal shield surrounding the cell during heat-capacity runs. A 1/2-w 10-ohm radio resistor was used as the temperature-sensing element. A 1.5-v battery supplied bridge current, and a series resistance was used to regulate

the detector current or sensitivity. The temperature was set by adjusting the ratio arm of the bridge. The unbalance of the bridge was amplified by a Kintel Model 204A Electronic Galvanometer. Its input sensitivity was about 0.5 μv and its output was ± 1 v at 1 ma. The output was amplified to a range of 0 to 50 v at 25 ma with a four-tube, linear, negative-feedback, amplifier. The power level available on a 2000-ohm heater with this arrangement was about 1 w. The circuit was adjustable with respect to gain and zero signal current through the heater. In practice, the power level was set at 5 v with the Kintel output at zero (temperature at desired value); -1 v on the Kintel gave 50 v on the amplifier, and a slight positive voltage on the Kintel output caused the heater to shut off.

The amplifier contained two stages of amplification followed by two cathode followers. The heater was the cathode resistor of the second cathode follower, and the desired power range was adjusted with a series resistance. The feedback was taken from the cathode of the last tube and applied to the cathode of the first tube. The gain of the circuit was adjusted by varying the feedback ratio. The zero level was adjusted by varying a resistor in the cathode of the first stage (but not in the feedback loop). The two cathode followers were necessary to get a low enough output impedance and to bring the output voltage close enough to ground. In practice, the circuit was found to be stable and to require little adjustment. In initial testing, the biases of the various parts of the circuit were fairly critical with respect to B^+ and B^- (300 v each), but the use of regulated power supplies removed the necessity for any later adjustments.

The available input sensitivity was better than 1 $m^oK/\mu v$ at 20^oK and was greater at lower temperatures. The full-scale power level of the heater was stepwise adjustable from 11μw to 1.25 w. The wide range was desirable because the heat capacity of the thermal shield was much less than that of the bath. A steady heating power of 10 mw was fairly common for the bath. The steady heating rate was determined by the rate of pumping on the bath. Higher powers were needed to change the bath temperature in reasonably short times. It is felt that the quality of temperature regulation was limited by the response of the bath rather than by the circuitry. The rate of distribution of heat in the bath (especially for the case of solid hydrogen) could probably be increased by soldering copper fins in the bath.

Thermocouples

A thermocouple of copper containing 0.0111 wt % iron versus copper was glued to the rear vapor-pressure bulb and used as an auxiliary thermometer for temperature calibrations. The wire was supplied by Sigmund Cohn Corporation, and contained a lower iron concentration than was specified in the order (0.015 wt %). For this reason, the sensitivity was less than hoped for, but the thermocouple was still useful.*

Different thermocouples of the same copper-iron alloy versus copper were used between the inner and outer bath and between the inner bath and the shield. Since the diameter of the wire was 0.010-in., the heat conductivity was too large to allow a difference thermocouple between the cell and shield. The potentials of the difference thermocouples were read on a Leeds and Northrup Electronic D.C. Type 9834 null detector. The potential of the auxiliary thermometer thermocouple was read on the White potentiometer of 10,000 μv maximum range. Several copper-constantan thermocouples were used in the calorimeter as well as in other parts of the apparatus, and these were usually read on the Leeds and Northrup recorder or on the K-3 potentiometer.

III. PRESSURE SYSTEM

General Description

The purpose of the pressure system was to develop a pressure as much in excess of 5000 atm as possible on a known amount of solid hydrogen sufficiently isolated from its environment to allow an accurate determination of its heat capacity. The general technique was similar to that used by Dugdale and Simon for studying the thermal properties of solid helium to 3000 atm.[37] In their experiments, a U-shaped container half filled with mercury was charged with helium gas on one side and then closed off from the tank. Oil pressure was applied to the mercury in the other arm then compressed the sample into the cell through stainless steel capillary tubing. After the pressurization, the

---

* A sample of copper wire containing 0.015 wt % iron was kindly supplied by Dr. E. R. Grilly of Los Alamos Scientific Laboratory. This wire was used in a test apparatus but not in the actual calorimeter.

helium was frozen in the capillary, and the sample in the cell was cooled and frozen at constant volume.

For the experiments on hydrogen, the higher pressures required and the problem of hydrogen embrittlement of ordinary high-strength steels made the apparatus problems a good bit more complicated. A schematic diagram of the pressure system for the present experiments is shown in Fig. 12. A bomb and three mercury U-tubes were used to raise the pressure from 1 atm to the vicinity of 10,000 atm.

After purification or preparation, the gas was initially stored at 1 atm in one or more of four 5-liter bulbs on the preparation rack. It was then condensed into a bomb with a total volume of 73 cm^3 which was cooled to the hydrogen triple point or lower. The volume of liquid hydrogen was always less than 30 cm^3. The bomb was closed off from the bulbs and heated, the sample expanding into a 2-liter volume on one side of the low-pressure U-tube at a pressure of 10 atm. The U-tube was closed off from the bomb and the mercury pushed up by nitrogen-gas pressure on the other side. The sample thus was compressed into the gas side of the medium pressure U-tube at about 100 atm and a volume about 200 cm^3. The medium-pressure U-tube was closed off from the low-pressure U-tube and the mercury forced up by oil pressure on the other side, the gas being compressed into the high-pressure U-tube at about 1000 atm and 20 cm^3. In order to isolate the medium pressure U-tube from the higher pressures, the mercury was pushed up into the 1/8-in.-o.d. by 0.024-in.-i.d. capillary at the end of the U-tube and frozen. The freezing point was determined by a cold finger attached to the capillary. The frozen mercury "valves" served to seal the high-pressure sample and to define the high-pressure volume closely. The mercury in the high-pressure U-tube was then pushed up by the action of an intensifier, and the sample was pushed into the cell. The mercury was pushed into the capillary at the end of the U-tube and frozen as with the medium-pressure U-tube. The inner bath of the calorimeter was then filled with liquid hydrogen or helium and the hydrogen rapidly froze at the point of contact of the capillaries with the inner bath. The hydrogen in the cell cooled more slowly and froze at constant volume. At the end of the experiment, the pressurizing procedure was reversed. The gas sample was let out into one or more of four 5-liter bulbs in a Styrofoam-insulated box, and the pressure read to determine the number of moles that had been in the high-pressure system. Samples could be

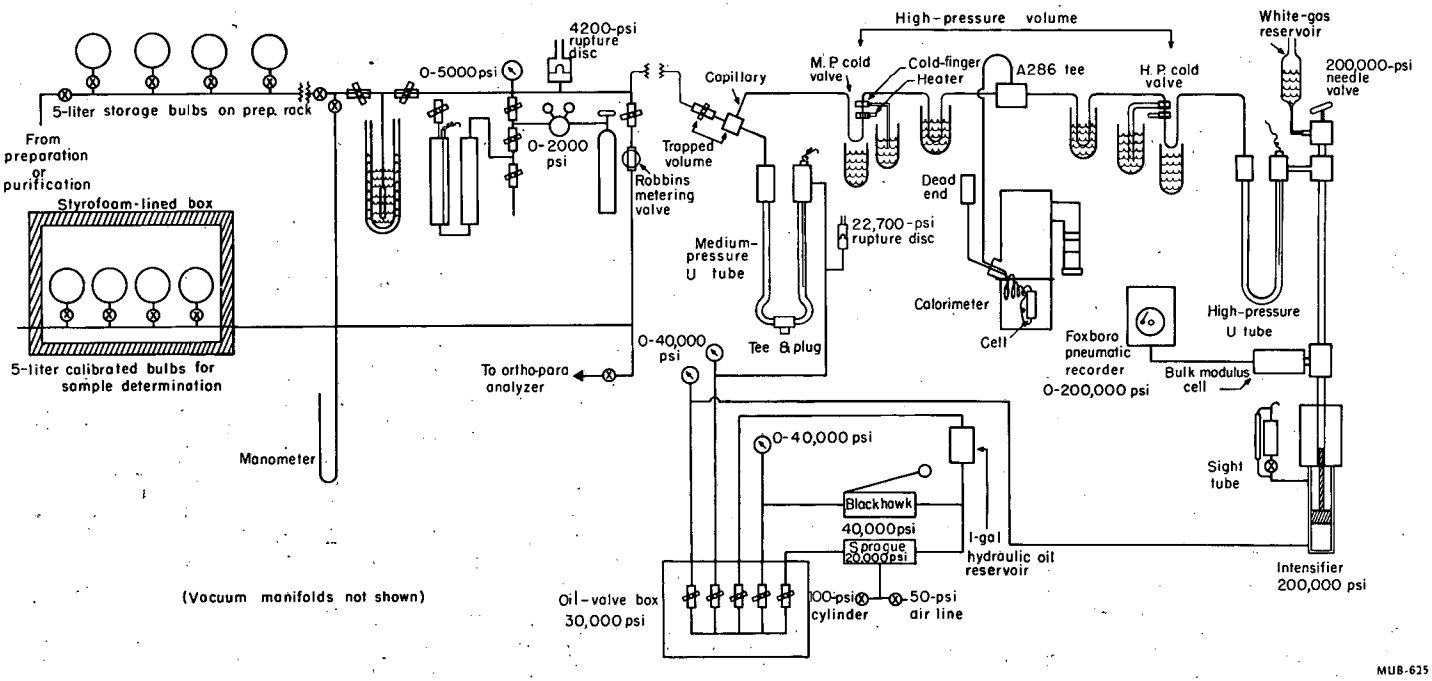

Fig. 12. Schematic of pressure system.

taken for the ortho-para analyzer before or after a pressurization. A more detailed description of the various parts of the pressure system is given below.

Low-Pressure System

Condensing Bomb

The bomb shown in Fig. 13 was of welded nonmagnetic stainless steel construction. It was connected to the manifold by 1/4-in.-o.d. by 0.049-in.-wall type 304 stainless steel tubing and was pressure tested to 5000 psi. The bomb was cooled in a glass double dewar arrangement equipped for use with liquid hydrogen or helium. A heater consisting of 27 ft of No. 24 insulated manganin wire with a total resistance of 20 ohms was wrapped around the outside of the bomb and baked on with formvar enamel. Enough voltage was supplied to give a maximum heat input of about 15 w. The temperature of the bomb could be determined by a thermocouple or by the bath vapor pressure.

Low-Pressure U-tube

Two 52-in.-long o.d. by 0.218-in. wall stainless steel tubes formed the arms of the U-tube as shown in Fig. 14. Heavy stainless steel caps screwed over the ends and were sealed with O-rings. Parker fittings were used to connect the caps to 1/4-in.-stainless steel tubing. The bottoms of the two arms were connected by 1/4-in.-o.d. by 0.049-wall stainless tubing. An electrical lead assembly was fitted into one of the top caps and the U-tube assembly was tested to 5000 psi. The U-tube was half filled with mercury, and the level followed by measuring the capacitance of a Formvar-insulated No. 16 copper wire suspended from the electrical connection and supported by the sides of the U-tube. The circuit used to make the depth measurement is discussed later in the Mercury-Depth Indicator section. The hydrogen sample was compressed in one arm of the U-tube by pressurizing the other side with nitrogen gas from a tank connected through a regulator adjustable from zero to tank pressure. The danger of mercury getting into the manifold was reduced by having a valve at the top of the U-tube which could be quickly closed until the driving pressure was released. An indication that the mercury was near the top was provided by a shorting wire glued to the Formvar of the depth-gauge wire.

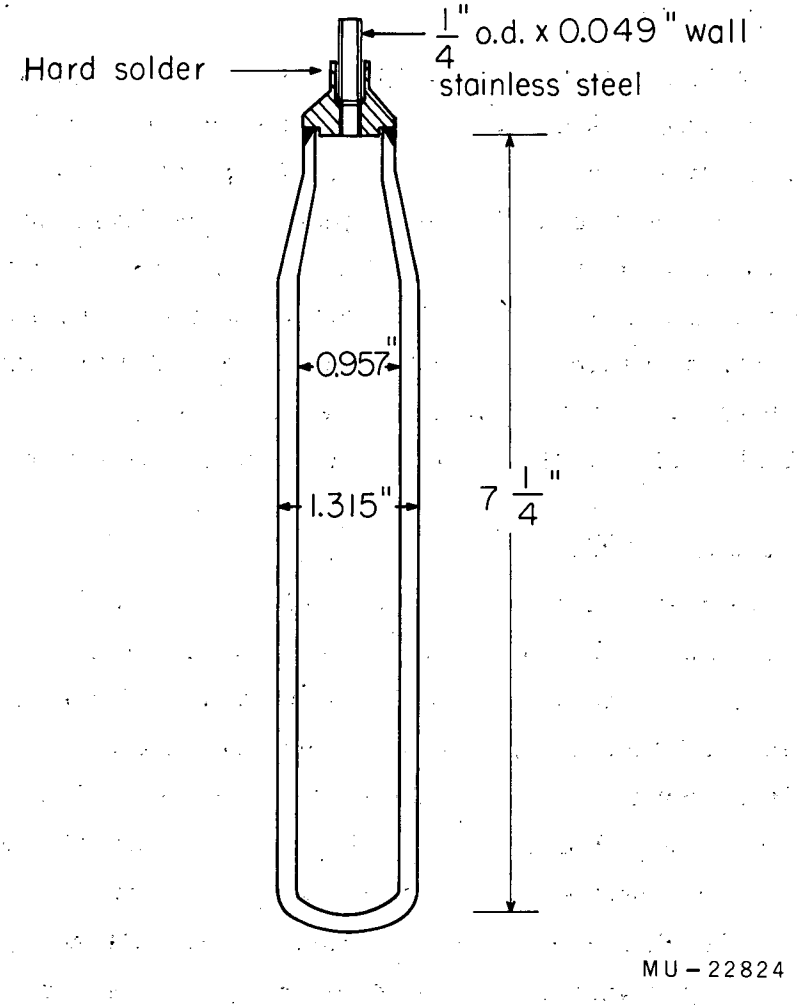

Fig. 13. Condensing bomb.

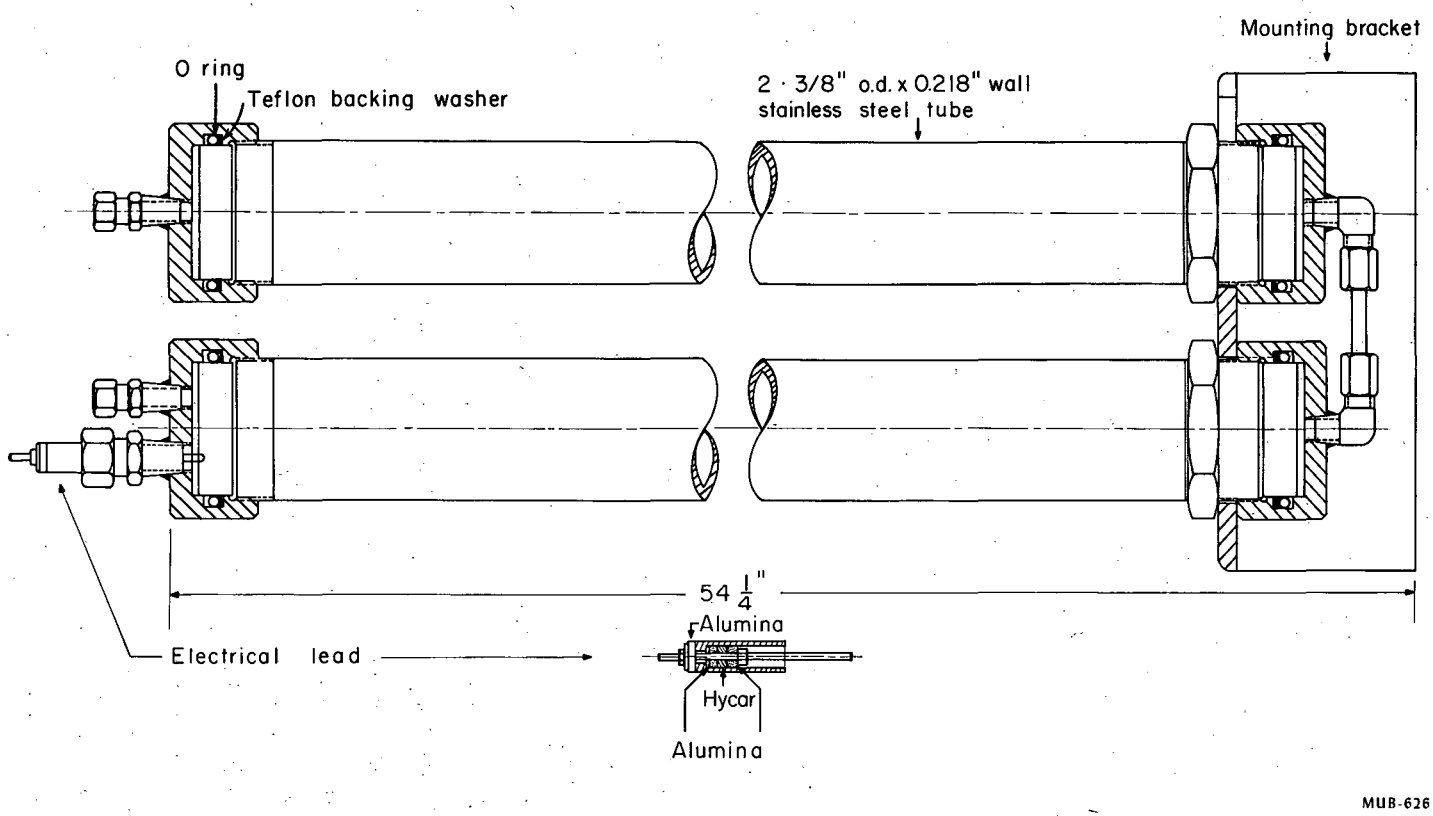

Fig. 14. Low-pressure U-tube.

Low-Pressure Manifold

Up to the bomb, 1/4-in.-o.d. by 0.049-in.-wall stainless tubing was used and 1/4-in.-o.d. by 1/16-in.-i.d. tubing was used beyond the bomb. American Instrument Co. parts used in the low-pressure manifold included "quick-connect" flareless fittings, valves (Cat. No. 44-1203), and a blowout assembly (45-9011) with a rupture disc to hold 4200 psi. The valves had O-ring seals on the stems and were helium leak-tight at 2000 psi through the stems and seats. A 0 to 5000-psig (47-8205) was attached to the low-pressure manifold for operational purposes. Several metering valves were tried for the purpose of letting the gas from the tank at 100 atm into the evacuated 5-liter bulbs. The most satisfactory was a stainless steel type with a Kel-F seat and an O-ring stem seal made by Robbins Aviation Co. (INS G 103-1P).

The condensing bomb, low-pressure U-tube, and manifold are shown in Fig. 15.

Mercury Depth Indicator

Initially it was hoped to follow the depth of the mercury in the U-tubes by measuring the resistance of a wire supported in the tube. Stainless steel wire was tried, but the mercury deposited a layer of insulating material on the wire which made the resistance measurement very erratic. The effect was apparently due to an interaction between the mercury and the steel, and did not seem to depend on the initial cleanliness of the mercury. A similar effect was observed by Bridgman.[38]

In order to avoid this problem, it was decided to measure the capacitance of a Formvar-insulated copper wire suspended in the mercury. The internal diameters of the low-, medium-, and high-pressure U-tubes were 2 in., 5/16 in., and 1/8 in., respectively. The lengths of the depth gauges were made 4 ft, 12 ft, and 160 cm, respectively. Number 16 (51-mil) wire used in the low-pressure U-tube and No. 20 (32 mil) was used in the medium- and high-pressure U-tubes. The thickness of the Formvar insulation was measured and found to be 1.6 mils. By taking the dielectric constant of Formvar as 3.12 and using the expression for the capacitance of a cylindrical condenser, the sensitivity of the low-pressure U-tube was roughly estimated to be 29 μμf/cm and that of the medium- and high-pressure U-tubes to be 18 μμf/cm. The circuit is shown in Figure 16. The capacitance of the wire was made 10% of that of one arm of

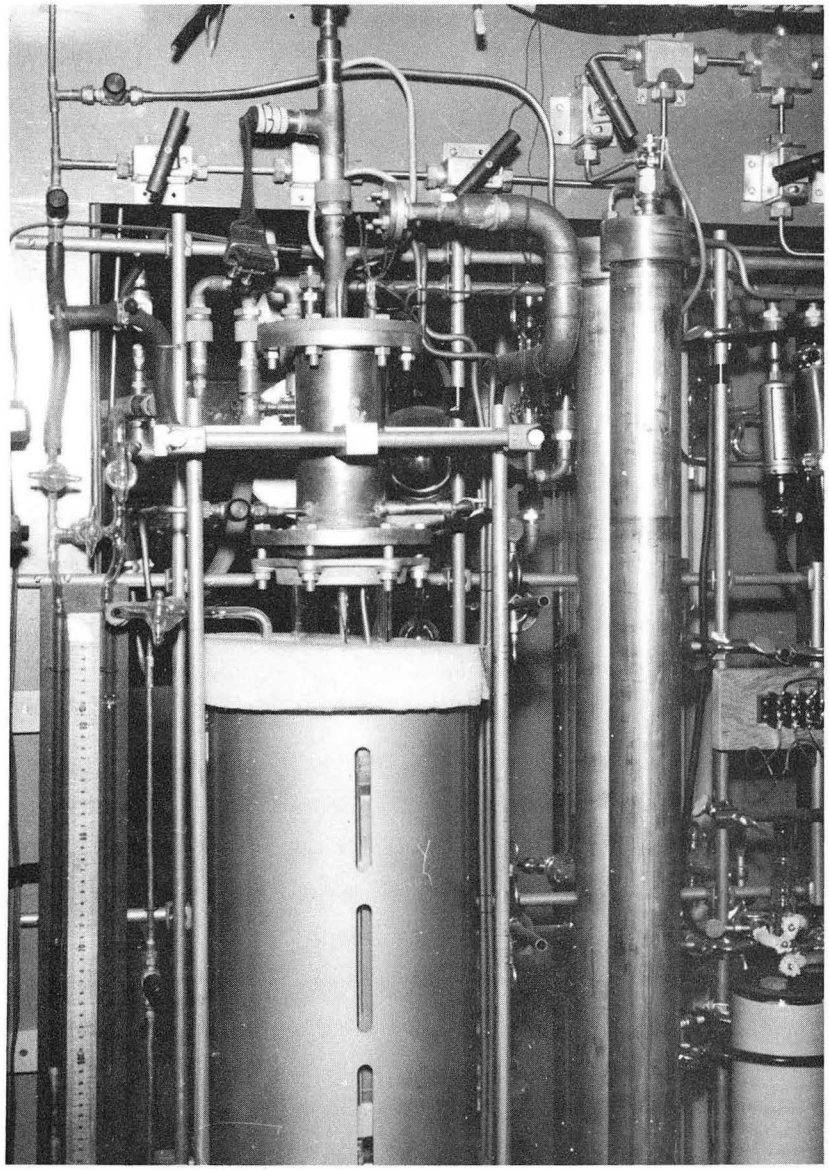

ZN-2732

Fig. 15. Condensing bomb and low-pressure U-tube arrangement.

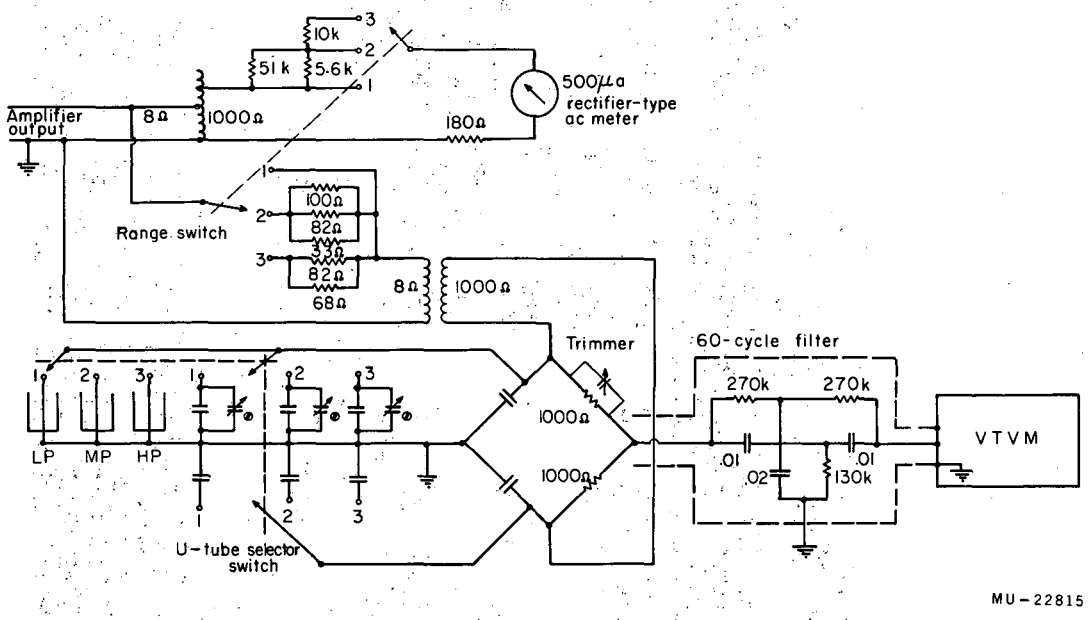

Fig. 16. Mercury U-tube depth-gauge circuit.

a Wheatstone bridge. The depth of the mercury was indicated by the unbalance of the bridge, which deviated about 5% from linearity at full-scale unbalance. Three sensitivities were incorporated: low, medium (4x), and high (10x). A General Radio 1-kc tuning-fork oscillator was used with a 10-w high-fidelity audio amplifier to power the bridge. A Triad S-25Z Autoformer and a Triad S-78Z Output Transformer were connected in parallel to the output of the amplifier, the former to supply current to a Weston 500-μa rectifier-type ac ammeter, and the latter to isolate the bridge from the meter and the sensitivity switch. A shielded 60-cycle twin-T filter was found necessary at the input of the detector, a Shasta vacuum-tube voltmeter. The bridge current was adjusted by setting the meter to 220 μa with the amplifier gain control, and the vacuum-tube voltmeter was used on the 10-mv scale. Adjustment of the bridge zero was provided by 200-μμf screwdriver-actuated capacitors on the front panel for the three U-tubes. The bridge was not accurate enough to give quantitative indications of the mercury depth, but was an indispensible aid in operating the U-tubes.

Shielding

The part of the pressure system involving gas above 100 atm was largely enclosed in 1-in.-thick mild-steel plate. The general features of the shield are shown in Fig. 17. The design was based on information available to us concerning safety features desirable with high pressure apparatus.[39] The main working area in the shield was a 3-ft-wide, 4-ft-high, and 18-in.-deep box with sliding doors on both sides. The sliding doors moved on roller bearings and proved to be very convenient. A small welded 1/2-in. steel box was also included in the shield for pressure testing the cells. The box was just large enough to hold a quart dewar. The medium- and high-pressure U-tubes extended from the bottom of the box through a trap door to the floor below. They were enclosed in a 1-in.-thick by 14-in.-diam. steel pipe to the bottom of the high-pressure U-tube, and in 1/2-in. steel pipe to the bottom of the medium-pressure U-tube. A 1/2-in.-thick steel box shielded the bottom of the medium-pressure U-tube and provided access to the fittings there. The medium-pressure U-tube was assembled in the 1/2-in. shielding and then pulled into the shield from two floors down through a second trap door. The high-pressure U-tube was lowered into the shield through a trap door from the floor above before the roof of the shield was installed. The bottom of the calorimeter

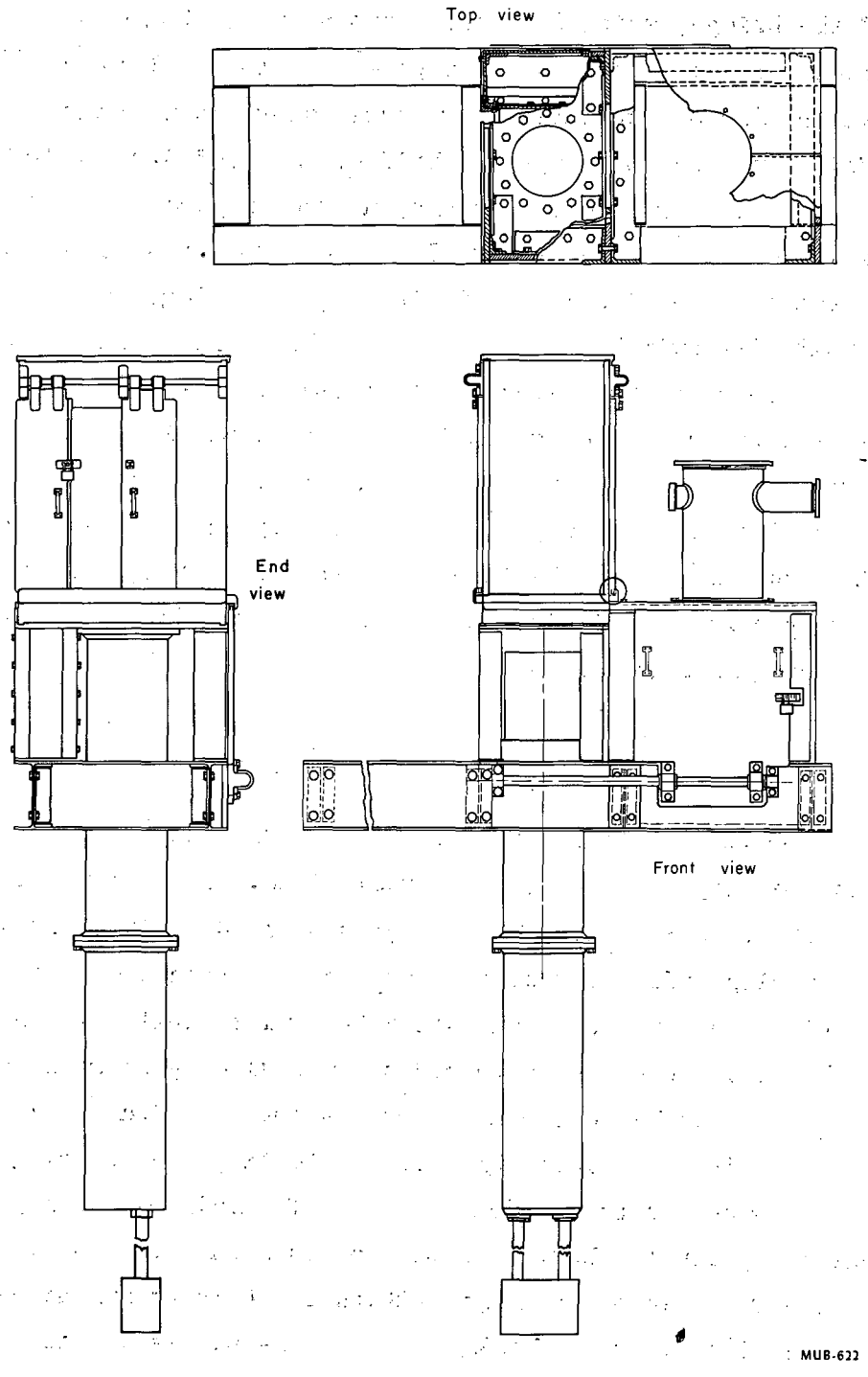

Fig. 17. High-pressure shielding arrangement.

was also shielded with 1-in. steel plate which was attached to the side of the box containing the high-pressure fittings. The shielding and enclosed equipment weighed about 5 tons and were supported by two 12-in. steel I-beams which rested on two of the concrete beams in the floor.

Medium-Pressure System

Two oil pumps were used: an air driven one for handling the large volumes required by the medium-pressure U-tube and the intensifier, and a hand pump for the slow movement needed when pushing the mercury into the capillaries. The air-driven pump was made by the Sprague Engineering Corporation, whose designation was S-440-200. About 100 psi of air were required to generate an output of 20,000 psi in the oil. The pump maintained the pressure to which it was set, and had a capacity of more than 300 cm^3/min -- much more than required. A 50-psi house air line was used for pressures up to about 11,000 psi, and a cylinder of compressed air was used for higher pressures. The hand pump was a Blackhawk Model P-228, rated for use to 40,000 psi. At low pressures its stroke was rated at 0.4 cm^3, but was smaller above 10,000 psi. For the 0-20,000 psi oil system 1/4-in.-o.d. by 1/16-in. i.d. tubing was used with American Instrument Co. connectors (45-1310). American Instrument valves (44-3105) rated to 30,000 psi were used in the oil manifold. A rupture-disc assembly (45-9103) was used in the medium-pressure U-tube line with a disc to hold up to 22,500 psi. Blackhawk LX-21 hydraulic oil was used in the pumps, medium-pressure U-tube, and low-pressure part of the intensifier.

Originally it was thought that fairly short large-diameter cylinders would be used to separate the hydrogen from the oil. The cost of constructing these parts from metals resistant to hydrogen embrittlement would have been quite high and, in the case of failure, the cost of replacement would have been equal to the initial expenditure. After consultation with Mr. Donald H. Newhall, President of Harwood Engineering Co., it was decided to use very long small-diameter composite tubing for both the medium-pressure and high-pressure systems. Although the use of these tubes raised space and installation problems, the much lower initial and replacement cost made their use worthwhile. The composite tubing consisted of stainless steel jacketed with alloy steel.

The medium-pressure U-tube, for use to 20,000 psi, was 15/16-in.-o.d. by 5/16-in. i.d. Each arm was a separate piece 14 ft, 8 in. long. The length of the straight portion was about 13 ft, 9 in. Harwood Engineering Co. 15LH type fittings were used to connect the U-tube to the rest of the system. The sealing elements to the tubing were lens rings. A tee with a cap was put at the bottom to join the two arms. During the bending of the tubing, the jacket stretched over the inner stainless tube by a small amount at the lower end. The angle on the lens ring was great enough to keep the seal on the inner tube, but in the tightening, the outer tube was pulled further over the inner one and on one side of the U-tube the seal shifted to the outer tube. This effect was not discovered until mercury had been forced all the way up the U-tube between the two layers of metal and out at the top. The difficulty was remedied by refacing the end of a new tube after it had been bent to the proper shape.

The oil was brought into the U-tube through a tee at the top. An electrical lead was brought in through the top of the tee on the oil side. A lava cone was used as the insulating seal. The dimensions of the electrical lead are shown in Fig. 18. Originally it was hoped to have the electrical lead on the gas side, but the cone could not be made leaktight against helium. Several attempts were made with the cone lightly coated with rubber cement. A thin layer of red iron oxide was also tried but the helium leak rate was always unacceptable. Although switching the lead to the oil side made the indication of the mercury level on the gas side more indirect, it solved the critical leak problem, and also eliminated one of the trapped volumes in the gas system. As shown in Fig. 19, 1/4-in.-o.d. by 1/16-in.-i.d. tubing was connected to the top of the U-tube on the gas side. This tubing sloped gradually upwards to a tee, one arm of which was connected to a valve for closing off the low pressure system. The other arm was adapted to 1/8-in.-o.d. by 0.024-in.-i.d. hard-drawn stainless steel capillary tubing leading to the high-pressure system. The arm leading to the valve constituted the only trapped volume in the gas system. The capillary tubing was arranged to come out the top of the tee so that any droplets of mercury coming over from the low-pressure system would tend to go into the U-tube.

The mercury-depth indicator consisted of a 12-ft piece of No. 20 Formvar-insulated wire. The end was coated with GE 7031 cement which was baked on to give chemical resistance to the hydraulic oil. A thin stainless steel wire

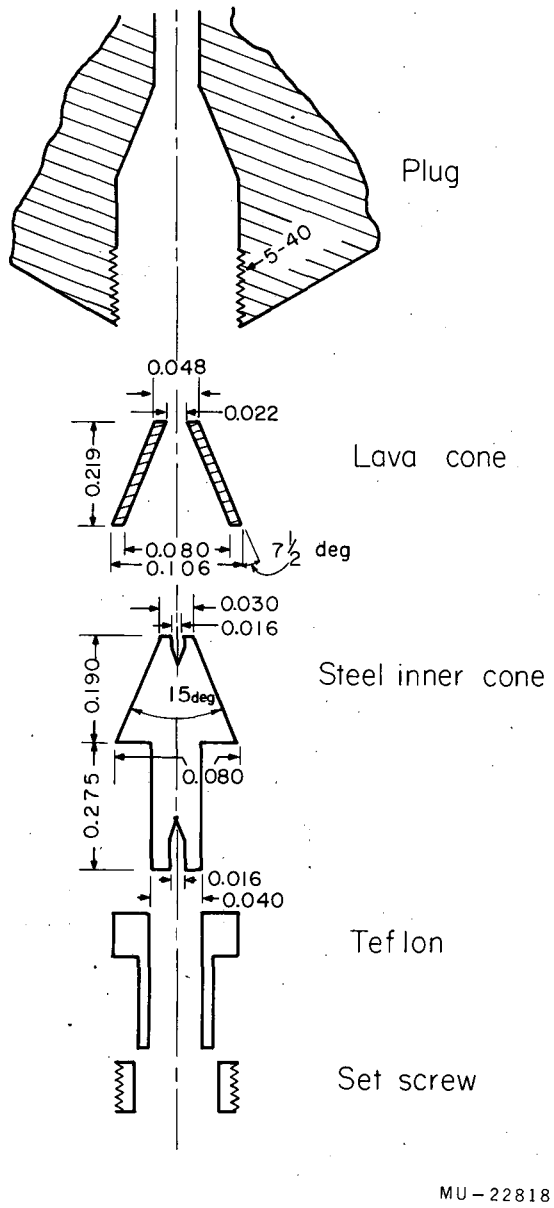

Fig. 18. Details of Harwood electrical-lead assembly.

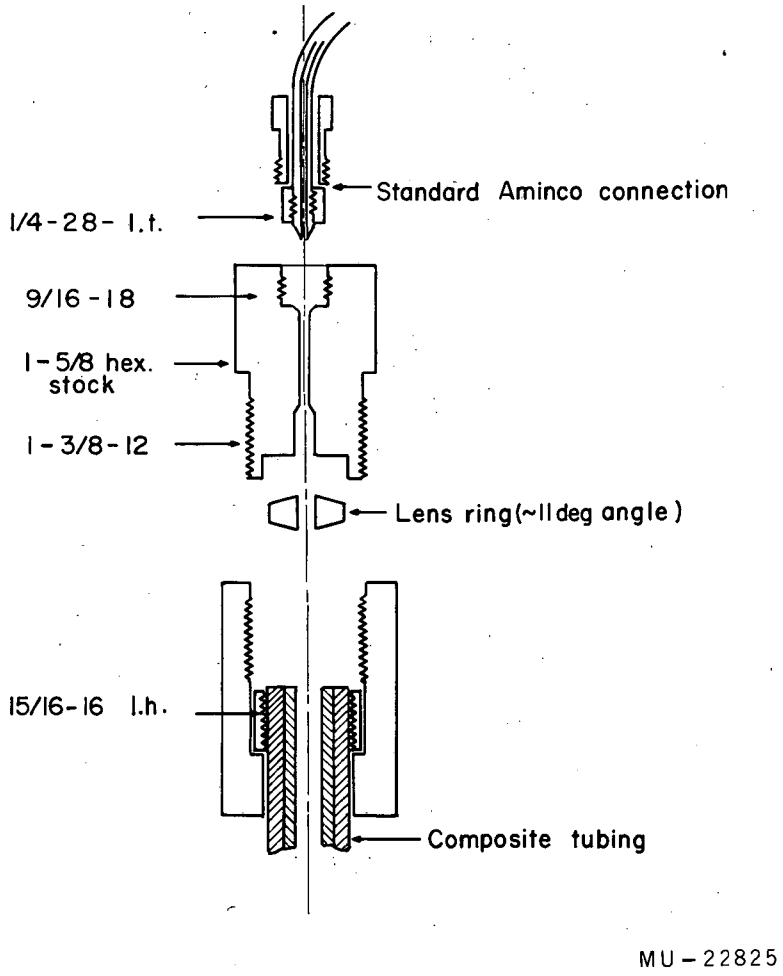

Fig. 19. Top of gas side of medium-pressure U-tube.

was soldered to the lead at the top and glued to the copper wire so that its end was several inches below the side arm of the tee on the oil side. Its purpose was to short the indicator when the mercury was in danger of going back into the oil system. It was easy to tell when the mercury went off the low end of the wire because the indicator stopped moving. The medium-pressure depth indicator was set up so that the bridge was balanced when the mercury was all of the way up on the gas side, hence the highest sensitivity could be used to determine when the mercury went off the end of the wire. The mercury level was adjusted so that it was at the top of the U-tube (within a few cm) on the gas side at 1 atm when it was at the end of the wire on the oil side.

After reaching the end of the U-tube, the mercury was pushed up into the smaller tubing, through two arms of the tee, and into the capillary tubing. This operation was carried out with fairly slow strokes of the Blackhawk pump. Upon reaching the cold finger-heater arrangement clamped to the capillary, the mercury froze. The purpose of the heater was to give a sharp temperature gradient at the cold finger in order to fix the freezing point of the mercury more closely. The temperature of the capillary under the cold finger was about -80°C. and the temperature under the heater was about room temperature. Mercury freezes at -39°C. The motion of the mercury in the capillary was monitored with a copper-constantan thermocouple soldered just past the cold finger. Before the mercury froze, each stroke of the pump caused gas to rush through the capillary at the thermocouple, giving a slight but sharp temperature rise (about 0.1 mv under typical conditions). This signal was amplified by a factor of ten and displayed on a recorder. The freezing of the mercury at the cold valve was then indicated by the lack of response of the thermocouple to further strokes of the Blackhawk pump.

This technique worked well except when there was a leak in the high-pressure system beyond the cold finger. Then the presence of the trapped gas volume seemed to cause a mixture of mercury and gas to be pushed into the capillary. Application of higher pressure on the other side after freezing the cold valve behind the cold finger then usually pushed the mercury back, probably because there was not enough frozen to make a good plug. It was found necessary to lower the cold-finger dewar after freezing the cold valve. This left a puddle of liquid which then filled in the cracks formed by the contraction of the mercury on freezing. When the mercury was pushed up to

the cold finger slowly enough, it seemed to freeze before getting past the cold finger. Evidence for this was given by the fact that a slight release of pressure caused the plug to break and move back. On the other hand, if the mercury was moved up to the cold finger with full sharp strokes of the Blackhawk, it did not unplug when the pressure was released slightly. Since the cell was made of a copper alloy, it had to be protected from mercury contamination. For this purpose a U-tube was put in the capillary past the cold finger and maintained at acetone—dry-ice temperature. Experience indicated that this protection was necessary and adequate.

High-Pressure System

A single piece of 3/4-in.-o.d. by 1/8-in.-i.d. composite tubing was bent into the proper shape. The total depth of the U-tube was 10 ft. A Harwood Engineering Co. A-2.5J intensifier was used as a source of pressure. Its range was 0 to 200,000 psi output for 0 to 15,000 psi input. The high-pressure stroke was 20.1 cm^3. The volume on top of the low-pressure piston was 303 cm^3. It was filled with hydraulic oil and connected to a sight tube for the purpose of indicating the position of the piston. The large ratio of volumes (15:1) made it very sensitive. White gasoline was used in the high-pressure system. Hydraulic oil was used in the low-pressure side, and the Sprague and Blackhawk pumps were used to pressurize the intensifier.

Some trouble was experienced with the packing of the high-pressure piston. A wax-impregnated leather washer contained by triangular cold-rolled steel washers was used. During shipment, the wax had dissolved out of the packing and it could not be made leaktight. A plastic impregnated washer was tried, and this proved satisfactory after it had been pressurized a few times. The intensifier was dead-ended and pumped up for the purpose of breaking in the new washer. The manner of connecting the intensifier to the U-tube is illustrated in Fig. 10. Harwood type-12H fittings were used.

The pressure-measuring cell was connected to a tee directly above the intensifier. It was supplied by the Harwood Engineering Co. Its principle of operation involved the bulk compression of a steel rod which was connected by a probe to a pneumatic system manufactured by the Foxboro Co. The pressure was read on a recorder driven by the pneumatic system. The recorder could be read to $\pm$ 500 psi.

A 12H valve was included in the white gasoline system for the purpose of adjusting the amount of fluid. The electrical lead was brought in through the top of the tee on the white-gasoline side. The same principle for obtaining an insulated seal was used as with the lead in the medium-pressure U-tube. The seal leaked when first pumped to about 40,000 psi, but after the pressure was raised to about 100,000 psi, it was leaktight at all pressures. On the gas side of the U-tube, capillary tubing was connected directly to the top of the U-tube with the arrangement shown in Fig. 20. The method of connecting the capillary tubing was described by Paul and Warshauer.[40] The high-pressure U-tube, medium-pressure U-tube, and cell were connected together by a tee made from Allegheny Ludlum A-286 stainless steel, which was required by the presence of hydrogen and mercury. All of the Paul-and-Warshauer fittings were also made of A-286. The sealing surfaces of the fittings galled badly and had to be re-faced periodically. A cold finger, cold valve, heater, and acetone—dry-ice trap identical to those used in the medium-pressure system were used between the top of the high-pressure U-tube and the A-286 tee. The 1/8-in. holes in the tee were stuffed with gold foil to act as a quick indicator of the presence of mercury.

The filling of the high-pressure system with mercury and white gasoline was not as trivial an operation as with the medium-pressure system because the compression of both the white gasoline and mercury at the higher pressures was a large fraction of the intensifier stroke. In addition, the amount of white gasoline had to be fixed before the pressurization. The following considerations illustrate the conditions for the maximum stroke of the high-pressure piston. It was desired to have the mercury 30 cm below the top of the tube on the white gasoline side under 1000 atm compression. With the intensifier all of the way back, the amount of white gas in the system was about 25 cm^3. If we assume a compression of 12% at 1000 atm, the 1-atm volume of the white gasoline was 28.4 cm^3. Since the cross section of the U-tube was 0.079 cm^2, the mercury was 73 cm below the top of the U-tube at 1 atm. On the gas side, it was desired to have the mercury at such an initial height that it could be pushed to the cold finger at the end of the stroke. If we take the volume of mercury as about 37 cm^3 and the compression between 1000 and 10,000 atm as 3%, the amount of the intensifier stroke that went into the compression of the mercury was 1.1 cm^3. Taking the compression of the white gasoline as 25% from 1000 to 10,000 atm, 7.1 cm^3 of the stroke went into its compression. Hence the net high-pressure stroke available for compressing

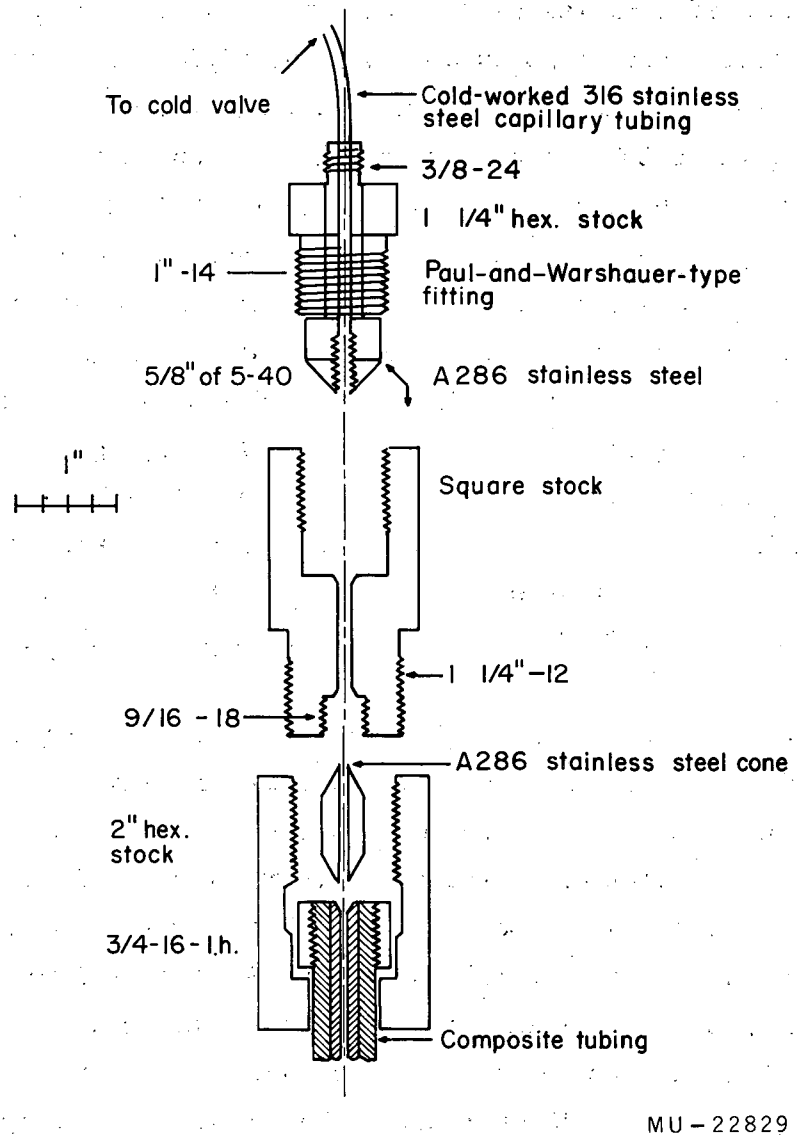

Fig. 20. Top of gas side of high-pressure U-tube.

the hydrogen was 11.9 cm^3. Allowing a 10% margin, one finds that the mercury will be about 82 cm below the top of the tube at 1 atm and 126 cm below the top at 1000 atm. By using the above considerations, the mercury level was adjusted to 78 cm below the top of the U-tube and checked on both sides to make sure that there was no air trapped in the mercury. The depth-indicator wire was attached in the same way as in the medium-pressure tube except that the length was 160 cm. Hence when the mercury was 10 cm below the top on the gas side, it left the end of the wire on the white gasoline side.

It was found that the Formvar insulation cracked after being in the white gasoline for a while and then shorted when the pressure was raised above about 1000 atm. The white gasoline seems to have dissolved the plasticizer and made the Formvar brittle. Teflon insulated wire made by American Super-Temperature Wires, Inc. is now being tried.

High-Pressure Cells

General

The general requirements for the metal used in the high-pressure cell were high mechanical strength, small heat capacity, reasonable heat conductivity, resistance to hydrogen embrittlement, lack of magnetization, and resistance to mercury attack. The only metals which seemed to be reasonable possibilities were stainless steels (cold-worked 316 or A286) and beryllium copper. The stainless steels did not match up to the beryllium copper in mechanical strength or in heat conductivity, although they were not vulnerable to mercury attack. Since it was possible to eliminate mercury from the cell by taking precautions in the connecting parts, it was decided to use the beryllium-copper alloy. This material has been used previously for high-pressure vessels.[41]

Berylco No. 25 rod was obtained from the Beryllium Corporation in the annealed condition. Its nominal composition was 1.8-2.05% beryllium, 0.18 to 0.30% cobalt, and the balance copper. The following properties were given in the supplier's literature. In the annealed (1450°F) condition, its tensile strength is 60,000 to 80,000 psi. After heat treating at 600°F for 3 hr, its tensile strength could be raised to about 180,000 psi. The hardening was caused by a precipitation process. The yield strength for 0.1% offset in the hardened condition was about 130,000 psi. The elastic modulus in tension at 20°C was 19,000,000 psi. The linear thermal expansion per °C in the range 20 to 100°C was 1.67×10^{-5}. Poisson's ratio was 0.3, and the density increase

on heat treatment was 0.6%.

Thermal Expansion

The thermal expansion of the material from the lowest temperature to room temperature was estimated by assuming the thermal expansion to be proportional to the heat capacity (Gruneisen's Law). Preliminary experiments indicated that the hardened beryllium copper had a heat capacity very similar to that of copper, for which $\Theta_D = 340^\circ K$. The proportionality between thermal expansion and heat capacity was found at room temperature, and the change of volume was determined from available tables of the integral of the Debye function.[42] A change in volume of 1.0% from 0 to 300°K was estimated. This value compares favorably with Swenson's estimate of 0.9 ± 0.3%.[43] The volume change below 77°K amounts to less than 0.1%.

Pressure and Volume Considerations

During the course of setting up the apparatus, three types of cell were made. The first design consisted of a hardened inner cylinder with an annealed cylinder shrunk over it. The second design had the same dimensions as the first except for a somewhat larger outside diameter, but was made from a single piece and hardened. It was made as insurance in case the first design proved unreliable. Trouble was experienced in keeping the Bridgman seals leaktight during the cool-down on the above designs, so a low-pressure cell with the ends screwed in and soft-soldered was constructed for the purpose of obtaining data while the technique of sealing the high-pressure cells was being perfected. Drawings of the cells are shown in Figs. 21 and 22.

Calculation of Pressure Effects

In the following considerations, the pressure dividing elastic from inelastic flow is first calculated, and then the burst pressure is estimated. The volume changes in the elastic and plastic regions are then estimated and the uncertainties are discussed. The low-pressure and solid cell are considered first for cross section and longitudinal stretch. The effect of the Bridgman-seal end plugs on the solid cell is then calculated. The properties of the composite cell are calculated last. The problem of seals on the high-pressure cells is then discussed.

Pressure Limit for Elastic Flow

Formulas for calculating the properties of pressure vessels have been

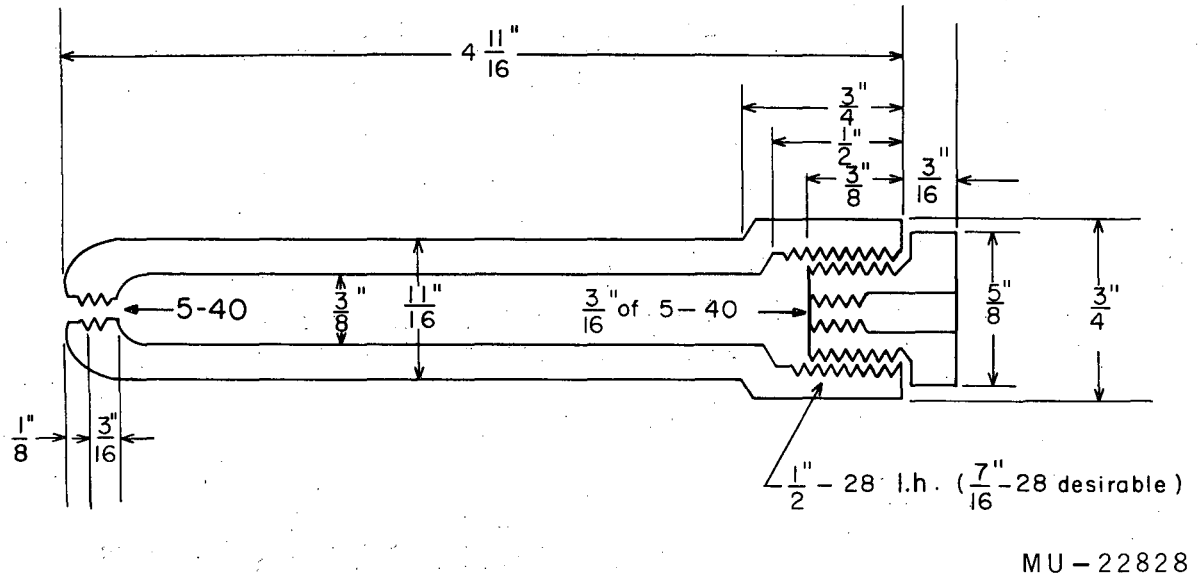

Fig. 21. Low-pressure cell.

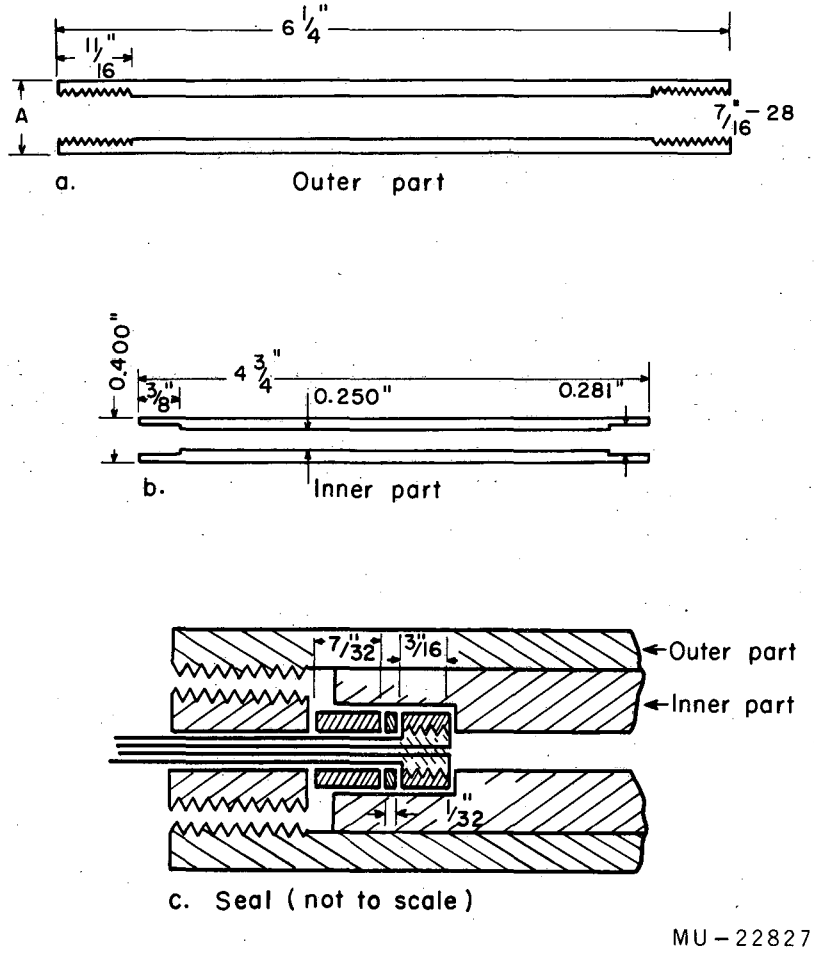

Fig. 22. High-pressure cells. (a) Outer part, with A = 11/16 in. for composite cell and 0.730 in. for solid cell; (b) Inner part of composite cell; (c) Seal (not to scale). Parts a and b on composite cell have 0.003-in. interference fit.

discussed by Comings.[44] The most useful relations for the present purposes have been collected in Appendix B. The largest stresses are the tangential ones at the inner radius. If a permanent volume increase of 0.2% is taken as the criterion of elastic behavior, there will be a permanent set of 0.1% in the radius. If σ_y is the stress that gives the permanent offset of 0.1% in the inner radius (or circumference), the Lamé formula gives for zero external pressure

$$P_y = \sigma_y \frac{K^2-1}{K^2+1} . \tag{4}$$

A more realistic formula is

$$P_y = \frac{\sigma_y}{\sqrt{3}} \frac{K^2-1}{K^2} . \tag{5}$$

If we have σ_y = 130,000 psi for 0.1% offset, we can calculate the pressures given in Table IV.

Table IV. Pressure limit for elastic flow

Cell	r_1	r_2	K	K^2	P_y [a]	P_y [b]
Low-pressure	0.375	0.688	1.83	3.36	70,400	52,700
Solid	0.250	0.730	2.92	8.53	102,800	66,200

[a] Eq. (4).
[b] Eq. (5).

Burst Pressure of Cell Walls

Using the criterion that the cell will burst when the plastic flow extends to the outer wall, it has been shown that we obtain

$$P_b = \frac{2\,\sigma_y}{\sqrt{3}} \ln K. \tag{6}$$

This formula ignores strain hardening. Two estimates are included--one for the yield strength (130,000 psi), and the other for the tensile strength (180,000 psi). The actual burst pressure probably lies between the two estimates. Estimates of the burst pressure are given in Table V.

Table V. Estimate of burst pressure

Cell	K	ln K	P_b (130,000)	P_b (180,000)
Low pressure	1.83	0.605	90,800	126,000
Solid	2.92	1.071	161,000	223,000

Volume Changes Below the Elastic Limit

The radial displacement is given by

$$\delta_1 = r_1 (\epsilon_t)_{r_1} \quad . \tag{7}$$

At r_1 with $P_2 = 0$, the tangential strain is

$$(\epsilon_t)_{r_1} = \frac{P_1}{E} \left[\frac{1 - 2\nu + (1 + \nu) K^2}{K^2 - 1} \right] . \tag{8}$$

Taking $E = 1.9 \times 10^7$ psi and $\nu = 0.3$, one obtains the percentage increase in cross section listed in Table VI.

Table VI. Percentage increase in cross section

Cell	P_y	K^2	$\frac{(\epsilon_t)_{r_1}}{P_1}$	$\frac{\delta A}{A} \simeq 2 (\epsilon_t)_{r_1}$ %
Low pressure	50000	3.36	1.06×10^{-7}	1.1
Solid	65000	8.53	0.81×10^{-7}	1.1

The changes at lower pressures should be linear in P. The longitudinal (see Table VII) strain for $P_2 = 0$ is given by

$$\epsilon_t = \frac{P_1}{E}\left(\frac{1 - 2\nu}{K^2 - 1}\right) . \tag{9}$$

Table VII. Longitudinal strain

Cell	P	ϵ_t/P_1	$\epsilon_t(\%)$
Low pressure	50000	8.95×10^{-9}	0.04
Solid	65000	2.80×10^{-9}	0.02

Hence the longitudinal strain below the elastic limit may be ignored.

Volume Changes Above the Elastic Limit

Assuming that the volume of an element remains constant as the inelastic strains are increased, and that the inelastic strains extend to the outer wall (burst pressure), Comings gives for the strain at r_1

$$(\epsilon_t)_{r_1} = (\epsilon_t)_{r_2} [K^2 (1- \nu/2) + \nu/2] , \tag{10}$$

where a realistic theory of yielding in cylinders gives

$$(\epsilon_t)_{r_2} \approx 0.866\, \epsilon_y = 0.866 \frac{S}{E} = 0.866 \frac{130,000}{1.9 \times 10^7} . \tag{11}$$

The results given in Table VIII do not include the effect of strain hardening.

Table VIII. Increase of cross section above elastic limit

Cell	$K^2 (1 - \nu/2) + \nu/2$	$\frac{\delta A}{A} \simeq 2 (\epsilon_t)_{r_1}$ (%)
Low pressure	3.01	3.58
Solid	7.40	8.80

The longitudinal strain at the burst pressure is still given by

$$\epsilon_z = \frac{P_1}{E} \left(\frac{1 - 2\nu}{K^2 - 1} \right) . \qquad (12)$$

Substitution of the appropriate values gives the results shown in Table IX.

Table IX. Longitudinal strain

Cell	P_b	ϵ_z/P_1	ϵ_z (%)
Low pressure	90,800	8.95×10^{-9}	0.08
Solid	161,000	2.80×10^{-9}	0.05

Uncertainties Above the Elastic Limit

The volume increases estimated above are probably too large because the effect of strain hardening has been neglected. An underestimate may be made by assuming that the elastic equations apply right up to the burst pressure. On this basis one would obtain the values shown in Table X.

Table X. Underestimate of volume increase above elastic limit

Cell	P_b	$(\epsilon_t)_{r_1}/P_1$	$2\,(\epsilon_t)_{r_1}$ (%)
Low pressure	90,800	1.06×10^{-7}	1.9
Solid	161,000	0.81×10^{-7}	2.6

The situation is illustrated in Fig. 23.

After stretching to a given pressure, the cell's behavior should be elastic below that pressure unless the release of pressure stresses the inner radius beyond the yield point in the reverse direction. Since the low-pressure cell should not be used over 50,000 psi, its volume should be readily known to better than 1%. Above 75,000 psi with the solid cell, however, it seems desirable to carry out test runs to determine the volume as a function of pressure and past history. The measurements could be made most easily by using two strain gauges to measure the tangential and longitudinal stresses at the outer radius, and by measuring the increase of the inner radius between pressurizations. The measurements could be made at room temperature. Swenson reports that Young's modulus increases by 10% at 77°K and stays constant at lower temperatures.[43]

Effect of the Bridgman Seals on the Cell Volume

The following effects must be considered:

(a) Longitudinal stretch of the cell walls between the step and the plug

(b) Compression of the beryllium-copper washers

(c) Bulk compression of the lead

(d) Redistribution effect of the lead due to the cell-wall stretch.

Judging from the longitudinal stretch of the whole cell at the burst pressure, (a) should be negligible. By using Young's Modulus (1.9×10^7), a total length of 7/16 in. and a cross section of 0.32 cm^3/cm, the compression of the washers is estimated to be 0.0028 cm^3 for a compressive stress of

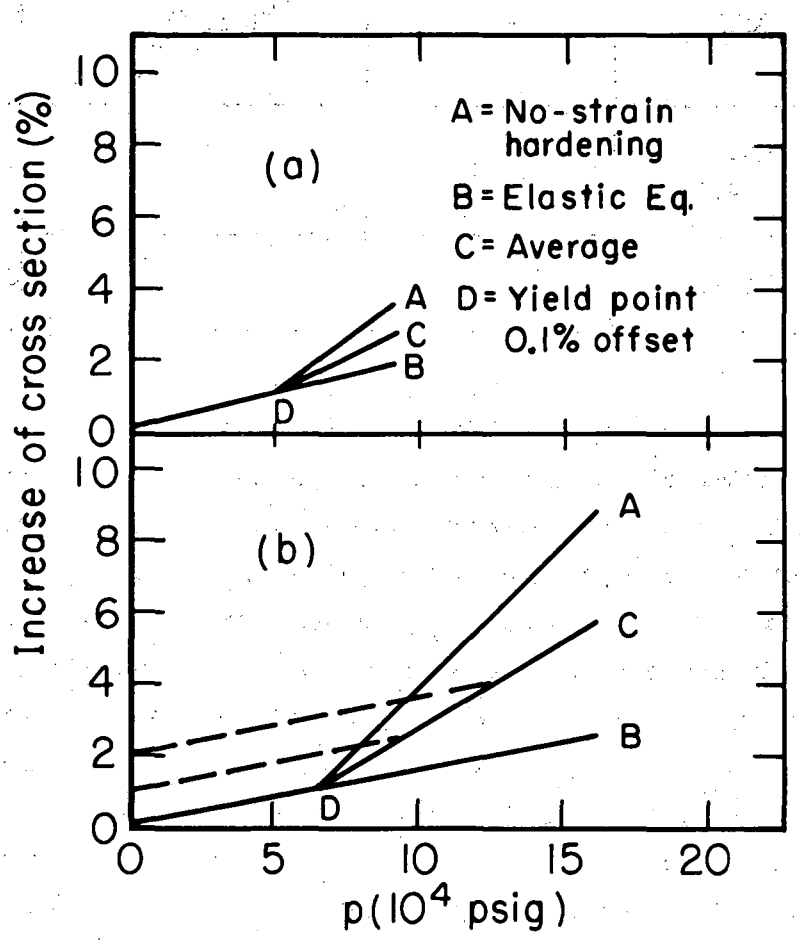

MU-23055

Fig. 23. Volume changes of (a) low-pressure cell, K = 1.83, and (b) solid cell, K = 2.92, with pressure. Dotted lines indicate increased range of elastic behavior when cell is stretched beyond point D.

150,000 psi. This value may be compared to a total cell volume of about 3 cm^3. The compression of the lead washers (0.051 cm^3 total volume) is estimated to be 0.0012 cm^3 if one uses the linear coefficient of the compressibility (23.7 x 10^{-7} per kg/cm^2). The thermal contraction of the lead washers relative to the beryllium copper is only 0.0006 cm^3 and can be neglected. If one assumes that the cross section of the bore increases 5%, then the length of the lead washers will decrease 5%, and the volume increase will be 0.0025 cm^3. The stretch of the bore around the front washer should also be about 0.1%. Hence the maximum correction for the end plugs at 10,000 atm should be about 0.5%.

Properties of the Composite Cell

The properties of the composite cell may be estimated by considering that the outer cylinder exerts a pressure on the inner one. Since the outer one is in the annealed state and is quite close to the yield point, it may be assumed that the pressure it exerts on the inner cylinder is constant with respect to stretch of the inner cylinder. The interference fit between the inner and outer cylinder was designed to be 0.003 in.

The tangential strain at the inner radius of the outer cylinder for $P_2 = 0$ is given by

$$(\epsilon_t)_0 E = P_1 \left[\frac{1 - 2\nu + (1 + \nu) K_0^2}{K_0^2 - 1} \right] . \qquad (13)$$

For $P_1 = 0$ the same quantity at the outer radius of the inner cylinder is

$$(\epsilon_t)_i E = P_2 \left[\frac{(\nu - 1) K^2 - (1 + \nu)}{K_i^2 - 1} \right] . \qquad (14)$$

The difference between the two strains should equal $0.003/0.400 = 7.5 \times 10^{-3}$. Also, P_1 equals P_2 at the interface. Subtraction gives

$$(7.5 \times 10^{-3})(1.9 \times 10^7) = P \left[\frac{0.4 + 1.3 K_0^2}{K_0^2 - 1} + \frac{0.7 K_i^2 + 1.3}{K_i^2 - 1} \right] .$$

Substituting $K_i^2 = 2.56$ and $K_0^2 = 2.96$, one obtains 34,600 psi as the pressure on the outside of the inner cylinder. The tangential stress on the inner radius of the outer cylinder corresponding to the above pressure is given by

$$(\sigma_t)_{r_1} = P_1 \left[\frac{K_0^2 + 1}{K_0^2 - 1}\right] = 2.02\ P_1 \tag{15}$$

$$= 70{,}000 \text{ psi.}$$

Since the yield strength of the annealed material is 60,000 to 80,000 psi, the inner surface of the outer cylinder should be at the yield point.

The tangential stress on the inner surface of the inner cylinder at the limit of elastic behavior is given by

$$\sigma_t = \frac{P_1 + K_i^2 (P_1 - 2P_2)}{K_i^2 - 1} \quad . \tag{16}$$

Solving for P_1 and substituting σ_y = 130,000 psi, we obtain

$$P_1 = \frac{\sigma_t (K_i^2 - 1) + 2\ P_2\ K_i^2}{K_i^2 + 1} \tag{17}$$

$$= 107{,}000 \text{ psi.}$$

A maximum burst pressure may be calculated by assuming a maximum stress in the walls of the inner cylinder equal to the ultimate strength (180,000 psi). This gives

$$P_1 r_1 - P_2 r_2 = \sigma_t (r_2 - r_1) \tag{18a}$$

$$P_1 = \sigma_t (K_i - 1) + P_2 K_i$$

$$= 166{,}000 \text{ psi.} \tag{18b}$$

High-Pressure Seals on the Cell

For the highest pressures, one must use a seal of the unsupported-area Paul and Warshauer type. The unsupported area-type is preferable, because it is not necessary to deform part of the cell to get a seal. However, the use

of the unsupported-area principle involves a soft packing which is likely to have a larger thermal-expansion coefficient than the cell material, so that maintaining a tight seal down to the lowest temperatures becomes a problem. Extrusion of the packing past its supporting parts can also be troublesome.

In the first cell design, a 1/8-in.-thick lead washer was used as the soft packing. The unsupported area was 0.079 cm^2 and the total area 0.34 cm^2, giving a packing pressure 30% greater than the pressure in the cell. The front beryllium-copper washer was 3/16-in. thick and the backing washer was 1/8-in. thick. The machining tolerances were poorer than 0.001 in. and it was found that the lead extruded past the backing washer above 50,000 psi. When the cell was cooled to liquid-nitrogen temperature below 20,000 psi, it leaked badly.

In the second attempt, the sealing surface was reamed out to 0.281 in. to get a larger step. The lead washers were made 1/32-in. thick and a 3/64-in. copper washer was placed on each side of the lead. The copper was dead soft, and it was hoped that this would prevent the extrusion of the lead. By using a thinner lead washer, it was hoped that enough initial compression could be obtained in the lead and copper washers to compensate for the thermal contraction of the lead. A simple calculation indicated that this was a reasonable expectation. After one compression to 50,000 psi and one cooling cycle, however, it was not possible to raise the pressure above 32,000 psi because of a large leak at that pressure. It appeared that the front copper washer spread and work-hardened, and effectively supported the front beryllium copper washer, keeping the lead from sealing the gas.

In view of this experience, it was decided to abandon the idea of the copper washers and try to get a close tolerance fit of the beryllium-copper washers in the bore. This was done in a lathe, and a tolerance of about 0.0005-in. was achieved. The threaded front washer was still 3/16 in., but the back one was made 7/16 in., the lead washer still being 1/32 in. When assembling these parts it was noticed that the 5-40 threads on the stainless capillary did not seem to be quite parallel to the axis of the tubing. This had the effect of putting the two washers at an angle to each other. This arrangement was found to leak between 30,000 and 40,000 psi, but not above or below. The explanation seemed to be that the front washer was supported by the bore and could not effectively compress the lead below 40,000 psi. The composite cell was used in this test. The pressure was raised to 94,000 psi, when failure of the capillary tubing at a bend halted the test. Evidence for

extrusion of the lead was still found, although it was not as bad as previously. The problem of the 5-40 threads can be solved by using a guided die-holder, or by cutting the threads on a lathe. (The latter operation is not convenient with a long piece of tubing.)

It was suggested[45] that the seal could be made good to low temperatures by backing the lead washer with an annealed gold washer. On cooling, the gold should maintain the initial seal, and the lead would take over at higher pressures. It is hoped that this approach will make the next test successful. If it is not possible to maintain a leaktight seal during the cooling with a low pressure in the cell, a workable but somewhat inconvenient method would be to cool the cell under a high pressure of helium, and then put in the sample under pressure before cooling further.

IV. SAMPLE PREPARATION AND ANALYSIS

Para Hydrogen Converters

Two catalyst chambers were constructed: one for use with liquid oxygen or nitrogen, and one for use with liquid hydrogen. Drawings are shown in Figs. 24 and 25, respectively. The liquid-nitrogen chamber was placed in a quart dewar which could be connected to the house vacuum, giving a readily available temperature range of about 60 to 90°K (35 to 57% ortho hydrogen). The liquid-hydrogen chamber was usually used at the noraml boiling point (20.4°K) at which the concentration of ortho hydrogen was 0.2%.

The catalyst used was unsupported ferric hydroxide gel, which has been found to convert the hydrogen to its equilibrium composition very rapidly.[46,47,48] It was prepared by adding NaOH solution to $FeCl_3$ solution and collecting and washing the precipitate to remove NaCl. After drying for 24 hr at 85°C and for 24 hr at 105°C, the lumps were broken up with a mortar and pestle and particles between No. 30 and No. 50 mesh were collected. About 50 g of catalyst were put in the liquid-nitrogen cell and evacuated at room temperature. After a day and a half, the pressure over the catalyst had reached 40 μ. It was then heated to 110°C. After about 12 hr, the pressure was back to 40 μ and the temperature was raised to 180°C. After 3 hr, the pressure was down to 50 μ, and the vacuum was broken with hydrogen gas and the catalyst was allowed to

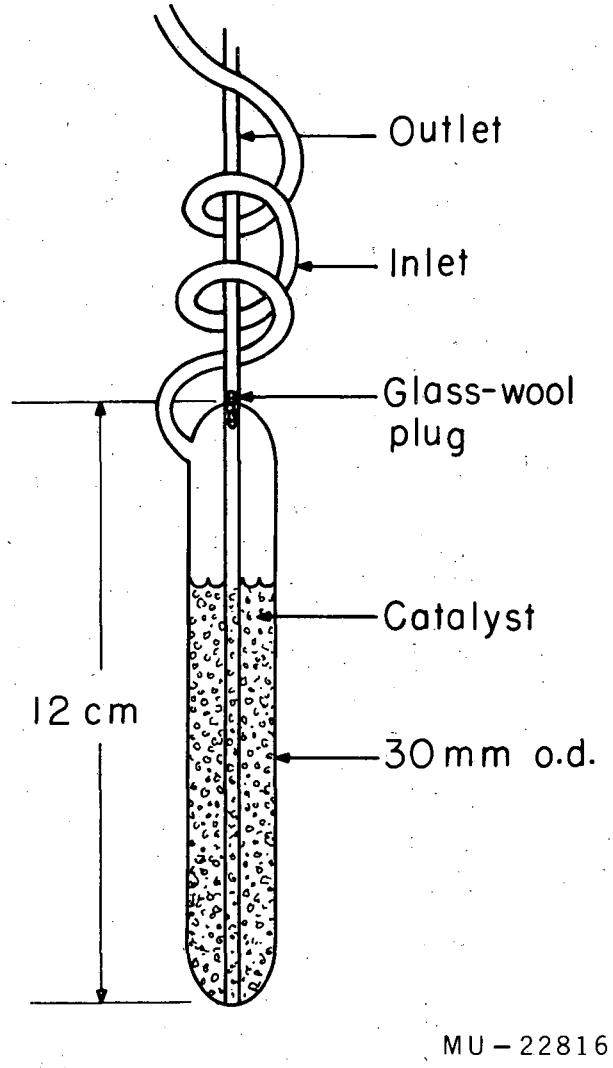

Fig. 24. Parahydrogen converter, liquid-nitrogen chamber.

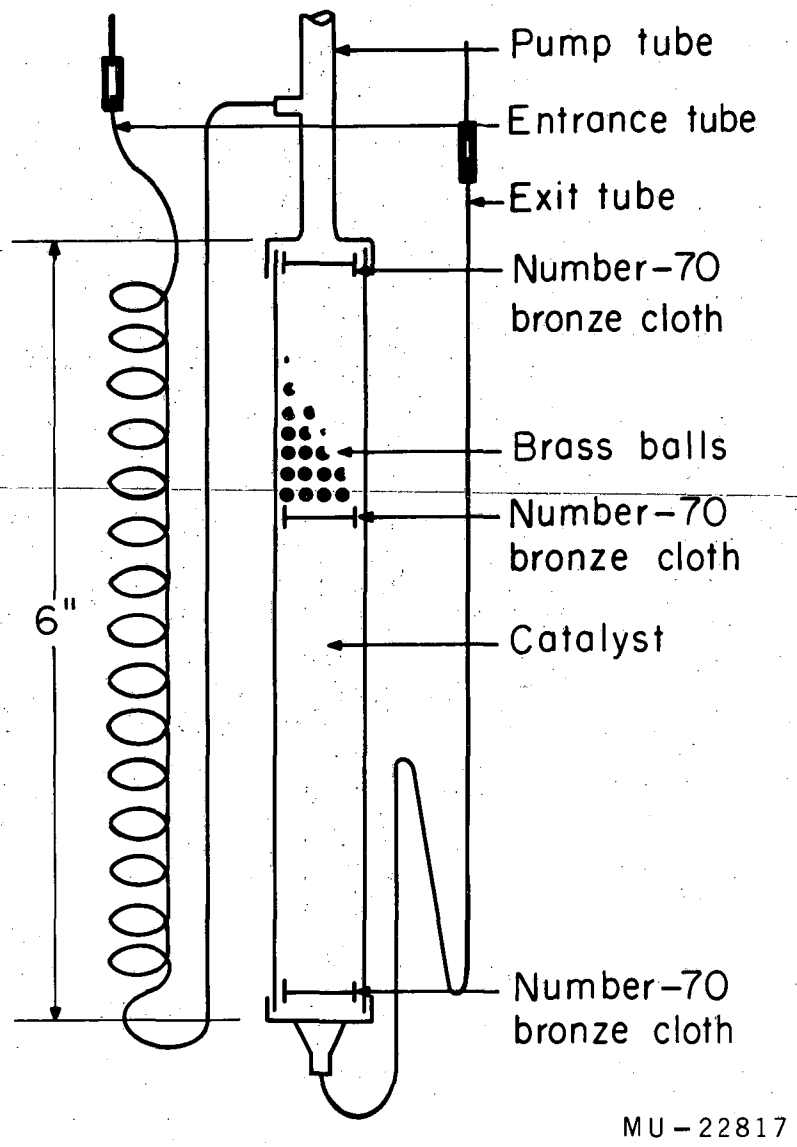

Fig. 25. Parahydrogen converter, liquid-hydrogen chamber.

cool. In the liquid-hydrogen converter, the temperature in the last step was limited to 150°C because the cell was soft-soldered together. Flow rates were controlled with a metering valve and monitored with a flow gauge. The rate was kept below 200 cm^3/min (STP). After a run was finished, the liquid-hydrogen cell was vented through a mercury bubbler attached to the pump-out tube while being warmed up.

Ortho-Hydrogen Separators

Three units of the type described by Cunningham, Chapin, and Johnston were constructed.[49] The separation was based on the preferential adsorption of ortho hydrogen (or para deuterium) on alumina at 20.4°K. The method consisted of passing normal hydrogen over the catalyst until equilibrium between the gas and adsorbed phases was reached. The gas space was then evacuated for a brief period and the catalyst was heated, the desorbed ortho hydrogen being collected after passing through the three stages. The valve panel used to connect the catalyst chambers to the gas source, mercury bubblers, sample bulb, and vacuum manifold is shown in Fig. 26. Hoke packless brass valves were used in the manifold. A view of the rear of the preparation rack is shown on Fig. 27.

One of the inserts was assembled and tested. The mechanical operation was satisfactory, although the alumina catalyst had not been properly activated[50] so that the separation of ortho hydrogen was not observed.

Hydrogen Purifier

Before being used, all of the hydrogen was passed through a quartz tube stuffed with copper turnings at 600°C and then through a liquid-nitrogen trap stuffed with glass wool.

Ortho-Para Analyzer

The thermal-conductivity method was used to analyze the gas mixtures. Adequate discussions of the theoretical aspects are available,[51,52] and a number of analyzers similar to the one used are described in the literature.[53,54] A drawing of the analyzer and the circuit used to measure the resistance of the platinum wire is given in Figs. 28 and 29. The cell was immersed in liquid nitrogen, and the wire temperature was raised to about 160°K by a current of

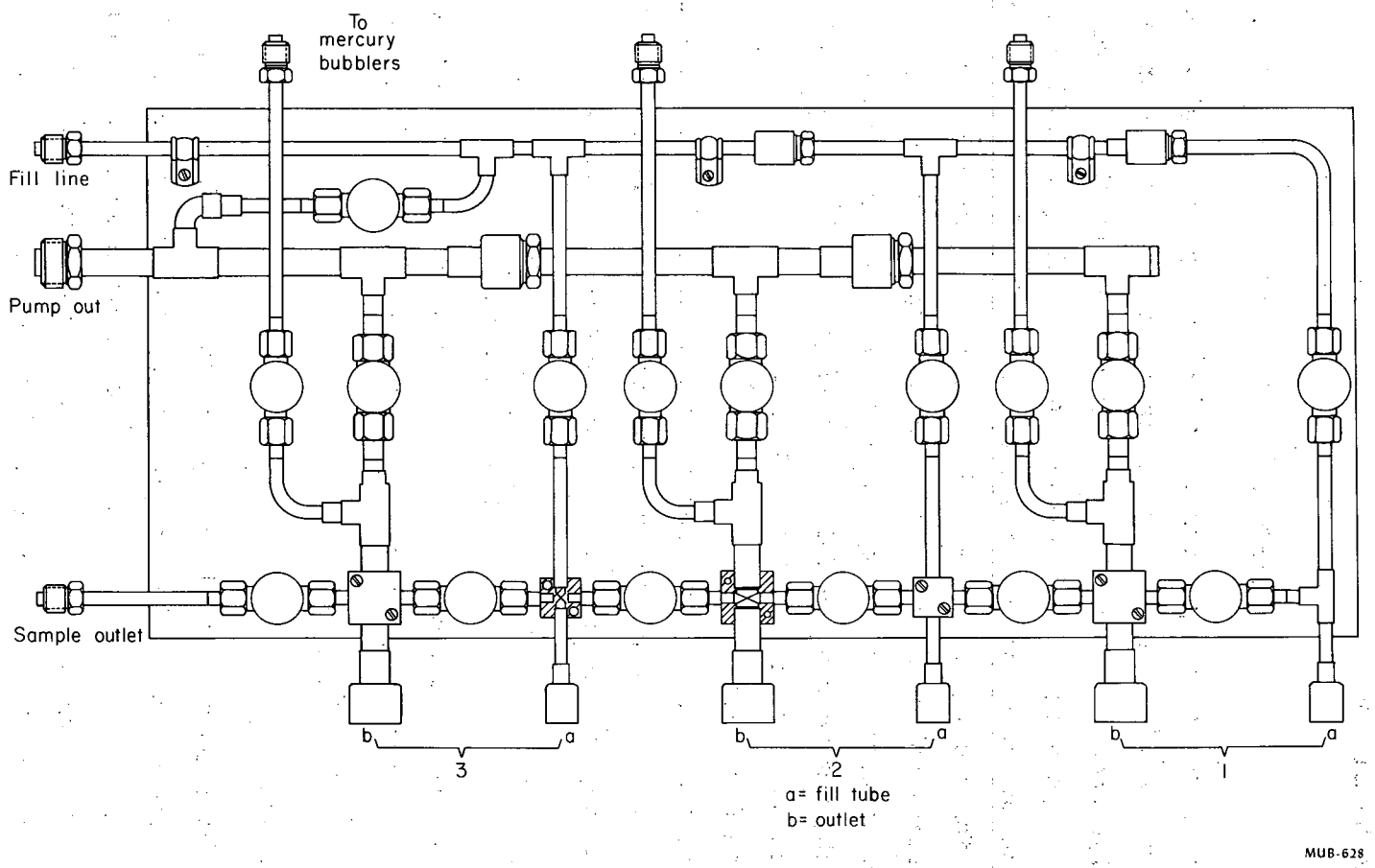

Fig. 26. Orthohydrogen separator manifold.

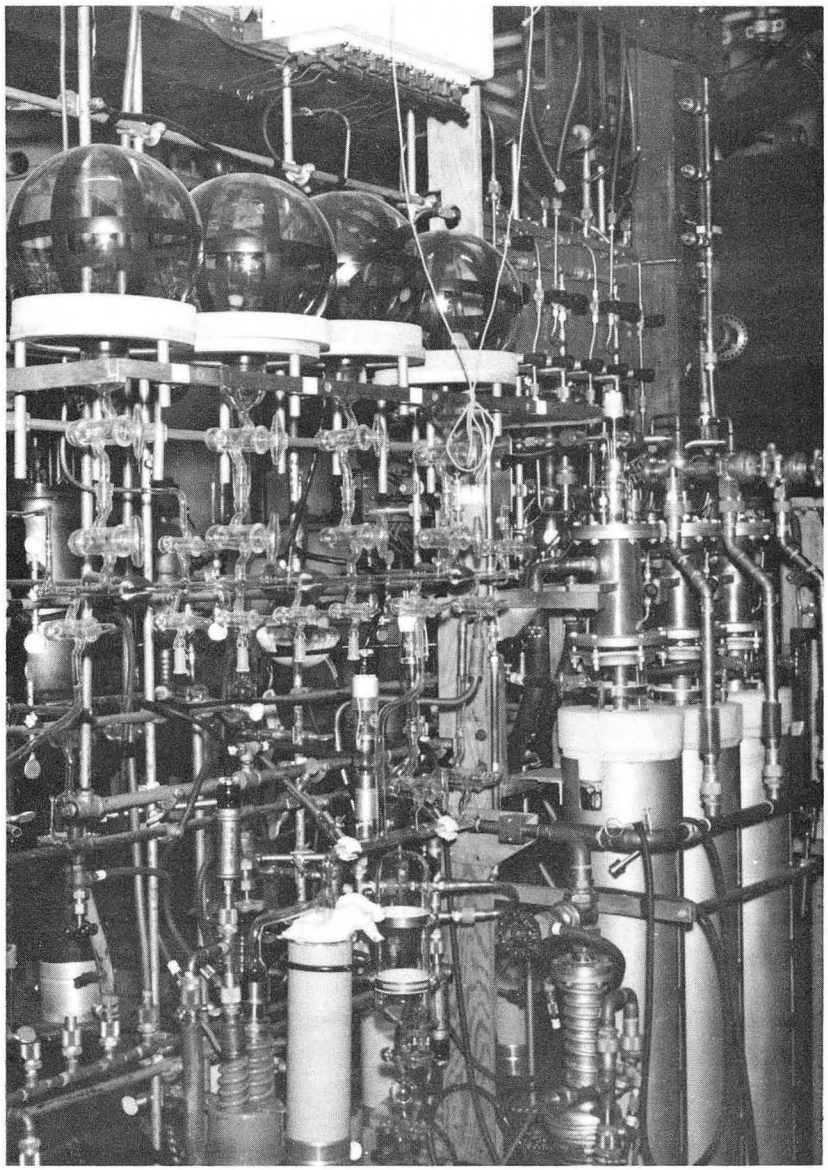

ZN-2733

Fig. 27. Rear view of preparation rack.

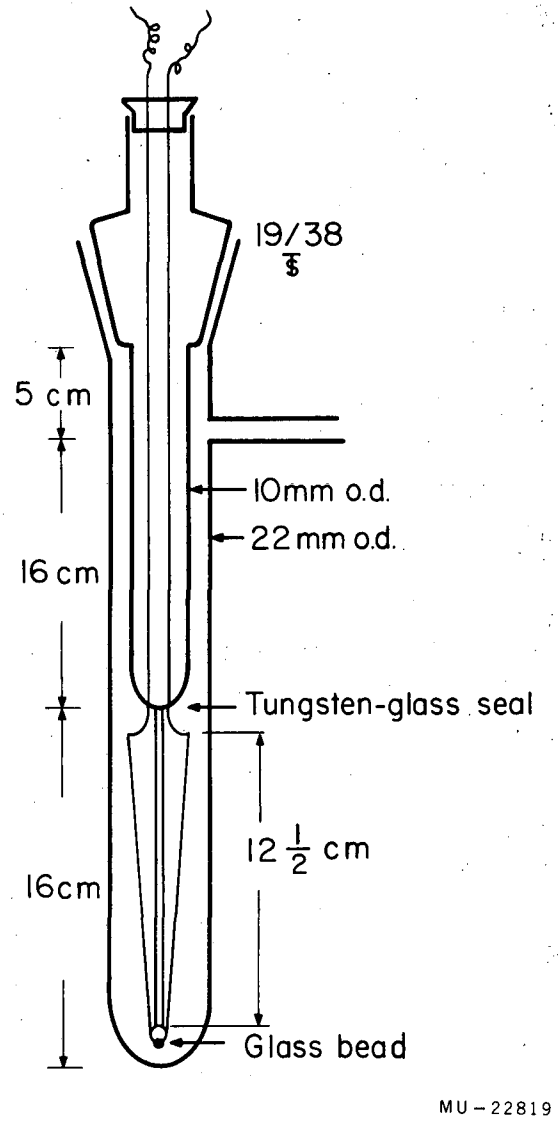

Fig. 28. Ortho-para analyzer cell.

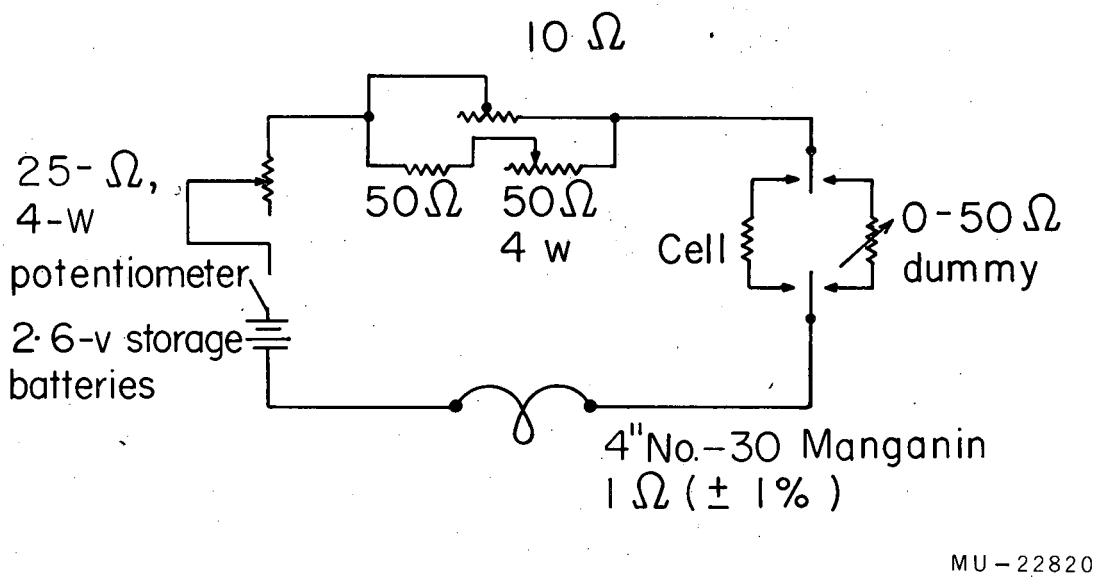

Fig. 29. Ortho-para analyzer circuit.

0.255 amp. Since the thermal conductivity is proportional to the heat capacity, the measurements were sensitive in the above temperature region, where the difference in heat capacity of ortho and para hydrogen is large.

The 1-mil platinum wire was 26 cm long, and a glass bead was suspended from the bottom of the wire to keep it taut. The pressure was adjusted to 40 ± 0.1 mm before each reading. After the current was adjusted so that the voltage across the manganin wire was 0.2550 v, the voltage across the platinum wire was read. When data (% ortho versus microvolts) from 0 to 75% ortho hydrogen were plotted, there was a slight curvature. Data taken on different days were shifted, although the shape of the calibration appeared to be the same; hence it was necessary to calibrate the cell each time it was used. The precision of the measurements was 0.5% in the ortho concentration or slightly better. The sensitivity of the measurements and the linearity of the plot might be improved by raising the wire temperature to about 200°K.

V. THERMAL MEASUREMENTS

Thermometer Calibration

The carbon composition resistors and the copper-iron—versus—copper thermocouple were calibrated against the vapor pressure of liquid para hydrogen in the region 20 to 14°K. Solid para hydrogen was used from 14 to about 9.5°K. The vapor-pressure—temperature relations were obtained from the literature.[55] Liquid helium was used below 4.2°K, with the 1955 vapor-pressure—temperature scale.[56] In the region between 9.5 and 4.2°K, the only absolute method of calibration involves the use of gas thermometry. Since this technique is difficult and time-consuming, it was not attempted in the present experiments. Various schemes for interpolating the data from the two calibrated regions are discussed in more detail below.

Temperature Regulation

Since the precision of the calibration data could be no better than the quality of temperature regulation, the technique used deserves some discussion. The rate of pumping on the inner bath was regulated by a metering valve in the pump line. The heater-regulator was mounted on the copper bottom plate of the bath, and its steady heating power was adjusted so that it just balanced the

heat loss from the vaporizing liquid. A steady level of about 10 mw was fairly common for the bath. With liquid and solid hydrogen and helium I, there was an appreciable temperature gradient in the bath because of the poor heat conductivity of the material. However, the thermometer and vapor-pressure bulbs were all in thermal contact with the copper bottom plate of the bath, and hence at the same temperature. The most serious difficulty in connection with the poor thermal conductivity of the bath involved the establishment of the steady state. Although it would have been possible to set the heater-regulator for a desired temperature, hours would have been required to reach a steady state. By heating the bath to approximately the right temperature, manually holding the temperature constant until a steady state was set up, and then letting the regulator function, it was possible to take between one and two readings per hour, depending on the temperature. Below 12° with solid hydrogen, a great deal of patience was required to reduce the oscillations of the temperature of the bottom of the bath sufficiently to take a set of readings. Above 12°, the establishment of the steady state was considerably more rapid, and in the liquid-hydrogen region, it was possible to set up the steady-state temperature in about ten min and complete a set of readings in about 1/2 hr. A heating power of about 1 w was used to raise the bath temperature from one setting to the next. Liquid helium I appears to behave like liquid hydrogen, although not much experience has been obtained in this region as yet. No points have been taken in the helium-II range so far, but the establishment of the steady state should be much easier than in any of the other regions because of its excellent thermal conductivity.

Procedure for Taking Readings

About 10 min after establishing the steady state, readings were taken of the vapor pressure, thermometer current and resistance, and thermocouple potential. The thermometer current was read on the K-3 potentiometer and the potential on the recorder. The zero and sensitivity were checked for each point in the same way as with a galvanometer. Thermometer current and input to the Rubicon potentiometer were also reversed at each reading to determine the thermals up to the potentiometer. These were less than 1 μv, and depended mainly on the cell temperature. It is reasonable to assume that the origin of the potential was in the vicinity of the copper-manganin junction at the shield.

Since the thermometer resistance and sensitivity varied so rapidly with temperature, it was necessary to change the current frequently in order to maintain the power dissipated and voltage sensitivity within acceptable limits. Table XI illustrates the temperature intervals in which the various currents were used and also gives approximate values of the resistance and sensitivity in each interval.

Table XI. Current settings at various temperatures

°K	Current (μa)	Approx. resistance	Approx. m(°K/μv)
10 ohm			
1 - 2	0.8	3000 - 300	0.15 - 5
2 - 3	2.0	300 - 140	2 - 9
3 - 4	5.0	140 - 85	3.5 -10
56 ohm			
1 - 2	0.07	50000 -5000	0.1 - 2
2 - 3	0.2	5000 -1800	0.7 - 5
3 - 4.5	1.0	1800 - 800	1 - 5
4.5 - 6	3.0	800 - 500	2 - 5
6 - 11	10	500 - 270	1.5 - 7
11 - 14	15	270 - 220	5 - 8
14 - 18	20	220 - 180	6 -11
>18	30	>180	>8

The sensitivities are of interest in connection with the size of the temperature increments, which are discussed in connection with drifts and precision in a later section.

Treatment of the Calibration Data

To the present, only two test calibration runs have been made. The first covered the liquid- and solid-hydrogen regions and included two points in the helium-I region. The thermocouple and 10-ohm resistor were calibrated against

the vapor pressure. In the second run, the 56-ohm resistor and thermocouple were calibrated in the liquid and solid hydrogen regions. Both runs were prematurely ended by unexpected difficulties so that neither set was a complete calibration.

A rough R - T table was calculated for the carbon thermometers from the raw data, and $(\log R/T)^{1/2}$ was plotted against $\log_{10}R$ to detect errors and bad points. This type of plot is almost a straight line.[57,58] The equations for the straight lines that fit the data are, for the 10-ohm resistor,

$$\sqrt{\frac{\log_{10}R}{T}} = 0.738 \log_{10}R - 0.735 , \qquad (19)$$

and for the 56-ohm resistor,

$$\sqrt{\frac{\log_{10}R}{T}} = 0.547 \log_{10}R - 1.104 . \qquad (20)$$

The data were fitted to the following equation with a least-squares procedure by the IBM 650 computer at the Lawrence Radiation Laboratory:

$$\frac{\log_{10}R}{T} = C_1 + C_2 \log_{10}R + C_3 (\log_{10}R)^2 + C_3 (\log_{10}R)^3 . \qquad (21)$$

The computer made 2-, 3-, and 4-parameter fits and printed out the coefficients for each. The residuals were printed out in the following form:

$$\text{Res.} = \frac{\log_{10}R}{T} - \frac{\log_{10}R}{T_{\text{calc.}}} . \qquad (22)$$

If one defines

$$\beta = \frac{T_c - T}{T_c} = \frac{(\text{Res})}{(\log R/T)} , \qquad (23)$$

then one has $T = T_c(1 - \beta)$. The quantity $(\log R/T)$ is printed out by the computer, so that β is readily obtained from the residuals. A plot of β

versus T for the four-parameter fit of the data for the second test run (56-ohm resistor) is shown in Fig. 30, which in included only to illustrate the precision or smoothness of the data. The uncertainties were estimated from the precision of reading the vapor pressure, the quality of the temperature regulation, and the precision of determining the thermometer resistance, and are shown in Fig. 31. At the lower temperatures, the greatest uncertainties are in the reading of the vapor pressure. For example, at $10^{\circ}K$ with the oil manometer, a precision of $\pm$ 0.1 mm corresponds to $\pm$ $0.005^{\circ}K$. The difficulty of regulating the bath temperature below $12^{\circ}K$ is also an important source of error.

The thermocouple data taken in the first run covered the region from 20 to $12^{\circ}K$, with points at 3.19 and $2.73^{\circ}K$. The data from the second run covered the region from 20 to about $9.2^{\circ}K$. Above $13^{\circ}K$ the data were very linear. The data from the first run were fitted to the two-parameter equation

$$T = 80.718 - 0.13544\ V \qquad (24)$$

by the least-squares routine of the IBM 650. The two liquid-helium points were not included in this fit. The reciprocal of the second coefficient indicates a sensitivity of 7.34 $\mu v/^{\circ}K$ in the liquid-hydrogen region. A difference plot of the actual temperature, T, minus the calculated temperature, T^{*}, is shown in Fig. 32. The data from the second run are also shown on Fig. 33. It can be seen that above $13^{\circ}K$ there is a difference of about $0.1^{\circ}K$, or 0.73 μv. During the first run, the thermocouple was glued directly to the cell, but was moved to the rear vapor-pressure bulb for the second run. Whether the difference between the two sets of data resulted from the operation of moving the thermocouple or from different thermal voltages in other parts of the circuit during the two runs is not clear from the limited data available. The possibility of an $0.1^{\circ}K$ temperature difference between the cell and vapor-pressure bulb has not been ruled out, although such an effect does not seem likely since one would expect such a difference to be opposite in sign. Further comments on this subject must await the availability of more data.

Since one hopes to use the thermocouple data to aid in determining the temperatures between 10 and $4.2^{\circ}K$, one must fit the data to an equation so that a sensitive difference plot can be made. It is clear that a simple power series in V will not be appropriate over the whole temperature range

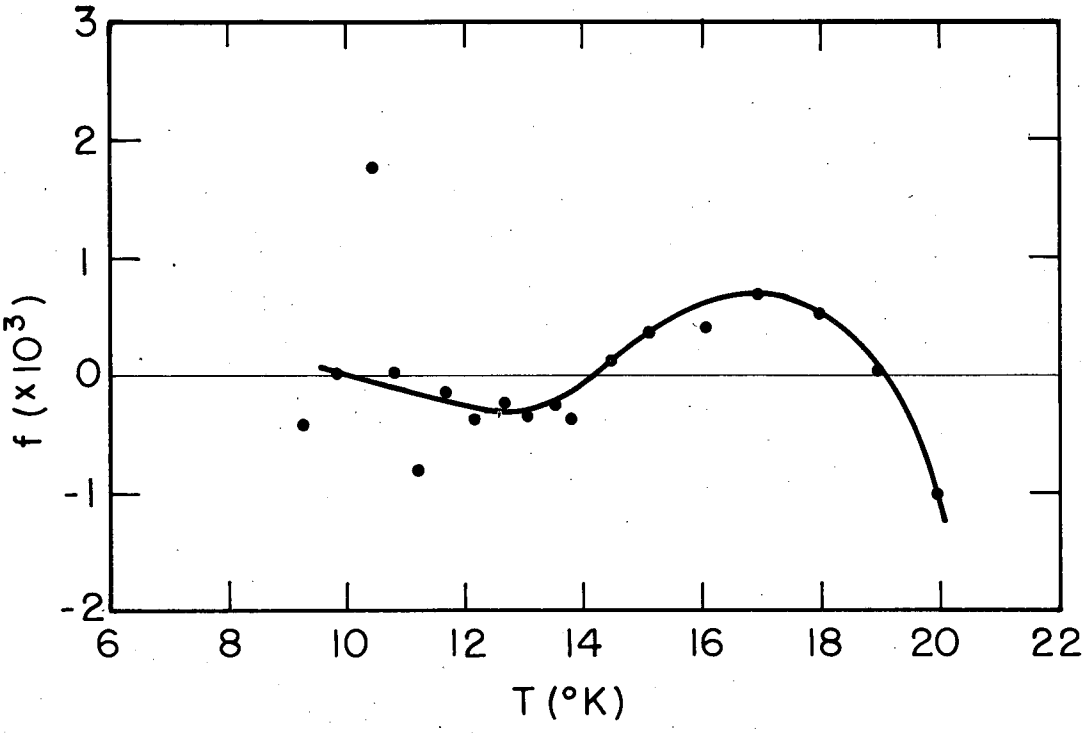

MU-23056

Fig. 30. Fractional deviation from four-parameter fit.

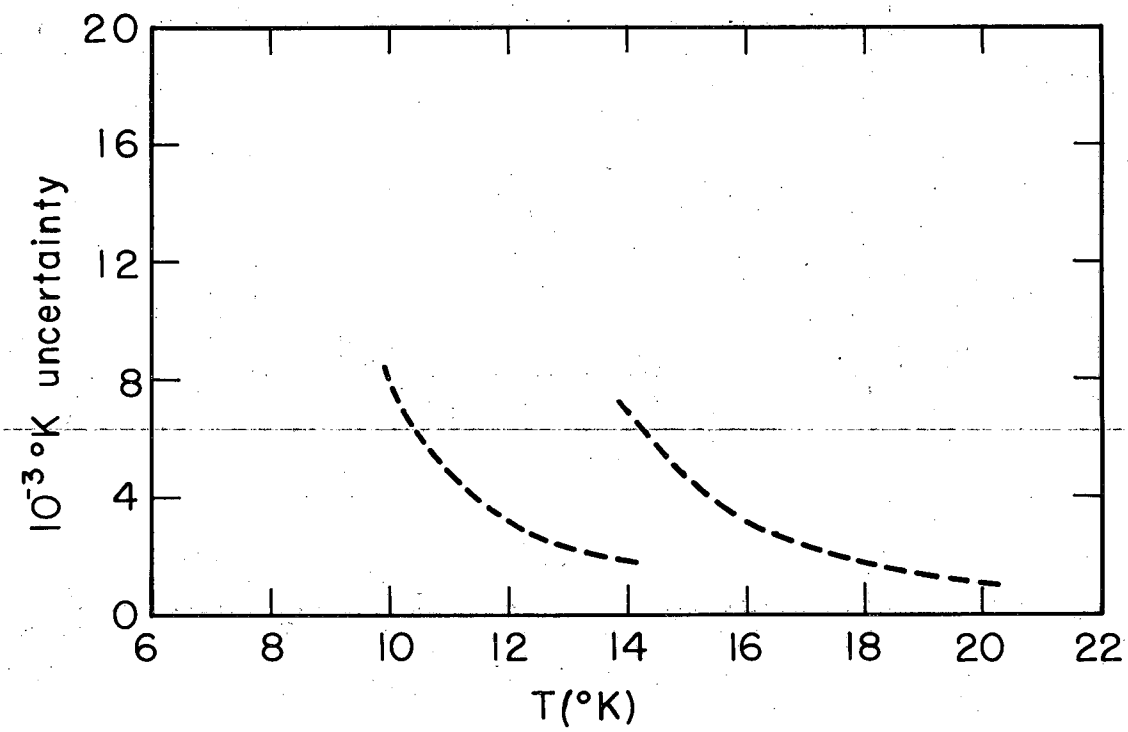

MU-23057

Fig. 31. Estimated uncertainties in data.

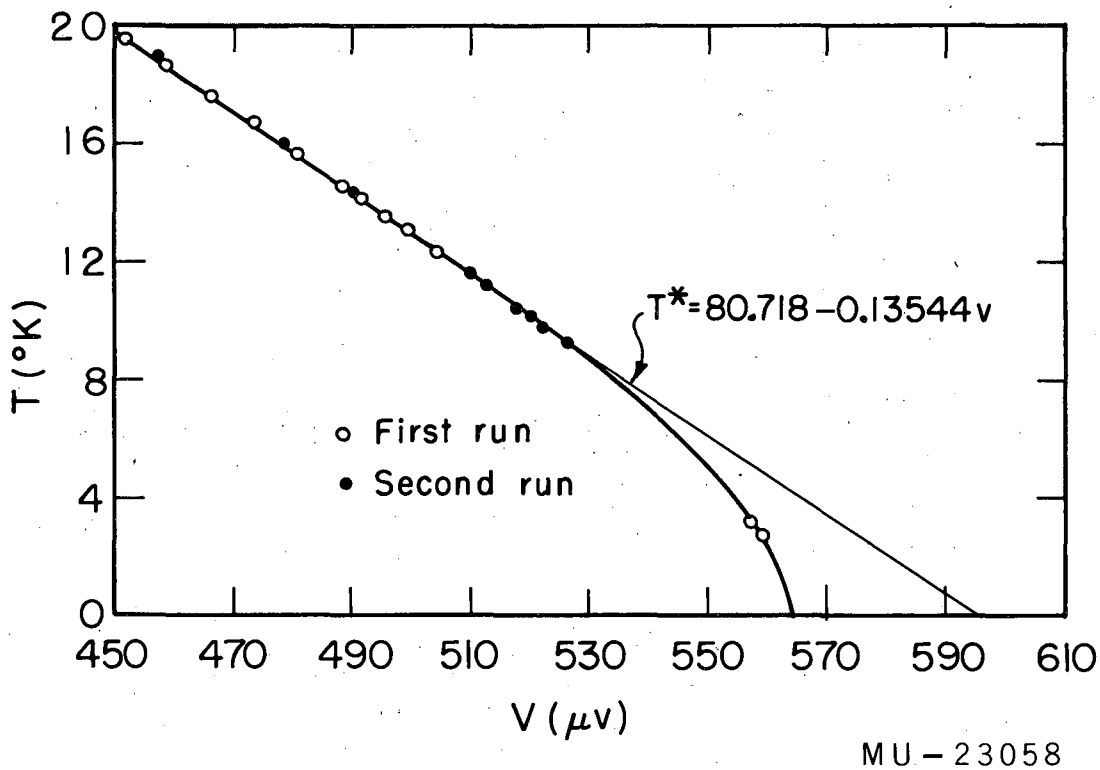

Fig. 32. Copper-iron-versus-copper thermocouple data.

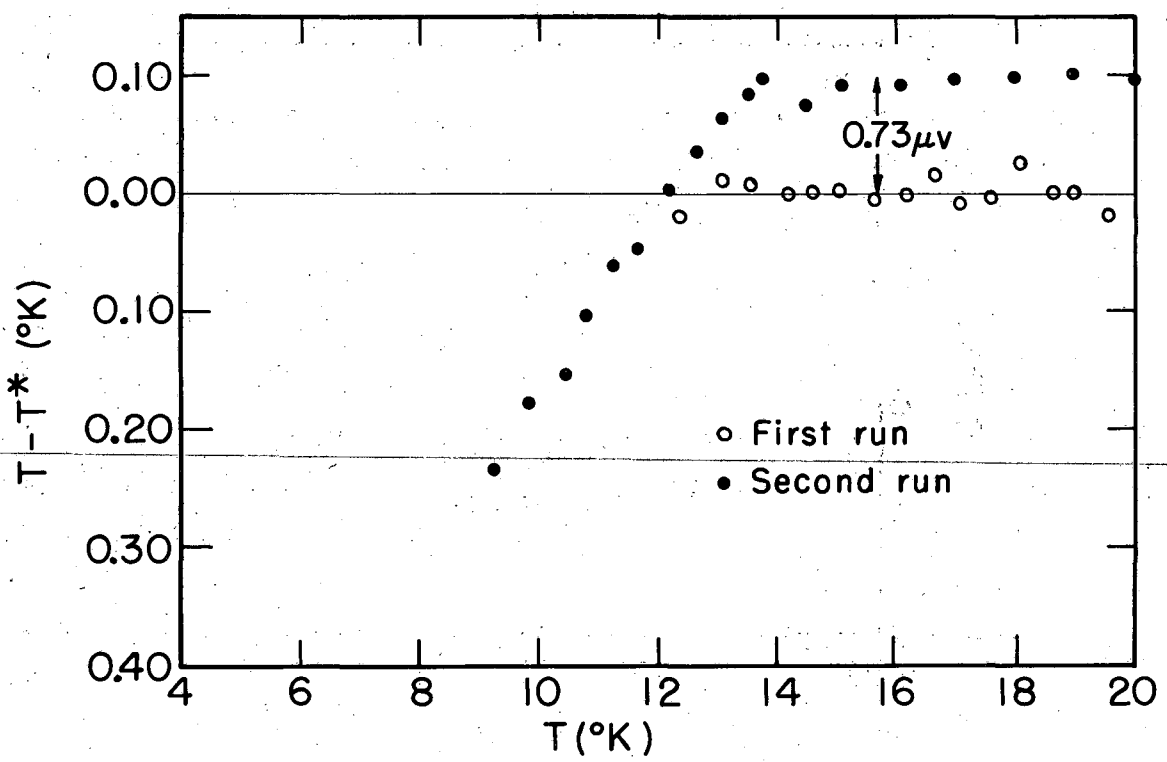

MU-23059

Fig. 33. Difference plot of copper-iron-versus-copper thermocouple data.

because of the linearity above 13°K. One way of getting around this might be to fit the data above 13°K to a straight line, and then fit the difference plot below 13°K to a power series in a quantity such as (T - 14).

The available data are not sufficient to test various methods of interpolation for the carbon thermometers into the 4.2 to 9.5°K region. Difference plots will have to be made for equations fitted over both the hydrogen and helium regions, and for equations fitted over only one region, and then compared. An interesting discussion of this problem is given in the literature.[57]

Estimate of Thermal Properties of the Isothermal Shield and Cell

The thermal conductivities of the materials were estimated from the graphical data given in the literature.[59] The data are probably within 50% of the actual values when applied to the present calculation. Table XII refers to the Debye temperature and γ to the coefficient of the linear electronic heat-capacity term. The heat capacity data were obtained from several sources.[60,61] The heat capacity of beryllium copper was assumed to be the same as that of copper, as suggested by preliminary experiments.

Table XII. Thermal Properties of materials

Material	$\mathcal{K}$ watts/cm °K (4 to 20°K)	Θ_D (°K)	$\gamma \times 10^4$ cal/mole(°K)^2
Copper	$2.1\ T^{0.75}$	340	1.7
Stainless steel	$0.42 \times 10^{-3}\ T^{1.29}$	390	8 (assumed)
Manganin	$1.4 \times 10^{-3}\ T^{1.43}$	---	---
Lead	---	96.3	8

Below the superconducting transition of lead at 7.22°K, the electronic heat capacity is $0.329 \times 10^{-4} T^3 (1 = 0.012T^2)$ cal/mole°K. The heat capacities of the soft solder on the leads and threads and of the electrical leads and GE cement were neglected.

Cell Heat Capacity

The cell body (first design) weighed 261 gm and the end screws weighed 22.1 gm. Both were of beryllium copper. The four beryllium copper and four copper washers weighed about 5.6 gm. The two lead washers weighed about 0.5 gm. The length of the 1/8-in. o.d. by 0.024-in. i.d. stainless steel capillaries between the cell and the shield was 16 in. ($\pm$ 1/2 in.), with 1-1/8 in. in each end plug. The cross section of the capillary hole was measured to be 0.00298 cm^2, while the over-all cross section was 0.0792 cm^2. Assuming a density of 7.8, one obtains 0.595 gm/cm. The lattice heat capacities were estimated by using the following equation:

$$C_L = (3R)(77.927)(T/\Theta)^3 . \qquad (25)$$

The lattice and electronic heat capacities of the various parts of the cell are listed in Table XIII. The superconducting lead electronic heat capacity at the transition temperature is less than 0.1% of the total cell heat capacity, and is neglected in this estimate.

Table XIII. Contributions to the cell heat capacity

Material	Weight	MW	$C_L \times 10^4 T^3$ (joules/°K)	$C_E \times 10^3 T$ (joules/°K)
Beryllium copper	289	63.5	2.25	3.24
2-1/4-in. capillary	3.4	55	0.02	0.21
10.0-in. capillary[a]	15.1	55	0.09	0.92
Lead	0.5	207	0.05	0.01

[a] The fraction of capillary to be included with the cell is discussed in the next section.

Summation then gives the following expression:

$$C_{total} = C_L + C_E = 2.41 \times 10^{-4}\ T^3 + 4.38 \times 10^{-3} T. \qquad (26)$$

Shield Heat Capacity

The volume of copper on the shield may be roughly estimated as 120 cm^3. The volume of lead is roughly 24.4 cm^3. Using 8.92 and 11.34 for the densities, one obtains

$$C = 8.34 \times 10^{-4}\ T^3 + 1.2 \times 10^{-2}\ T \text{ joules}/^{o}K \qquad (27a)$$

for copper and

$$C = 29.2 \times 10^{-4}\ T^3 + 1.8 \times 10^{-4}\ T^3(1 + .012T^2)\ 4.184 \qquad (27b)$$

for lead with $T < 7.2$, and

$$C = 29.2 \times 10^{-4}\ T^3 + 0.4 \times 10^{-2}\ T \qquad (27c)$$

for $T > 7.2$.

Cell-Shield Heat Leak

The contributions from the cell-shield heat leak are:

Material	Heat Leak ($mw/^{o}K$)
8·10-cm No. 40 manganin wires	$5.5 \times 10^{-5}\ T^{1.43}$
2·48±2-mm No. 30 manganin wires	$1.2 \times 10^{-4}\ T^{1.43}$
2·14-7/8-in. stainless steel capillaries	$1.7 \times 10^{-3}\ T^{1.29}$

The sum of the above may be taken as $2.0 \times 10^{-3}\ T^{1.3}$ $mw/^{o}K$ for our purposes. The effect of the Formvar insulation was neglected.

Shield-Bath Heat Leak

The contributions from the shield-bath heat leak are:

Material	mw/°K
2·2-in. by 5/32-in.-diam. stainless steel rods	$0.020\ T^{1.29}$
2·2-1/2-in. by 8-in.-diam. stainless steel capillaries	$0.011\ T^{1.29}$
30 cm of copper wire: 30 No. 38 Formvar-insulated	$0.17\ T^{0.75}$
2·0.010-in.-diam. Cu-Fe thermocouple wires	$0.34\ T^{0.75}$

Summation gives $0.51\ T^{0.75} + 0.032\ T^{1.29}$ mw/°K. The heat capacities and heat leaks are given in Table XIV for the cell and shield as a function of temperature. The relaxation times ($C/\mathcal{K}$) are also given. The relaxation time, λ, of the capillaries between the cell and shield is also estimated with the aid of the following formula:

$$\lambda = \frac{l^2 C_l}{\pi^2 A \mathcal{K}} , \qquad (28)$$

where l is the length, A the cross section, and C_l the heat capacity per unit length of the capillaries. Substitution yields

$$\lambda = 2.06\ T^{1.71} + 164\ T^{-0.29}\ \text{sec.} \qquad (29)$$

Effect of Stainless Steel Capillaries on Heat-Capacity Measurements

From the theoretical estimate of the properties of the calorimeter, it can be seen that the heat capacity of the capillary tubes is not a negligible fraction of the total empty-cell heat capacity. The relaxation time of heat effects in the capillaries is also the same order of magnitude as the heating periods being used. Since it was not obvious how to account for the capillary effect, a theoretical calculation was carried out by using well-known methods,[62]

Table XIV. Estimate of thermal properties of shield and cell

T (^{o}K)	Cell					Shield			
	C_L (mjoules/^{o}K)	C_E (mjoules/^{o}K)	$C_{tot.}$ (mjoules/^{o}K)	$\mathcal{K} \times 10^3$ cell shield (mw/^{o}K)	τ_C (sec)	$C_{tot.}$ (mjoules/^{o}K)	$\mathcal{K}$ shield bath (mw/^{o}K)	τ_S (sec)	λ [a] (sec)
1.1	0.321	4.82	5.14	2.26	2270	19.2	0.58	33	162
1.5	0.813	6.57	7.38	3.39	2180	33.2	0.74	45	150
2.0	1.93	8.76	10.69	4.92	2170	60.1	0.94	64	141
4.0	15.4	17.5	32.9	12.16	2710	336	1.63	206	132
8.0	123	35.0	158	29.9	5290	2050	2.90	707	162
14.0	661	61.3	722	61.8	11700	10540	4.64	2280	263
20.0	1930	87.6	2018	98.2	20500	30350	6.35	4780	415
26.0	4240	114	4354	138	31500	66400	8.00	8280	604

[a] For a discussion of the significance of the relaxation times tabulated above, see the ensuing section on drifts.

and is given below.

The shape of a typical heat-capacity run (temperature versus time) is shown in Figs. 34 and 35. Here T_1 is the temperature of the shield; T_f the temperature of the cell at the end of the foredrift; T_a the temperature extrapolated from the afterdrift to the end of the heating period; T_p the maximum temperature reached; t_0 the time at the beginning of the heating period; and t_p the time at the end of the heating period. The brief temperature rise after the heater is turned off is probably due to a lag in the response of the thermometer or in the distribution of the energy from the heater. The ensuing rapid drop is due to heat flowing from the cell to the capillaries. The true afterdrift then occurs.

If one defines x as the distance along the capillary from the shield (x = 0) to the cell (x = L), and assumes that the shield temperature remains constant during a run, the amount of heat absorbed by the capillaries between t_0 and t_p is given by

$$C_L \int_0^L (T_a - T_f) \frac{x}{L} \, dx = \frac{1}{2} (L \, C_L)(T_a - T_f) = \frac{C'}{2}(T_a - T_f) , \qquad (30)$$

where the further assumption of a linear temperature distribution along the capillaries at t_0 and t_p has been made. In the above expression, C_L is the heat capacity per unit length, and C' is the total heat capacity of the capillaries. Hence, the effective heat capacity of the capillaries is 0.5 C' when the temperature distribution along the capillaries is linear at the beginning and end of the heating period.

The starting point for a more realistic calculation may be taken as the linear heat-flow equation:

$$\frac{d^2T}{dx^2} = \frac{C_L}{AK} \frac{dT}{dt} , \qquad (31)$$

where x and the other symbols are as previously defined. Consider a steady-state temperature distribution of the form

$$T(x,o) = (T_f - T_1) \frac{x}{L} . \qquad (32)$$

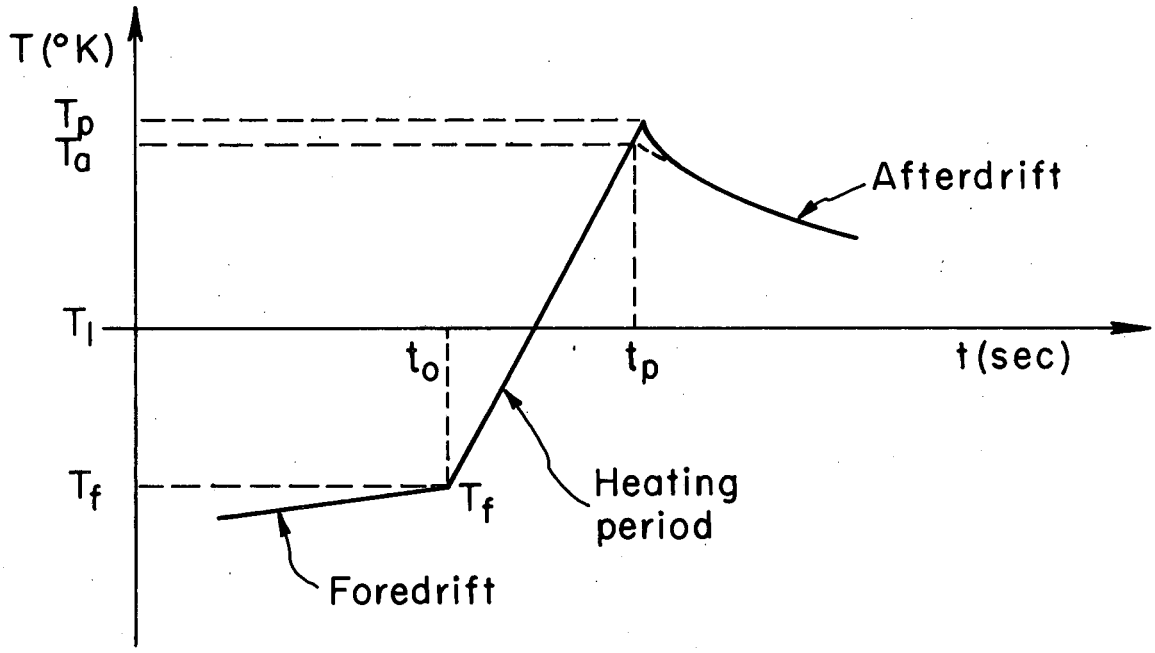

MU-23060

Fig. 34. Illustration of the time-temperature data for a heat-capacity run.

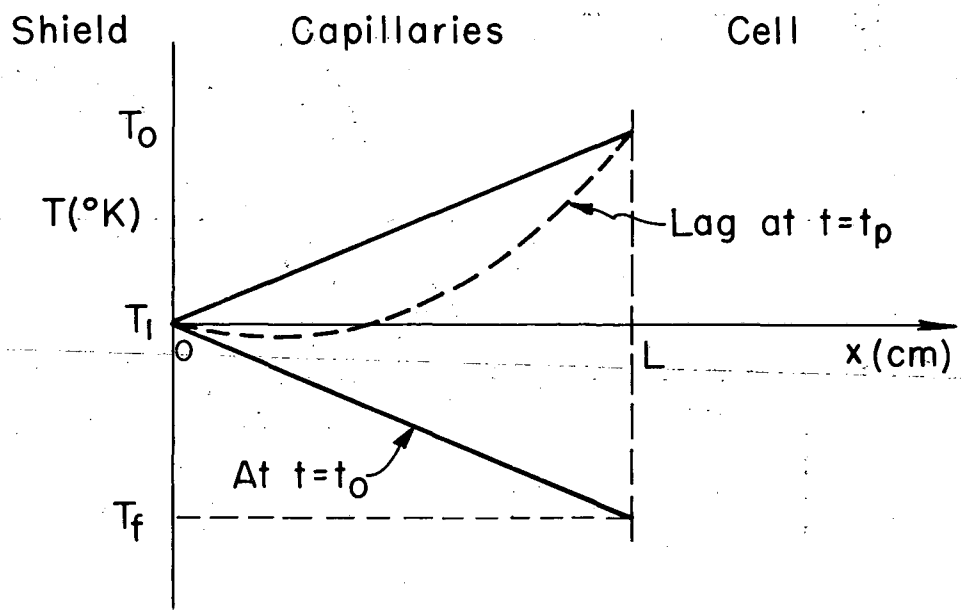

MU-23061

Fig. 35. Schematic diagram of the temperature-distance effects.

If the value of T_f is increased $1^{o}K$ at $t = 0$ and then held constant, the new steady state will be

$$T(x, \infty) = (T_f - T_1)\frac{x}{L} + \frac{x}{L} , \tag{33}$$

and the solution at arbitrary times is found to be

$$T(x,t) = (T_f - T_1)\frac{x}{L} + \frac{x}{L} + \frac{2}{\pi}\sum_{n=1}^{\infty}\frac{(-1)^n}{n}\sin\frac{n\pi x}{L}\, e^{-n^2 t/\lambda} . \tag{34}$$

The part of the temperature distribution resulting from the unit temperature rise is given by $A(x,t)$, which is defined by

$$A(x,t) \equiv T(x,t) - (T_f - T_1)\frac{x}{L} = \frac{x}{L} + \frac{2}{\pi}\sum_{n=1}^{\infty}\frac{(-1)^n}{n}\sin\frac{n\pi x}{L}\, e^{-n^2 t/\lambda} \tag{35}$$

If a series of temperature rises $F(0)$, $F(\tau_1) - F(0)$, $F(\tau_2) - F(\tau_1)$, ... take place at times $0, \tau_1, \tau_2, \ldots$, at $x = L$, the linearity of the problem may be utilized to obtain the temperature distribution at the instant following $t = \tau_n$ as follows:

$$\begin{aligned} T'(x,t) = F(0)A(x,t) &+ [F(\tau_1) - F(0)]\, A(x,t-\tau_1) \\ &+ [F(\tau_2) - F(\tau_1)]\, A(x,t-\tau_2) + \ldots \\ &+ [F(\tau_n) - F(\tau_{n-1})]\, A(x,t-\tau_n) , \end{aligned} \tag{36}$$

where

$$T'(x,t) = T(x,t) - (T_f - T_1)\frac{x}{L} . \tag{37}$$

If one writes

$$F(\tau_k) - F(\tau_{k-1}) = \Delta F_k \ , \ \tau_k - \tau_{k-1} = \Delta\tau_k \ , \tag{38}$$

Eq. (36) may be written

$$T'(x,t) = F(0)\, A(x,t) + \sum_{k=1}^{n} A(x,t-\tau_k) \left(\frac{\Delta F}{\Delta \tau}\right)_k \Delta\tau_k \ . \tag{39}$$

By allowing the number of jumps to become infinite while the jumps and intervals tend to zero, one obtains the following limiting form:

$$T'(x,t) = F(0)\, A(x,t) + \int_0^t A(x,t-\tau)\, F'(\tau)^{d\tau} \ . \tag{40}$$

For the duration of the heating period (taking t_o as 0), one may assume

$$F(t) = \left(\frac{T_p - T_f}{t_p}\right) t \ . \tag{41}$$

Combination of Eqs. (35), (40), and (41) gives

$$T'(x,t) = \frac{T_p - T_f}{t_p} \left[\frac{x}{L}\, t + \frac{2\lambda}{\pi} \sum_{n=1}^{\infty} \frac{(-1)^n}{n^3} \left(1-e^{-n^2 t/\lambda}\right) \sin \frac{n\pi x}{L}\right] , \tag{42}$$

from which one obtains the temperature distribution in the capillaries up to t_p:

$$T(x,t) = (T_f - T_1)\, \frac{x}{L} + \frac{(T_p - T_f)}{t_p}\, \frac{x}{L}\, t + \frac{2\pi}{\lambda} \sum_{n=1}^{\infty} \frac{(-1)^n}{n^3} \left(1-e^{-n^2 t/\lambda}\right) \sin \frac{n\pi x}{L} . \tag{43}$$

The temperature distribution after t_p is considered in a later paragraph.

The heat flow from the cell to the capillaries during the heating period is given by

$$Q_1 = AK\left(\frac{dT}{dx}\right)_{x=L} \tag{44}$$

and the heat flow from the capillaries to the block is

$$Q_2 = AK\left(\frac{dT}{dx}\right)_{x=0} . \tag{45}$$

The total heats flowing from the cell to the capillary and from the capillary to the block are

$$H_1 = \int_0^{t_p} AK\left(\frac{dT}{dx}\right)_{x=L} dt + \int_{t_p}^{t_s} AK\left(\frac{dT}{dx}\right)_{x=L} dt \tag{46}$$

and

$$H_2 = \int_0^{t_p} AK\left(\frac{dT}{dx}\right)_{x=0} dt + \int_{t_p}^{t_s} AK\left(\frac{dT}{dx}\right)_{x=0} dt , \tag{47}$$

where t_s is sufficiently greater than t_p that the steady-state drift has been established. The difference between Eqs. (46) and (47) represents the heat that goes to change the temperature of the capillaries. The first term of Eq. (47) represents the heat flow from the cell and capillaries to the environment during the heating period, and the second term represents the flow after the heating period.

At this point it becomes apparent that one of two approaches may be followed in order to treat the effect of the capillaries on the heat-capacity measurement:

a. The capillaries may be considered as part of the environment. The correction in this case would consist of calculating Eq. (46) and subtracting it from the heat input in order to obtain only the heat capacity of the cell and contents.

b. The capillaries may be considered as part of the cell. The correction to the heat input in this case involves only the amount of heat that passes from the capillaries to the environment during the heating period and during the time necessary to attain the steady state in the

capillaries.

Since most of the heat absorbed by the capillaries comes from the cell, the second approach is the more reasonable, because it should involve the smallest calculated correction.

The calculation is carried out as follows: The first term of Eq. (47) is evaluated to give the heat flow from the capillaries to the environment during the heating period. The second term is evaluated by making the approximation that the cell temperature remains at a constant temperature (T_a) while the capillaries relax to the linear temperature distribution: $T = T_1 + (T_a - T_1)x/L$. The difference between the heat that would flow from the capillaries to the environment if the steady state had already been reached, and the amount that actually flows, gives the correction.

The appropriate derivative during the heating period is

$$\left(\frac{dT}{dx}\right)_{x=0} = \left(\frac{T_f - T_1}{L}\right) + \left(\frac{T_p - T_f}{t_p}\right)\frac{t}{L} + \frac{2\lambda}{L}\sum_{n=1}^{\infty}\frac{(-1)^n}{n^2}\left(1 - e^{-n^2 t/\lambda}\right) \tag{48}$$

and the integral is

$$t_p\,\frac{A\chi}{L}\,\frac{1}{2}(T_f + T_p) - T_1 + \frac{2\lambda}{t_p}(T_p - T_f)\left[\sum_{n=1}^{\infty}\frac{(-1)^n}{n^2} - \frac{\lambda}{t_p}\sum_{n=1}^{\infty}\frac{(-1)^n}{n^4}\left(1-e^{-n^2 t/\lambda}\right)\right] \tag{49}$$

For Eq. (49) to be useful, the block temperature must be eliminated since it is not readily determined during an experiment. Since the fore and after drifts are easily determined, one may write

$$\frac{dT_f}{dt} = \frac{1}{\tau}(T_1 - T_f)$$
$$\frac{dT_p}{dt} = \frac{1}{\tau}(T_1 - T_p)\ , \tag{50}$$

where

$$\tau = \frac{LC}{\chi A} \tag{51}$$

and C is the heat capacity of the cell. Manipulation of the above yields

$$\frac{1}{2}(T_f + T_p) - T_1 = -\frac{1}{2}\tau\left(\frac{dT_f}{dt} + \frac{dT_p}{dt}\right). \tag{52}$$

Since dT_a/dt, the afterdrift after capillary effects have died out, is known rather than dT_p/dt, further manipulation yields

$$\frac{dT_p}{dt} = \frac{dT_a}{dt} - \frac{1}{\tau}(T_p - T_a) \tag{53}$$

The second term above is a second-order correction and may be neglected for all practical purposes. The first part of Eq. (49) then becomes

$$-\frac{1}{2}t_p C\left[\frac{dT_f}{dt} + \frac{dT_a}{dt}\right], \tag{54}$$

which is the same as the customary drift correction. The second part of Eq. (49) may be written

$$C(T_p - T_f)\left(\frac{\lambda}{\tau}\right)\left(2\sum_{n=1}^{\infty}\frac{(-1)^n}{n^2}\right)\left[1 - \frac{\lambda}{t_p}\left(\frac{\sum_{n=1}^{\infty}\frac{(-1)^n}{n^4}(1-e^{-n^2 t_p/\lambda})}{\sum_{n=1}^{\infty}\frac{(-1)^n}{n^2}}\right)\right]. \tag{55}$$

The sum $\sum_{n=1}^{\infty}\frac{(-1)^n}{n^2}$ appears to be equal to $\pi^2/12$ to at least four decimal places. The amount of heat flowing from the capillaries to the shield during the heating period may then be written:

$$-\frac{1}{2}t_p C\left[\frac{dT_f}{dt} + \frac{dT_a}{dt}\right] - \frac{C'}{6}(T_p - T_f)\left[1 - \left(\frac{\lambda}{t_p}\right)\frac{12}{\pi^2}\left\{\sum_{n=1}^{\infty}\frac{(-1)^n}{n^4}(1-e^{-n^2 t_p/\lambda})\right\}\right]. \tag{56}$$

Here $C\lambda/\tau$ has been replaced by C'/π^2, where C' is the heat capacity of the capillaries.

The correction for the transient after the end of the heating period may now be considered. At t_p the deviation of the temperature from the steady state

is given by

$$T(x,t) - (T_a - T_1)\frac{x}{L} = \frac{T_a - T_f}{t_p}\,\frac{2\lambda}{\pi}\sum_{n=1}^{\infty}\frac{(-1)^n}{n^3}\left(1-e^{-n^2 t_p/\lambda}\right)\sin\frac{n\pi x}{L}\,. \qquad (57)$$

Taking $t = 0$ at t_p, the time-dependent equation for the relaxation to the steady state is

$$T(x,t) - (T_a - T_1)\frac{x}{L} = \frac{T_a - T_f}{t_p}\,\frac{2\lambda}{\pi}\sum_{n=1}^{\infty}\frac{(-1)^n}{n^3}\left(1-e^{-n^2 t_p/\lambda}\right)\sin\frac{n\pi x}{L}\,e^{-n^2 t/\lambda}\,. \qquad (58)$$

The desired heat flow from the capillaries to the shield is

$$H = A\mathcal{K}\int_0^{\infty}\left(\frac{dT}{dx}\right)_{x=0} dt\,, \qquad (59)$$

which yields

$$H = \frac{2A\mathcal{K}}{L}(T_a - T_f)\,\frac{\lambda^2}{t_p}\sum_{n=1}^{\infty}\frac{(-1)^n}{n^4}\left(1-e^{-n^2 t_p/\lambda}\right)\,. \qquad (60)$$

Comparison with Eq. (56) shows that this term cancels its equivalent member, so that all that remains of the correction is

$$-\frac{1}{2}\,t_p C\left(\frac{dT_f}{dt} + \frac{dT_a}{dt}\right) - \frac{C'}{6}(T_a - T_f)\,. \qquad (61)$$

This result simply means that, to a first approximation, the correction for the capillaries is independent of the heating period. The validity of the approximation depends on the smallness of the ratio $(T_p - T_a)/(T_a - T_f)$, which was usually well below 0.1.

Since the effective heat capacity of the capillaries is $1/2\ C'$, the fraction of the total heat capacity of the capillaries which appears with the cell is $1/2 - 1/6 = 1/3$. This quantity also indicates the fraction of the sample in the capillaries during a run that should be added to the amount in the cell.

Heat-Capacity Measurements

Temperature Increments

The Δ T's were made small enough so that the drifts were not too rapid and large enough so that the error due to thermometer sensitivity was about 0.2% or less. About 0.1° was used at 1°K and about 1° was used at 20°K.

Energy Input

In the region from 10 to 17°K, the temperature dependence of the manganin heater was found to be approximately 0.06% per $^{\circ}$K. The heating times and currents were decided upon after considering various factors. A minimum heating period of about 30 sec was required to obtain a precision of about 0.01% in the time measurements. Heating currents varied from 150 μa near 1°K to 3 ma above 14°K. To obtain large enough Δ T's at the highest temperatures, one had to increase the heating periods, so that at 20°K, a 200-sec heating time was used.

Drifts

Observation of Table XIV indicates that the thermal-relaxation time of the cell to the shield temperature is always much longer than the heating period, while the relaxation of the shield to the bath is usually the same order of magnitude as the heating period. In practice, the net effect of this arrangement is a nonlinear afterdrift of the cell, because the shield has usually not reached its equilibrium temperature with respect to the bath by the end of the heating period, and the drift of the cell with respect to the shield, which is proportional to the temperature difference between the two, is no longer linear. Thus the afterdrifts must be plotted on semi-log paper to obtain the drift of the cell with respect to the shield at the end of the heating period. The error introduced into the heat-capacity drift correction by the drifting shield temperature is of importance only if the drift is nonlinear during the heating period. It seems likely that this correction to the correction is small.

Measurements Below $2^{o}K$

In this region the large heat capacity and rate of heat generation in normal hydrogen make it convenient to measure the heat capacity simply by allowing the cell and contents to warm up and then analyzing the time-temperature curve. This approach was used by Hill and Ricketson in the first measurements of the anomalous heat capacity.[8] Since the present apparatus has a heavier cell and larger heat leaks than that used by Hill and Ricketson, the applicability of the method to the present data must be considered.

The situation at $2^{o}K$ with normal hydrogen is considered here to give a basis for the following statements. The cell heat capacity at $2^{o}K$ is approximately 2.5×10^{-3} cal/^{o}K. At 1 atm, the cell contains about 0.13 moles of normal hydrogen which has a heat capacity of about 0.6 cal/mole ^{o}K at this temperature. The ratio of sample to cell heat capacity is then about 32 (for $\rho = 0.089$ gm/cm^3). At lower temperatures, the cell heat capacity decreases almost linearly with temperature, while the anomalous heat capacity of the sample rises to a maximum of about 15 cal/mole ^{o}K, so that the ratio becomes even more favorable. The heat leak between cell and shield is about 1×10^{-6} cal/sec ^{o}K at $2^{o}K$, while the heat generation in 0.13 moles of normal hydrogen is about 125×10^{-6} cal/sec. From the above numbers it can be seen that if the cell heat capacity and the heat leak to the environment are completely ignored, the over-all data between $1^{o}K$ and $2^{o}K$ would still be good to about 1%. By keeping the shield within a few tenths of a degree of the cell, the heat-leak error could be reduced. A very rough correction for the heat capacity of the cell would be more than adequate.

Since the rate of heat generation varies with ortho-hydrogen concentration and pressure, one must be able to calibrate it. This should be easily accomplished by using the heater on the cell to change the heating rate by known amount. The change in the rate of temperature change would give the heat capacity of the sample, from which the rate of heat evolution in the sample could be calculated. The uncertainty in the rate of heating would undoubtedly be the largest source of error in the measurements below $2^{o}K$. The effect of pressure on the conversion rate is discussed in a later section. Experiments of the type just described have not yet been carried out because of difficulties with the pressure seals on the calorimeter.

VI. EXPERIMENTAL ASPECTS OF HIGH-PRESSURE MEASUREMENTS

The determination of the number of moles of hydrogen in the cell is probably the most difficult of the measurements in a run. The total number of moles of gas in the system is determined after the run by expanding the sample into large bulbs to a pressure below atmospheric. The problem then reduces to the determination of the fraction of the total sample that was in the cell. The solution of this problem involves the determination of (a) all of the volumes in the high-pressure system, (b) the nature of the thermal gradients between room and cell temperatures, (c) the stretch of the various parts of the system with pressure, and (d) the equation of state of the gas in the temperature and pressure region of interest. Each of these items is discussed below in connection with the related uncertainties in the final result.

Errors due to Uncertainties in the Volumes of the High-Pressure System

Consider the high-pressure system shown in the schematic diagram (Fig. 36).

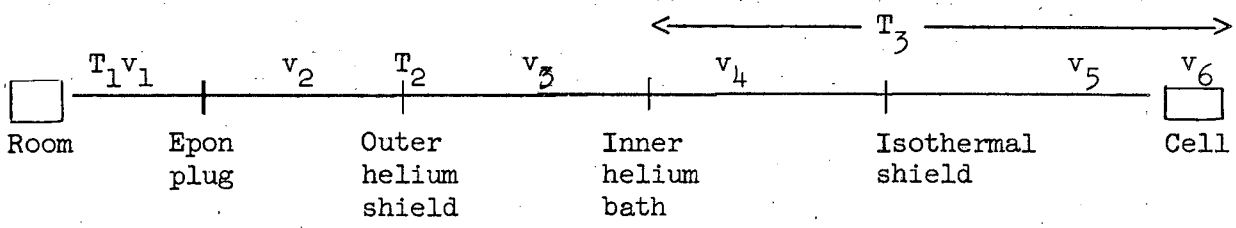

Fig. 36. Schematic diagram of high-pressure system

Here T_1 is room temperature and v_1 is the volume of the high-pressure system from the cold valves to the Epon plug at the calorimeter; T_2 is the temperature of the outer helium shield at the capillary contact and v_2 is the volume in the capillaries between the Epon plug and the outer helium shield; v_3, v_4, and v_5 have analogous meanings; v_6 is the cell volume; and T_3 is the temperature from the inner helium bath to the cell, which is assumed to be constant for this calculation. Let $v_7 = v_4 + v_5 + v_6$ be the volume which is isolated at temperature T_3 when the hydrogen is first frozen in the capillaries at the inner helium bath.

The total number of moles of hydrogen in the high-pressure system is given by

$$n = n_1 + n_2 + n_3 + n_7 \ . \tag{62}$$

The molar volume at a given pressure and temperature may be represented by $V(T)$. It is also convenient to represent the molar volume at a temperature half-way between T_1 and T_2 by $V(T_{12})$.

The number of moles in v_7 at a given pressure for a given temperature configuration is given by

$$n_7 = n \left[\frac{\dfrac{v_7}{V(T_3)}}{\dfrac{v_1}{V(T_1)} + \dfrac{v_2}{V(T_{12})} + \dfrac{v_3}{V(T_{23})} + \dfrac{v_7}{V(T_3)}} \right] , \tag{63}$$

where a linear temperature distribution has been assumed along the capillaries. If one represents the term in brackets by f, then one has

$$n_7 = nf, \tag{64}$$

and

$$\left| \frac{\Delta n_7}{n_7} \right| = \left| \frac{\Delta n}{n} \right| + \left| \frac{\Delta f}{f} \right| . \tag{65}$$

Substituting back, one has that

$$\left| \frac{\Delta f}{f} \right| = \frac{V(T_3)}{v_7} \left\{ (1 - f) \left| \frac{\Delta v_7}{V(T_3)} \right| + f \left[\left| \frac{\Delta v_1}{V(T_1)} \right| + \left| \frac{\Delta v_2}{V(T_{12})} \right| + \left| \frac{\Delta v_3}{V(T_{23})} \right| \right] \right\}, \tag{66}$$

which indicates that as the fraction of the volume not in the cell decreases, the effect of uncertainties in the cell volume becomes smaller, although the effect of uncertainties in the other volumes remains large. In order to estimate the quantities in the above equations, one must consider in detail the various volumes in the high-pressure system together with their uncertainties. Uncertainties in the molar volumes as a function of pressure and temperature are not included in the above error analysis and are considered in a later section.

Volumes in the Pressure System

The following volume measurements were made in July, 1960. Changes have been made since then, but the values serve to illustrate the sample distribution in the high-pressure system and to indicate the errors involved. The cell volume refers to one of the solid cells (designated JB 1) before it had been pressurized. The volume measurements were all made at 1 atm, and the calculated values also refer to 1 atm.

The volumes in the high-pressure system (beyond the frozen-mercury cold valves) are listed first. The total volume of the capillaries leading to the cell was measured by filling with mercury. The volumes from point to point were estimated by measuring the lengths and using the value 0.00298 cm^3/cm.

Item	Dimensions	Volume (cm^3)
1. Cell (measured)	1/4 in. i.d. by 4 in. length	3.217 ± .005
2. Two capillaries, total (meas.)	99 in. + 104 in. ± 2 in.	1.541 ± .002
3. Sections of capillaries	(0.00298 cm^3/cm assumed)	
a. Cell to shield	16.1/4 in. + 16.7/16 in.	0.248
b. Shield to inner bath	3.1/8 in. + 3.1/8 in.	0.047
c. Inner bath to wires	1.1/8 in. + 1.1/4 in.	0.018
d. Wires to outer bath	7.3/8 in. + 7.11/16 in.	0.114
e. Outer bath to wires	1.5/16 in. + 1 1/2 in.	0.021
f. Wires to epon inside	25.1/16 in. + 27 1/4 in.	0.395
g. Epon outside to end	37.1/4 in. + 41.7/8 in.	0.599
4. Dead end (calc.)		0.071 ± .007
5. A286 tee (meas. and calc.)		0.545 ± .030
6. Capillary (MP cold valve to A286 tee)	105.5 ± 1 cm	0.314 ± .006
7. Capillary (HP cold valve to A286 tee)	107 ± 1 cm	0.319 ± .006
	Total high-pressure volume	6.007 ± .056

The volume between the medium pressure cold valve and the trapped volume is listed next. Correction is made for the fact that the low-pressure tee is at an angle.

8. Capillary (MP cold valve to LP tee)	56.5 ± 1 cm	0.168 ± .006
9. Top arm of LP tee (calc.)		0.088 ± .005
	Total	0.256 ± .011

The contributions to the trapped volumes are:

10. Valve (calc.)	0.302 ± .020
11. Arm of tee (calc.)	0.088 ± .005
12. Tubing (calc.)	0.170 ± .005
Total	0.560 ± .030

The determination of the number of moles in the high pressure system is critical with respect to the above volumes. The following volumes are needed to calculate a small correction to the 5-liter bulbs during the low-pressure determination of the number of moles.

Top of high-pressure U-tube:

	Item	Dimensions	Volume (cm^3)
13.	Capillary (cold valve to fitting)	69 ± 1 cm	0.206
14.	Fitting (calc.)	1/8 in. i.d. by 1·1/4 in. length	0.252
15.	Cone (calc.)	1/16 in. i.d. by 1·3/8 in. length	0.069
16.	U-tube (calc.)	1/8 in. i.d. 0.0792 cm^3/cm	
		Total	0.527

Medium-pressure U-tube up to trapped volume:

17.	Tubing (U-tube to tee)	1/16 in. i.d. by 10·1/4 in. length	0.515
18.	Fitting (calc.)(U-tube to tubing)		0.700
19.	Lens ring (calc.)	5/16 in. i.d. by 1/4 in. length	0.314
20.	U-tube (calc.)	5/16 in. i.d. 0.494 cm^3/cm	
		Total	1.529

Low-pressure system:

21.	Total	14.45 ± 1.4

Measuring bulbs in Styrofoam box:

22.	Bulb I	5169 ± 25
23.	Bulb II	5141 ± 25
24.	Bulb III	5120 ± 25
25.	Bulb IV	5183 ± 25
26.	Manometer and connections	319 + 0.0458 P (mm Hg)

The volumes in cm^3, and their uncertainties needed for the evaluation of $|\Delta f/f|$ in Eq. (66) are found from the above listing to be:

$$v_1 = 1.848 \pm .049$$
$$v_2 = 0.405 \pm .010$$
$$v_3 = 0.133 \pm .019$$
$$v_4 = 0.056 \pm .009$$
$$v_5 = 0.248 \pm .010$$
$$v_6 = 3.217 \pm .005$$
$$v_7 = 3.521 \pm .024$$
$$\text{Total} = 5.907 \pm .102; \quad f = 0.596.$$

For the purposes of this calculation, a pressure of 4000 atm may be taken, and the molar volume as a function of temperature may be taken as

$$V(T) = 16.39 + 0.0172\ T\ cm^3 . \tag{67}$$

The subject of molar volumes is discussed more thoroughly in a later section. If one takes $T_1 = 300^oK$, $T_2 = 100^oK$, and $T_3 = 77^oK$, then one has $T_{12} = 200^oK$, and $T_{23} = 88^oK$. The molar volumes are $V(T_1) = 21.56\ cm^3$, $V(T_2) = 18.11$, $V(T_3) = 17.71$, $V(T_{12}) = 19.83$, and $V(T_{23}) = 17.91$. For the purposes of a rough calculation the molar volumes are close enough to be cancelled in the equation for $|\Delta f/f|$, so that one can use

$$\left|\frac{\Delta f}{f}\right| \cong (1 - f) \left|\frac{\Delta v_7}{v_7}\right| + \frac{f}{v_7}\left(|\Delta v_1| + |\Delta v_2| + |\Delta v_3| \right) . \tag{68}$$

Substitution gives

$$\left|\frac{\Delta f}{f}\right| = 0.003 + 0.013 = 0.016\ (1.6\%) .$$

Uncertainties From Other Sources

Errors due to Temperature Uncertainty

Starting with the expression for f, one may deduce the following expression by considering only the errors in the molar volumes. The rough equality of the molar volumes was used in one step to obtain a simplified expression in the same manner as described above. We have

$$\left|\frac{\Delta f}{f}\right| \cong (1-f)\frac{\Delta V(T_3)}{V(T_3)} + \frac{f}{v_7}\left[v_1 \left|\frac{\Delta V(T_1)}{V(T_1)}\right| + v_2 \left|\frac{\Delta V(T_{12})}{V(T_{12})}\right| + v_3 \left|\frac{\Delta V(T_{23})}{V(T_{23})}\right| \right] . \tag{69}$$

If one assumes a temperature uncertainty of $\pm\ 2^oK$, then, on the basis of the linear approximation, the volume uncertainty at each temperature is $\pm\ 0.034\ cm^3$. Substitution in the above gives a resulting uncertainty of 0.14%.

Errors due to the Trapped Volume

The uncertainty here can be considered as a contribution to $|\Delta n/n|$. Let N be the total number of moles of gas, n be the number of moles in the high-pressure system, v be the volume of the high-pressure system, and v_T be the trapped volume. If temperature effects are not considered, we obtain

$$n = N \frac{v}{v + v_T} \tag{70}$$

and

$$\left| \frac{\Delta n}{n} \right| = \left| \frac{\Delta n}{N} \right| + \frac{v_T}{v + v_T} \left| \frac{\Delta v}{v} \right| + \left| \frac{\Delta v_T}{v + v_T} \right| . \qquad (71)$$

If one uses $v = 6.007 \pm .056$ and $v_T = 0.560 \pm .030$ cm^3, the contribution of the last two terms is 0.5%.

Uncertainty in N from the Low-Pressure Measurement

The dominant error in this case is the uncertainty in the volume of the 5-liter bulbs, amounting to about 0.5%. The sum of all of the errors considered above is 2.8%. The effect of pressure in increasing the various volumes has not been considered above, although there is reason to expect some cancellation of the uncertainties in the value of f. The above uncertainty is absolute, and it is hoped that the relative precision will be greater.

The Equation of State of Hydrogen

To evaluate the number of moles of hydrogen in the cell, one must know the equation of state along and above the melting curve. The available data on this subject are summarized below.

Bridgman[38] measured the compressibility of hydrogen in 1923 at 65°C from 2000 to 15,000 kg/cm^2. The piston-displacement method was used and the gas was compressed in contact with kerosene, lowering the accuracy of the experiments. The thermal-expansion data are not reported, but it is stated that the thermal expansion of hydrogen seemed to increase somewhat with pressure. Stewart measured the compression of solid hydrogen and deuterium to 20,000 kg/cm^2 at 4.2°K,[28] connecting his data to that of Megaw.[13] Michels et al. measured the compressibility isotherms of hydrogen and deuterium between -175°C and + 150°C.[63] Below room temperature, their data are all well below 1000 kg/cm^2. Accurate P-V-T data on normal hydrogen from 0 to 200 atm between 35°K and 300°K have been obtained by Johnston and coworkers.[64]

The melting curve of hydrogen was determined by Simon, Ruhemann, and Edwards in 1930,[65] and, more recently, Mills and Grilly have determined the melting curves of hydrogen, deuterium, and tritium.[66] Bartholome measured the volume of the liquid and the volume change on melting up to 152 kg/cm^2 (18.24°K) with hydrogen and up to 98.7 kg/cm^2 (20.97°K) with deuterium.[67] His data indicate that the entropy of melting decreases gradually as the pressure increases.

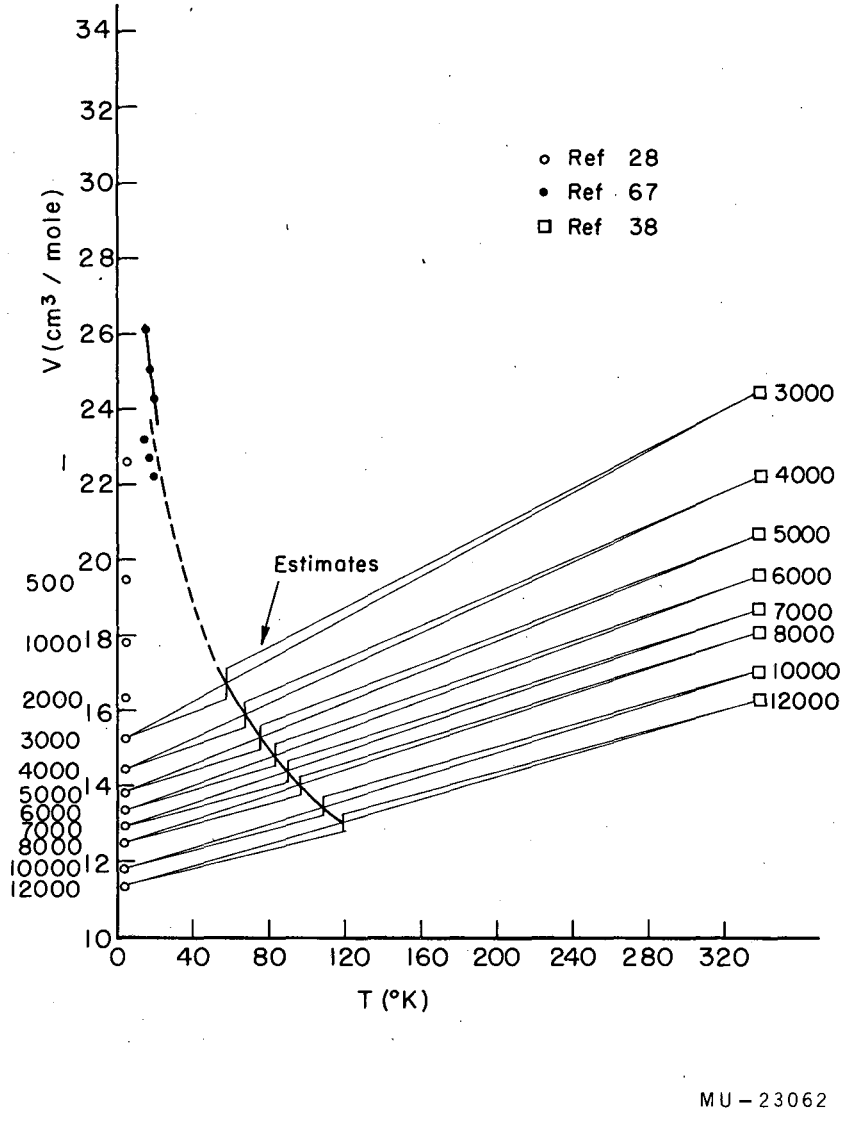

Fig. 37. Estimate of hydrogen isobars above 3000 kg/cm^2.

The simplest way of estimating the equation of state in the region of interest (20 to 120°K, 1,000 to 12,000 kg/cm^2) is to plot the data of Bridgman and Stewart on a molar-volume-versus-temperature graph and then draw linear isobars. This has been done in Fig. 37. Since the melting temperature is known as a function of pressure, the molar volume at which melting occurs may be obtained on the basis of the above approximation. An upper limit to the volume change with melting may be calculated by using a constant entropy of melting in the Clausius-Clapyron equation along with the melting-curve data. A value of 2.00 cal/mole/°K was taken, and the above calculation was carried out. These volume discontinuities were added to the melting curve in Fig. 37, as may be seen. The linear interpolation above 3000 kg/cm^2 may be off by 10% or more, so that it will be necessary to determine the equation of state in the region of interest for the present experiments.

Below 3000 kg/cm^2 it is certain that the isobars are curved, and there is very little data on which to base interpolations, so that no attempt has been made to estimate the P-V-T properties in this region. Measurements of the equation of state will be required in this region also. Since the P-V-T measurements can be made in the calorimeter in the same cell to be used for the heat-capacity measurements and to the same precision obtainable in the heat capacity work, no special problems arise from this difficulty. Fig. 37 may be used to obtain an estimate of the highest pressure obtainable by the blocked-capillary method. Assuming that 12,000 kg/cm^2 is the highest pressure that can safely be generated, the linear interpolation indicates that the molar volume of the fluid at the melting point is 13.3 cm^3. At 4.2°K, this corresponds to a pressure of about 6,000 kg/cm^2. To obtain higher pressures, one may have to use a method suggested by Nesbitt and Fiske[68] of the General Electric Co., Schenectady, N. Y. An insulated heater wire (such as Formvar-covered manganin) could be threaded into the capillary from the room-temperature end down to the cell. By keeping the temperature in the capillary above the melting point, it would be possible to raise the pressure in the cell to the value obtainable at the other end of the system. Since this technique would probably be tricky to apply, it seems best to obtain as much data as possible by using the blocked-capillary method first.

Extrusion of Hydrogen Through Capillaries

The extrusion pressures of hydrogen through a hole of 1/8 in. diam. and unspecified length (probably 1/2 in., as estimated from drawing) were measured by Stewart to be 240 kg/cm^2 and 290 kg/cm^2, respectively.[27] These data may be

used to obtain a rough estimate of the highest pressure differences that may be used in the present experiments without having extrusion of the hydrogen in the capillaries, and hence, failure of the blocked-capillary method. The analysis of the stress-strain pattern of a solid in a tube with a pressure at one end is analogous to the analysis of the viscous flow of a fluid in a capillary. Consider the case of an incompressible solid. Let R be the radius of the capillary, S be the tangential stress on a curved surface perpendicular to a radius of the capillary, G be the modulus of elasticity in shear of the hydrogen in the capillary, and l be the length of the capillary sustaining the pressure difference P. It can be shown that the maximum shearing stress occurs at the radius of the capillary, and is expressed by

$$S = \frac{PR}{2l} . \tag{72}$$

If the yield pressure is 240 kg/cm^2 for a 1/8-in. diameter and 1/2-in. length, then the above equation allows the yield pressure for a 0.025-in. diameter and 3-in. length (a practical situation in the present experiments) to be estimated as 7200 kg/cm^2. Since the solid is actually compressible, this estimate is too large. On the other hand, one would expect the solid to become harder as the pressure is increased.

A calculation may be carried out which takes the compressibility of the solid into account. Aside from being rather complicated, the result depends on the value of the shear modulus, G, which cannot be evaluated accurately enough from the available data, and whose pressure dependence is unknown. Although it seems unlikely that extrusion in the capillaries will be a problem, one should test for the effect in the first runs by following the pressure on the room-temperature side as the capillary is frozen and the cell cooled.

VII. THEORETICAL CONSIDERATIONS

Introduction

Although no high-pressure heat-capacity data are yet available for analysis, a fair amount of 1-atm data on the heat capacity of solid hydrogen and deuterium has appeared in the literature during the past two years. Since the phenomena occurring at 1 atm will be relevant to high-pressure studies, and since the data are interesting in themselves, it was desirable to consider these data and the theoretical interpretations which have been made.

The modern data on the anomalous heat capacity of solid hydrogen and deuterium have been published in four papers from two laboratories. In 1954 Hill and Ricketson published data on solid hydrogen between 2 and 14°K on samples containing 0.5, 7, 25, 41, 56, 66, and 74% o-H_2.[8] At the two higher concentrations, the data were extended to 1.15°K. and a λ anomaly was discovered. In the next year, the same authors extended the measurements to 0.2°K and found that the λ anomaly did not occur below about 60% o-H_2 concentration.[9] In 1957 Gonzalez, White, and Johnston published data on solid deuterium between 0.3 and 13°K on samples containing 3, 14.5, 18.5, and 33.3% p-D_2.[14] No λ anomaly was discovered because the concentration of p-D_2 was not high enough. In 1959 Hill and Lounasmaa obtained data on the lattice heat capacities of solid hydrogen and deuterium by reducing the o-H_2 and p-D_2 impurity concentration as much as possible.[69] By having the conversion catalyst in the sample and equilibrating for 2 hr at the triple point before freezing the sample and taking measurements, they obtained a nominal o-H_2 concentration of 0.02%, and nominal p-D_2 concentrations of 1.5 or 2.15%, depending on the temperature of equilibration. The solid-hydrogen data were fitted by a function of the type, $C_p = AT^3 + BT^5$, as were the deuterium data after the anomalous contribution of the p-D_2 was subtracted empirically.

The interpretation of the above data has been the subject of several other papers. Tomita applied the Bethe approximation in the statistical treatment of the cooperative phenomenon and calculated the temperature dependence of the peak of the anomaly with respect to o-H_2 concentration.[10] The theory predicted the lowest concentration for the occurrence of the λ anomaly to be 16.7%, as compared with the experimental value of 60%.

Nakamura[70] considered the valence, electrostatic quadrupole, and London dispersion forces in the pairwise interaction of adjacent ortho molecules and calculated the magnitude of the high temperature "tail" of the anomaly, using

Hill and Ricketson's data.[8] This calculation applied only to the region where the anomalous heat capacity was proportional to T^{-2}. Nakamura also calculated the pairwise energy levels for quadrupolar interaction and compared the predicted heat capacity with Hill and Ricketson's 7% data.[8] The data were about a factor of two larger than the theoretical result. He then fitted the discrepancy with the expression for a two-level anomaly (upper-level degenerate) proportional to the o-H_2 concentration. (The pairwise energy was proportional to the square of the concentration.) A fit was obtained by using a splitting of 2×10^{-16} ergs per molecule (since Nakamura seems to have counted some of the o-H_2 molecules twice in this calculation, the numerical value is in doubt). In order to explain the contribution dependence on the first power of the o-H_2 concentration, Nakamura postulated a splitting of the rotational levels by the lattice motion of the molecules. In a later paper, Nakamura and Uryu calculated the quenching of the rotational states of ortho hydrogen in the solid state by using the Einstein model for lattice vibrations and obtained a splitting of 0.72×10^{-16} ergs between the $M = 0$ and ± 1 levels.[71]

In the present work, it was of interest to reexamine Nakamura's conclusions in the light of all of the recent data. From the experimental point of view, his result was based on a single experiment, and might be altered by small discrepancies. From the theoretical point of view, Nakamura did not explicitly consider isolated ortho molecules, isolated pairs of ortho molecules, and more complicated configurations at the 7% concentration. On this basis, it was still of interest to determine whether a realistic calculation based on the angular potential energy between ortho molecules could account for the size and shape of the heat-capacity anomaly.

At high pressures the different shape and repulsive energies between ortho-ortho and ortho-para pairs becomes important, and one might expect that such effects can no longer be neglected in calculating the splitting of the ortho-hydrogen sublevels. The energy-level system of a pair of ortho molecules in solid hydrogen was calculated considering these effects. The case of three ortho molecules in a row was also treated in the quadrupolar approximation. The two models had appreciably different level systems and heat capacities. The energy-level system for pairwise interaction was calculated as a function of intermolecular separation, and it was found that, although only the quadrupole interaction is important at 1 atm, valence forces become important at 5000 atm. The experimental data at various o-H_2 and p-D_2 concentrations were compared with the calculations, and the present understanding of the situation was discussed.

Interaction Between Two Hydrogen Molecules

The various contributions to the interaction between two hydrogen molecules have been discussed by Hirschfelder, Curtiss, and Bird.[52] Three effects are important in the angular dependence of the intermolecular potential. These are (a) the chemical or valence energy (sometimes called the exchange repulsion), (b) the electrostatic quadrupole-quadrupole interaction, and (c) the inverse sixth-power dispersion energy. The inverse eighth-power dispersion energy is small, and its angular dependence is considered negligible by Hirschfelder et al.[52]

Because of its convenience, de Boer's theoretical result for the valence energy[31] is used. Over the range $4a_o$ to $10a_o$ ($a_o = 0.529A$), de Boer's result was expressed as

$$V^{(val)} = 2.78 \frac{e^2}{a_o} \left[e^{-1.87r_{ac}/a_o} + e^{-1.87r_{bc}/a_o} + e^{-1.87r_{ad}/a_o} + e^{-1.87r_{bd}/a_o} \right], \tag{73}$$

where nuclei ab and cd form the two molecules. The following approximation, recommended by de Boer for the region $6a_o$ to $8a_o$, shows the angular dependence explicitly:

$$\begin{aligned} V^{1(val)} = \frac{e^2}{a_o} \Big\{ & 48{,}000 \left(\frac{a_o}{r}\right)^{11} + 129{,}360 \left(\frac{a_o}{r}\right)^{13} [13 \cos^2 \theta_{ab} + 13 \cos^2 \theta_{cd} - 2] \\ & + 412{,}010 \left(\frac{a_o}{r}\right)^{15} [1 - 15 \cos^2 \theta_{ab} - 15 \cos^2 \theta_{cd} - 195 \cos^2 \theta_{ab} \cos^2 \theta_{cd} \\ & + 2 \left\{ \sin \theta_{ab} \sin \theta_{cd} \cos (\phi_{ab} - \phi_{cd}) - 14 \cos \theta_{ab} \cos \theta_{cd} \right\}^2] \\ & + 68{,}640 \left(\frac{a_o}{r}\right)^{15} [6 - 90 \cos^2 \theta_{ab} - 90 \cos^2 \theta_{cd} \\ & + 2255 \cos^4 \theta_{ab} + 2255 \cos^4 \theta_{cd}] \Big\} \end{aligned} \tag{74}$$

The electrostatic quadrupole-quadrupole interaction is given by[52]

$$\begin{aligned} V^{(Q-Q)} = \frac{3Q_aQ_b}{16\, r^5} \Big\{ & 1 - 5 \cos^2 \theta_a - 5 \cos^2 \theta_b - 15 \cos^2 \theta_a \cos^2 \theta_b \\ & + 2 [\sin \theta_a \sin \theta_b \cos (\phi_a - \phi_b) - 4 \cos \theta_a \cos \theta_b]^2 \Big\}, \end{aligned} \tag{75}$$

where Q is the cylindrically symmetric quadrupole moment about the internuclear axis. Harrick and Ramsey have measured the quadrupole moment of hydrogen by a molecular-beam microwave-resonance method.[72] They obtained a value for Q/e of 0.220×10^{-16} cm^2 relative to the internuclear axis. This numerical value pertains to the convention used by Hirschfelder et al.[53]

The dispersion potential at large separation may be represented as follows:[52,73]

$$V^{(dis)} = - \frac{C(\theta_a, \phi_a; \theta_b, \phi_b)}{r_{ab}^6} \tag{76}$$

where θ_a, ϕ_a; θ_b, ϕ_b refer to the intermolecular axis, and

$$C(\theta_a,\phi_a; \theta_b,\phi_b) = (A - B - B' + C)[\sin\theta_a \sin\theta_b \cos(\phi_a - \phi_b) - 2\cos\theta_a \cos\theta_b]^2$$
$$+ 3(B - C)\cos^2\theta_a + 3(B' - C)\cos^2\theta_b + (B + B' + 4C) \tag{77}$$

Here we define

$$A = \frac{h}{4}\alpha_{\parallel}(a)\,\alpha_{\parallel}(b)\,\frac{\nu_{\parallel}(a)\,\nu_{\parallel}(b)}{\nu_{\parallel}(a) + \nu_{\parallel}(b)}, \tag{78a}$$

$$B = B' = \frac{h}{4}\alpha_{\parallel}(a)\,\alpha_{\perp}(b)\,\frac{\nu_{\parallel}(a)\,\nu_{\perp}(b)}{\nu_{\parallel}(a) + \nu_{\perp}(b)}, \tag{78b}$$

and

$$C = \frac{h}{4}\alpha_{\perp}(a)\,\alpha_{\perp}(b)\,\frac{\nu_{\perp}(a)\,\nu_{\perp}(b)}{\nu_{\perp}(a) + \nu_{\perp}(b)}, \tag{78c}$$

where $\alpha_{\parallel}$ and $\alpha_{\perp}$ are the polarizabilities along and perpendicular to the molecular axis, respectively, and $\nu_{\parallel}$ and $\nu_{\perp}$ are the fundamental frequencies for (electronic) vibrations along and perpendicular to the molecular axis, the latter being doubly degenerate.

If we assume that molecules a and b are of the same kind, and set $\nu_{\parallel} = \nu_{\perp} = \nu = I/h$, where I is the ionization potential,[52] Eqs. (78) reduce to

$$A = \frac{\alpha_{\parallel}^{2} I}{8}, \quad B = B' = \frac{\alpha_{\parallel}\,\alpha_{\perp}\, I}{8}; \text{ and } C = \frac{\alpha_{\perp}^{2} I}{8} \tag{79}$$

If the anisotropy of polarizability, K, is defined by

$$K = \frac{\alpha_{\parallel} - \alpha_{\perp}}{\alpha_{\parallel} + 2\,\alpha_{\perp}}, \tag{80}$$

the combinations appearing in Eq. (77) become

$$(A - 2B + C) = \frac{I\alpha^2}{8}\left(\frac{\alpha_{\parallel} - \alpha_{\perp}}{\alpha}\right)^2 = \frac{I\alpha^2}{8}\,K^2, \tag{81a}$$

$$B - C = \frac{I\,\alpha_{\perp}\alpha}{8}\left(\frac{\alpha_{\parallel} - \alpha_{\perp}}{\alpha}\right) \simeq \frac{I\,\alpha^2}{8}\,K, \tag{81b}$$

and

$$2B + 4C = \frac{I\,\alpha_{\perp}}{4}\,(\alpha_{\parallel} + 2\,\alpha_{\perp}) \simeq \frac{3}{4}\,I\,\alpha^2. \tag{81c}$$

The approximation $\alpha_{\perp} \simeq \alpha$ seems justified for our purposes since we have $\alpha_{\perp} = (1 - 1/3\,K)\,\alpha$ and $K \simeq 0.1$. In order to replace $I\alpha^2$ in Eqs. (81) by a more empirical quantity, the London force between spherically symmetric molecules, $-3/4\,I\alpha^2/r^6$, may be compared with the coefficient of the empirically fitted Lennard-Jones 6-12 potential, $4\epsilon\,[\,(\frac{\sigma}{r})^{12} - (\frac{\sigma}{r})^6]$, which gives the result: $I\alpha^2 = 16/3\,\epsilon\sigma^2$. For hydrogen, we have $\epsilon/k = 37.00^{\circ}K$, and $\sigma = 2.928A$. If we replace σ by $5.55a_o$, the above equations may be combined and substituted into Eq. (76) to give a usable expression for the angular dependence of the London inserve sixth-power dispersion energy:

$$V^{(dis)} = -29{,}000\,\epsilon\,\left(\frac{a_o}{r}\right)^6 \Big[4 + 2K(\cos^2\theta_a + \cos^2\theta_b)$$

$$+ 2/3\,k^2\left\{\sin\theta_a \sin\theta_b \cos(\phi_a - \phi_b) - 2\cos\theta_a \cos\theta_b\right\}^2\Big]. \tag{82}$$

The value of K used for these calculations was 0.1173.[52]

The inverse eighth-power dispersion energy may be expressed as[52]

$$V^{(dis,8)} = -116\,\frac{e^2}{a_o}\left(\frac{a_o}{r}\right)^8 \tag{83}$$

Equations (74), (75), (82), and (83) may be added to give an expression of the form:

$$V = A + B\,(\cos^2\theta_a + \cos^2\theta_b) + C\cos^2\theta_a\cos^2\theta_b + D\sin^2\theta_a\sin^2\theta_b\cos^2(\phi_a - \phi_b)$$

$$+ E\sin\theta_a\cos\theta_a\sin\theta_b\cos\theta_b\cos(\phi_a - \phi_b) + F\,(\cos^4\theta_a + \cos^4\theta_b), \quad (84)$$

where the coefficients are collected in Table XV.

Table XV. Coefficients of angular potential energy

Coefficient	Valence	Q - Q	Dis-6 (and dis-8)
A	$\frac{e^2}{a_0}\left[48{,}000\,(\frac{a_0}{r})^{11} - 258{,}720\,(\frac{a_0}{r})^{13} + 823{,}850\,(\frac{a_0}{r})^{15}\right]$	$\frac{3}{16}\frac{Q^2}{r^5} \times 1$	$-29{,}000\,\epsilon\,(\frac{a_0}{r})^6 \times 4$ $-116\,\frac{e^2}{a_0}\,(\frac{a_0}{r})^8$
B	$\frac{e^2}{a_0}\left[1681680\,(\frac{a_0}{r})^{13} - 12357750\,(\frac{a_0}{r})^{15}\right]$	$-\frac{3}{16}\frac{Q^2}{r^5} \times 5$	$-29{,}000\,\epsilon\,(\frac{a_0}{r})^6 \times 2K$
C	$\frac{e^2}{a_0}\left[81165970\,(\frac{a_0}{r})^{15}\right]$	$\frac{3}{16}\frac{Q^2}{r^5} \times 17$	$-29{,}000\,\epsilon\,(\frac{a_0}{r})^6 \times \frac{8}{3}K^2$
D	$\frac{e^2}{a_0}\left[824020\,(\frac{a_0}{r})^{15}\right]$	$\frac{3}{16}\frac{Q^2}{r^5} \times 2$	$-29{,}000\,\epsilon\,(\frac{a_0}{r})^6 \times \frac{2}{3}K^2$
E	$-\frac{e^2}{a_0}\left[23072560\,(\frac{a_0}{r})^{15}\right]$	$-\frac{3}{16}\frac{Q^2}{r^5} \times 16$	$+29{,}000\,\epsilon\,(\frac{a_0}{r})^6 \times \frac{8}{3}K^2$
F	$\frac{e^2}{a_0}\left[17503200\,(\frac{a_0}{r})^{15}\right]$	0	0

Application of Perturbation Theory to Pairwise Interaction

A problem relating to the anomalous heat-capacity effects in solid hydrogen that can be treated with some degree of realism from the theoretical point of view is the pairwise interaction of two ortho molecules, each having eleven para-hydrogen neighbors. Since each ortho-hydrogen molecule ($J = 1$) has three degenerate orientational eigenstates in the absence of a perturbation, a pair of ortho molecules has nine degenerate states. Application of first-order perturbation theory to this problem yields the correct combinations and eigenvalues of the nine states under the applied perturbation.[74] Mathematically, the procedure involves the calculation of the matrix elements of the 9 by 9 array and the solution of the resulting secular equation.

The potential of interaction of the two ortho molecules is given by Eq. (84), as is the potential of interaction between each ortho molecule and each of its para neighbors. The unperturbed wave functions may be taken as follows:

Ortho Molecule at a

$$\psi_1^a = \frac{1}{2}\sqrt{\frac{3}{\pi}} \sin \theta_a \cos \phi_a \tag{85a}$$

$$\psi_2^a = \frac{1}{2}\sqrt{\frac{3}{\pi}} \cos \theta_a \tag{85b}$$

$$\psi_3^a = \frac{1}{2}\sqrt{\frac{3}{\pi}} \sin \theta_a \sin \phi_a \tag{85c}$$

Ortho Molecule at b

$$\psi_1^b = \frac{1}{2}\sqrt{\frac{3}{\pi}} \sin \theta_b \cos \phi_b \tag{85d}$$

$$\psi_2^b = \frac{1}{2}\sqrt{\frac{3}{\pi}} \cos \theta_b \tag{85e}$$

$$\psi_3^b = \frac{1}{2}\sqrt{\frac{3}{\pi}} \sin \theta_b \sin \phi_b, \tag{85f}$$

with all para states being represented by $\psi_i^p = 1/\sqrt{4\pi}$. For the rest of the discussion, a state such as $\psi_1^a \psi_3^b$ will be referred to as (13).

The interaction between an ortho molecule and one of its para neighbors is considered first. The three zeroth-order states will be of the form $\psi_1^a \psi_i^p$,

$\psi_2^a \psi_i^p$, $\psi_3^a \psi_i^p$. Hence Eq. (84) may be averaged over Θ_b, ϕ_b to obtain the potential

$$V = (A + \frac{1}{3} B + \frac{1}{5} F) + (B + \frac{1}{3} C) \cos^2 \Theta_a + \frac{1}{3} D \sin^2 \Theta_a + F \cos^4 \Theta_a . \tag{86}$$

Introducing the Legendre Polynomials, we have

$$P_2^o (\cos \Theta) = \frac{1}{2} (3 \cos^2 \Theta - 1) \tag{87a}$$

and

$$P_4^o (\cos \Theta) = \frac{1}{8} (35 \cos^4 \Theta - 30 \cos^2 \Theta + 3) . \tag{87b}$$

The potential may be written

$$V = (A + 2/3\, B + \frac{1}{9} C + \frac{2}{9} D + \frac{2}{5} F) + (\frac{2}{3} B + \frac{2}{9} C - \frac{2}{9} D + \frac{4}{7} F)$$

$$P_2^o (\cos \Theta_a) + \frac{8}{35} F P_4^o (\cos \Theta_a) . \tag{88}$$

Only the $P_2^o(\cos \Theta_a)$ causes a splitting, which is readily found to be

$$\Delta E \equiv E_2 - E_1 \; (= E_3) = \frac{2}{5} B + \frac{2}{15} (C - D) + \frac{12}{35} F. \tag{89}$$

This splitting is the same order of magnitude as that which results from the interaction of two ortho molecules and is caused by the valence and dispersion forces.

The next point of interest involves the summation of the ortho-para interaction over the eleven para neighbors of the ortho molecule. Since Eq. (86) is cylindrically symmetric about the ortho-para intermolecular axis, the addition theorem of spherical harmonics may be used to rotate the eleven-coordinate systems to a common axis to allow summation of the potentials. If γ is the polar angle about one of the intermolecular directions and α and β are the polar coordinate angles of this direction with respect to the common coordinate system, the addition theorem has the form[75]

$$P_n(\cos \gamma) = P_n(\cos \alpha)\, P_n (\cos \Theta) + 2 \sum_{m=1}^{n} \frac{(n - m)!}{(n + m)!} P_n^m (\cos \alpha)\, P_n^m (\cos \Theta) \cos m(\phi - \beta), \tag{90}$$

and Θ and ϕ are the angles in the common coordinate system. If the summation (for n = 2) is carried out for either the cubic close-packed or hexagonal close-

packed cases over twelve nearest neighbors, there is complete cancellation. This means that the potential of an ortho molecule surrounded by eleven para molecules and a hole may be expressed as

$$V = 11\left(A + \frac{2}{3}B + \frac{1}{9}C + \frac{2}{9}D + \frac{2}{5}F\right)$$

$$- \left(\frac{2}{3}B + \frac{2}{9}C - \frac{2}{9}D + \frac{4}{7}F\right) P_2^0(\cos\theta_a) \qquad (91)$$

where the $P_4^0(\cos\theta_a)$ contribution has been dropped. Writing in the expression for $P_2^0(\cos\theta_a)$ and filling the hole with an ortho molecule with eleven para neighbors, we obtain

$$V = 2\left(11A + \frac{23}{3}B + \frac{4}{3}C + \frac{7}{3}D + \frac{164}{35}F\right) -$$

$$- \left(B + \frac{1}{3}C - \frac{1}{3}D + \frac{6}{7}F\right)\left(\cos^2\theta_a + \cos^2\theta_b\right) + V_{ab}\,, \qquad (92)$$

where V_{ab} is given by Eq. (84). Substituting and collecting, we have

$$V = \left(23A + \frac{46}{3}B + \frac{8}{3}C + \frac{14}{3}D + \frac{328}{35}F\right)$$

$$-\left(\frac{1}{3}[C - D] + \frac{6}{7}F\right)\left(\cos^2\theta_a + \cos^2\theta_b\right) + C\cos^2\theta_a\cos^2\theta_b$$

$$+ D\sin^2\theta_a\sin^2\theta_b\cos^2(\phi_a - \phi_b)$$

$$+ E\sin\theta_a\cos\theta_a\sin\theta_b\cos\theta_b\cos(\phi_a - \phi_b) + F\left(\cos^4\theta_a + \cos^4\theta_b\right).$$

$$(93)$$

The matrix elements of the nine states obtained from Eqs. (85) with respect to the above potential have been calculated and are given in Table XVI. The quantity, $\left(23A + \frac{46}{3}B + \frac{193}{75}C + \frac{78}{15}D + \frac{322}{35}F\right)$, has been removed from each of the diagonal matric elements.

Table XVI. Matrix Elements for Pairwise Total Interaction

	(11)	(22)	(33)	(12)	(21)	(23)	(32)	(13)	(31)
(11)	0	$\frac{1}{25}$ E	$\frac{2}{25}$ D						
(22)	$\frac{1}{25}$ E	$\frac{4}{75}$(C-D)	$\frac{1}{25}$ E						
(33)	$\frac{2}{25}$ D	$\frac{1}{25}$ E	0						
(12)				$-\frac{4}{75}$(C+D)	$\frac{1}{25}$ E				
(21)				$\frac{1}{25}$ E	$-\frac{4}{75}$(C+D)				
(23)						$-\frac{4}{75}$(C+D)	$\frac{1}{25}$ E		
(32)						$\frac{1}{25}$ E	$-\frac{4}{75}$ (C+D)		
(13)								$-\frac{4}{25}$D	$\frac{2}{25}$ D
(31)								$\frac{2}{25}$ D	$-\frac{4}{25}$ D

If only the electrostatic quadrupole-quadrupole interaction is considered, all of the para molecules may be ignored, and Eq. (75) may be taken as the perturbing potential. The resulting matrix elements are shown in Table XVII. A factor of $3/100\ Q^2/r^5$ has been removed from each matrix element.

Table XVII. Matrix elements for pairwise quadrupole interaction

	(11)	(22)	(33)	(12)	(21)	(23)	(32)	(13)	(31)
(11)	3	-4	1						
(22)	-4	8	-4						
(33)	1	-4	3						
(12)				-4	-4				
(21)				-4	-4				
(23)						-4	-4		
(32)						-4	-4		
(13)								1	1
(31)								1	1

The eigenvalues of the 3 by 3 part of Table XVII (with the same factor removed) are 12, 2, and 0. The eigenvalues of the two center 2 by 2's are 0 and -8, and of the last 2 by 2 are 2 and 0. The eigenfunctions of the eigenvalues in the order listed above are

$$E = 12 : \quad \psi_1 = \frac{1}{\sqrt{6}} [(11) - 2 (22) + (33)] \tag{94a}$$

$$E = 2 : \quad \psi_2 = \frac{1}{\sqrt{2}} [(11) - (33)] \tag{94b}$$

$$E = 0 : \quad \psi_3 = \frac{1}{\sqrt{3}} [(11) + (22) + (33)] \tag{94c}$$

$$E = 0 : \quad \psi_4 = \frac{1}{\sqrt{2}} [(12) - (21)$$

$$\psi_5 = \frac{1}{\sqrt{2}} [(32) - (23)]$$

$$E = -8 : \quad \psi_6 = \frac{1}{\sqrt{2}} [(12) + (21)]$$

$$\psi_7 = \frac{1}{\sqrt{2}} [(32) + (23)]$$

$$E = 2 : \quad \psi_8 = \frac{1}{\sqrt{2}} [(13) + (31)]$$

$$E = 0 : \quad \psi_9 = \frac{1}{\sqrt{2}} [(13) - (31)] .$$

For the more general case represented by Table XVI, the calculations were carried out for internuclear distances of 3.75 A, 3.58 A, 3.45 A, and 3.15 A. The last two represent hydrogen at roughly 1000 and 5000 atm, respectively. The values of C, D, and E at these separations are shown in Table XVIII. The units of this calculation are 10^{-16} ergs.

Table XVIII. Numerical values of coefficients

	3.75	3.58	3.45	3.15
C	49.86	67.43	87.26	186.80
D	5.60	7.11	8.61	14.05
E	-46.48	-59.91	-73.93	-130.71

The eigenvalues are collected in Table XIX in the same order as in Eq. (94).

Table XIX. Eigenvalues

	3.75	3.58	3.45	3.15
1	3.956	5.248	6.648	13.199
2	0.401	0.462	0.551	0.705
3	-1.997	-2.493	-3.004	-4.691
4	-1.397	-1.957	-2.615	-6.233
5	-1.397	-1.957	-2.615	-6.233
6	-5.115	-6.751	-8.529	-16.689
7	-5.115	-6.751	-8.529	-16.689
8	-0.448	-0.569	-0.688	-1.124
9	-1.344	-1.707	-2.065	-3.372

In Table XX, the energy levels are rearranged and the lowest subtracted out. The quadrupole levels are also shown for comparison. The units are 10^{-16} ergs. The results are also shown in Fig. 38.

Table XX. Rearranged eigenvalues

	3.75		3.58		3.45		3.15	
	Total	Q - Q	Total	Q - Q	Total	Q - Q	Total	Q - Q
1	9.071	9.030	11.999	11.388	15.177	13.702	29.888	21.593
2	5.516	4.515(2)	7.213	5.694(2)	9.080	6.851(2)	17.394	10.796(2)
8	4.667		6.184		7.841		15.565	
9	3.771	3.612(4)	5.044	4.555(4)	6.464	5.481(4)	13.317	8.637(4)
4,5	3.718(2)		4.794(2)		5.914(2)		11.998	
3	3.118		4.258		5.525		10,456(2)	
6,7	0 (2)	0 (2)	0 (2)	0 (2)	0 (2)	0 (2)	0 (2)	0 (2)

It can be seen that the total interaction is almost the same as the quadrupole-quadrupole interaction at the larger two separations, but that at shorter distances, the differences become more noticeable. The lowest level is doubly degenerate at all separations.

Linear Arrangement of Three Ortho Molecules

The preceding calculation is readily extended to the case of three ortho molecules along a line (a, b, c). Since the quadrupole interaction is a good approximation to the total interaction at one atmosphere, only the quadrupole perturbation energy will be considered.

The perturbing potential may be taken as

$$V_{abc} = V_{ab} + V_{bc} , \tag{95}$$

where V_{ab} and V_{bc} are obtained from Eq. (75). The zeroth-order wave functions are obtained from Eq. (85) and $\psi_1^a \psi_3^b \psi_2^c$ will be denoted by (132) as before. It is easily seen that

$$\int (ijk)^* V_{abc} (i'j'k') \, d\tau_a \, d\tau_b \, d\tau_c = \delta_{kk'} \int (ij)^* V_{ab} (i'j') \, d\tau_a \, d\tau_b$$

$$+ \delta_{ii'} \int (jk)^* V_{bc} (j'k') \, d\tau_b \, d\tau_c \tag{96}$$

The matrix elements obtained from Table XVII by using this result are shown in Table XXI. The same factor of $3/100\ Q^2/r^5$ has been removed from each element. It can be seen that three 7 by 7 blocks and one 6 by 6 block are obtained after some rearrangement. The first and third 7 by 7 blocks are identical, as might be expected.

The following basis transformation was made:

$$\psi_1 = (111) \qquad \psi_8 = (222)$$

$$\psi_2 = (212) \qquad \psi_9 = (121)$$

$$\psi_3 = (313) \qquad \psi_{10} = (323)$$

$$\psi_4 = \frac{1}{\sqrt{2}}[(122) - (221)] \qquad \psi_{11} = \frac{1}{\sqrt{2}}[(211) - (112)]$$

$$\psi_5 = \frac{1}{\sqrt{2}}[(122) + (221)] \qquad \psi_{12} = \frac{1}{\sqrt{2}}[(211) + (112)]$$

$$\psi_6 = \frac{1}{\sqrt{2}}[(133) - (331)] \qquad \psi_{13} = \frac{1}{\sqrt{2}}[(332) - (233)]$$

$$\psi_7 = \frac{1}{\sqrt{2}}[(133) + (331)] \qquad \psi_{14} = \frac{1}{\sqrt{2}}[(332) + (233)]$$

ψ_{15} through ψ_{21} are the same as ψ_1 - ψ_7 with 1 and 3 interchanged

$$\psi_{22} = \frac{1}{\sqrt{2}}[(123) - (321)] \qquad \psi_{25} = \frac{1}{\sqrt{2}}[(132) + (312)]$$

$$\psi_{23} = \frac{1}{\sqrt{2}}[(123) + (321)] \qquad \psi_{26} = \frac{1}{\sqrt{2}}[(213) - (231)]$$

$$\psi_{24} = \frac{1}{\sqrt{2}}[(132) - (312)] \qquad \psi_{27} = \frac{1}{\sqrt{2}}[(213) - (231)] \,. \tag{97}$$

Table XXI. Matrix elements for the three-in-a-row model

	111	212	313	122	221	133	331	222	121	323	112	211	233	332	333	232	131	322	223	311	113	123	321	132	312	213	231
111	6	0	0	-4	-4	1	1																				
212	0	-8	0	-4	-4	0	0																				
313	0	0	2	0	0	1	1																				
122	-4	-4	0	4	0	-4	0																				
221	-4	-4	0	0	4	0	-4																				
133	1	0	1	-4	0	4	0																				
331	1	0	1	0	-4	0	4																				
222								16	0	0	-4	-4	-4	-4													
121								0	-8	0	-4	-4	0	0													
323								0	0	-8	0	0	-4	-4													
112								-4	-4	0	-1	0	0	1													
211								-4	-4	0	0	-1	1	0													
233								-4	0	-4	0	1	-1	0													
332								-4	0	-4	1	0	0	-1													
333															6	0	0	-4	-4	1	1						
232															0	-8	0	-4	-4	0	0						
131															0	0	2	0	0	1	1						
322															-4	-4	0	4	0	-4	0						
223															-4	-4	0	0	4	0	-4						
311															1	0	1	-4	0	4	0						
113															1	0	1	0	-4	0	4						
123																						-8	0	-4	0	-4	0
321																						0	-8	0	-4	0	-4
132																						-4	0	-3	1	0	0
312																						0	-4	1	-3	0	0
213																						-4	0	0	0	-3	1
231																						0	-4	0	0	1	-3

The result, after some rearrangement, is shown in Table XXII. The first and third 5 by 5's have eigenvalues of 13.085, 4, 1.602, 0, and -10.687. The second 5 by 5 has eigenvalues of 19.492, 1.403, 0, -11.403, and -11.492. The 3 by 3's have eigenvalues of 0, -4, -12, and 1.403, -2, -11.403, respectively. The first and third 2 by 2's have eigenvalues of 8, 0, and the middle 2 by 2 has eigenvalues of 0, -2. Note that two of the non-integral eigenvalues of the second 5 by 5 are degenerate with two of the second 3 by 3 eigenvalues. The eigenvalues are collected in Table XXIII, with the lowest subtracted out. The factor $3Q^2/100r^5$ is still factored out. The degeneracies are shown in parentheses. Two of the levels were combined for calculating purposes, as indicated. The levels are shown schematically in Fig. 39 and compared with the level system for two independent pairs. Since the latter system has 81 levels, its degeneracies have been divided by three to be comparable to the 27 levels of the present problem. It is clear that the two level systems are qualitatively different.

Table XXIII. Eigenvalues

31.492	(1)	
25.085	(2)	
20	(2)	
16	(2)	
13.602	(2)	13.500 (4)
13.403	(2)	
12	(7)	
10	(2)	
8	(1)	
1.313	(2)	
0.598	(2)	
0.508	(1)	
0	(1)	

Table XXII. Transformed matrix elements.

	1	2	3	5	7	4	6	8	9	10	12	14	11	13	15	16	17	19	21	18	20	22	24	26	23	25	27
1	6	0	0	$-\frac{8}{\sqrt{2}}$	$\frac{2}{\sqrt{2}}$																						
2	0	-8	0	$-\frac{8}{\sqrt{2}}$	0																						
3	0	0	2	0	$\frac{2}{\sqrt{2}}$																						
5	$-\frac{8}{\sqrt{2}}$	$-\frac{8}{\sqrt{2}}$	0	4	-4																						
7	$\frac{2}{\sqrt{2}}$	0	$\frac{2}{\sqrt{2}}$	-4	4																						
4						4	-4																				
6						-4	4																				
8								16	0	0	$-\frac{8}{\sqrt{2}}$	$-\frac{8}{\sqrt{2}}$															
9								0	-8	0	$-\frac{8}{\sqrt{2}}$	0															
10								0	0	-8	0	$-\frac{8}{\sqrt{2}}$															
12								$-\frac{8}{\sqrt{2}}$	$-\frac{8}{\sqrt{2}}$	0	-1	1															
14								$-\frac{8}{\sqrt{2}}$	0	$-\frac{8}{\sqrt{2}}$	1	-1															
11													-1	-1													
13													-1	-1													
15															6	0	0	$-\frac{8}{\sqrt{2}}$	$\frac{2}{\sqrt{2}}$								
16															0	-8	0	$-\frac{8}{\sqrt{2}}$	0								
17															0	0	2	0	$\frac{2}{\sqrt{2}}$								
19															$-\frac{8}{\sqrt{2}}$	$-\frac{8}{\sqrt{2}}$	0	4	-4								
21															$\frac{2}{\sqrt{2}}$	0	$\frac{2}{\sqrt{2}}$	-4	4								
18																				4	-4						
20																				-4	4						
22																						-8	-4	-4			
24																						-4	-4	0			
26																						-4	0	-4			
23																									-8	-4	-4
25																									-4	-2	0
27																									-4	0	-2

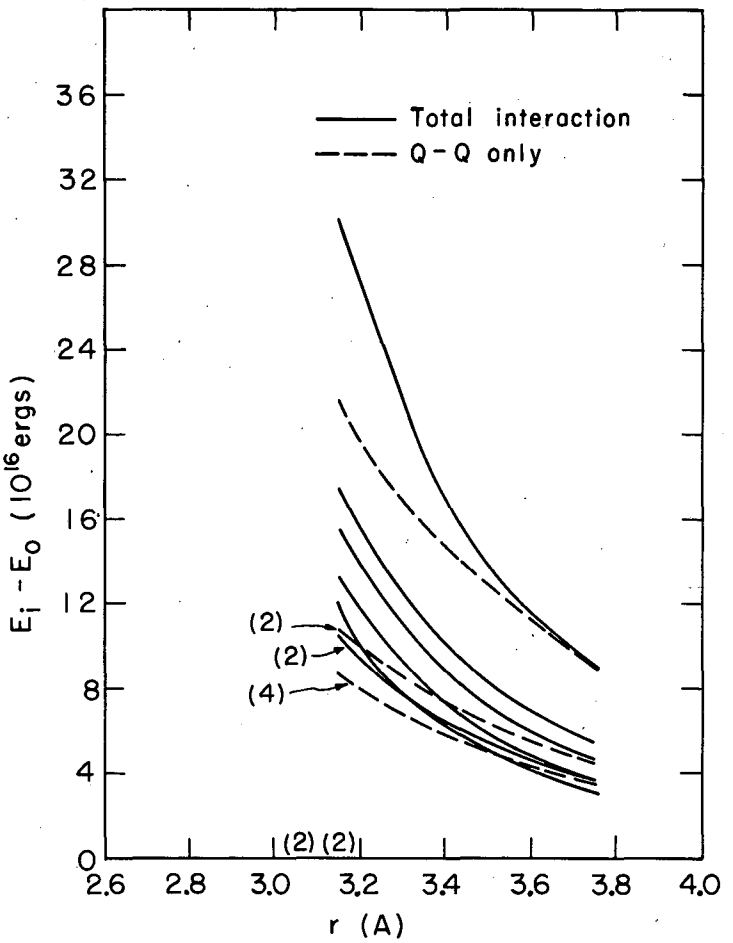

Fig. 38. The energy-level diagram for interaction between a pair of orthohydrogen molecules surrounded by para-hydrogen neighbors. The baseline represents the lowest level. — total interaction; --- quadrupole interaction. Parentheses indicate degeneracies.

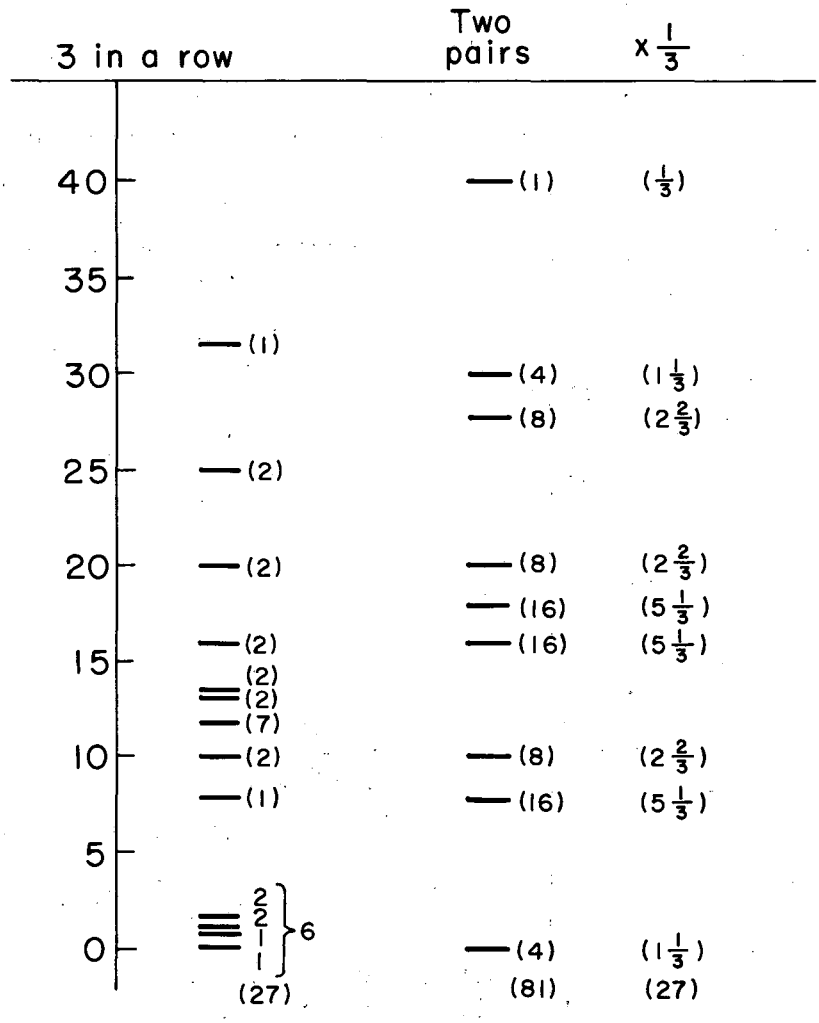

Fig. 39. Comparison of energy-level system for the "three-in-a-row" and isolated pair models.

Calculation of Heat Capacities from the Splittings

Rushbrooke has presented a simple discussion of this subject.[76] If the partition function is represented by

$$p.\ f. = \sum_i \omega_i\ e^{-\epsilon_i/kT}\ , \tag{98}$$

where ω_i is the degeneracy of the state having energy ϵ_i, we can write for the heat capacity of the system at constant volume

$$\frac{C_v}{R} = \frac{1}{(kT)^2}\ \frac{1}{(p.f.)^2}\left[\ (p.f.)\ (\sum_i \epsilon_i^{\ 2}\ \omega_i e^{-\epsilon_i/kT}) - (\sum_i \epsilon_i\ \omega_i\ e^{-\epsilon_i/kT})^2\ \right], \tag{99}$$

where R = Nk.

For the two-level system (upper level degenerate) and the three-level system (equal spacing), we have, respectively,

$$\frac{C_v}{xR} = \left(\frac{\epsilon}{kT}\right)^2 \frac{2e^{-\epsilon/kT}}{(1 + 2e^{-\epsilon/kT})^2} \tag{100}$$

and

$$\frac{C_v}{xR} = \left(\frac{\epsilon}{kT}\right)^2 e^{-\epsilon/kT}\left[\ \frac{1 + 4e^{-\epsilon/kT} + e^{-2\epsilon/kT}}{(1 + e^{-\epsilon/kT} + e^{-2\epsilon/kT})^2}\ \right]\ , \tag{101}$$

where ϵ is the energy spacing of the levels, and x is the mole fraction of ortho hydrogen. The heat capacity of the four-level pairwise quadrupolar interaction discussed below Table XVII is given as

$$\frac{C_v}{\frac{1}{2}\ RZx^2} = \left(\frac{\epsilon}{kT}\right)^2 (Ze^{-4\epsilon\ kT})$$

$$\left[\ \frac{64 + 50e^{-\epsilon/kT} + 4e^{-5\epsilon/kT} + 100e^{-6\epsilon/kT} + 72e^{-10\epsilon/kT} + 25e^{-11\epsilon/kT}}{(2 + 4e^{-4\epsilon/kT} + 2\ e^{-5\epsilon/kT} + e^{-10\epsilon/kT})\ 2}\ \right] \tag{102}$$

where $\epsilon = 3Q^2/50r^5$, z is the number of nearest neighbors, and x is the mole fraction of ortho hydrogen.

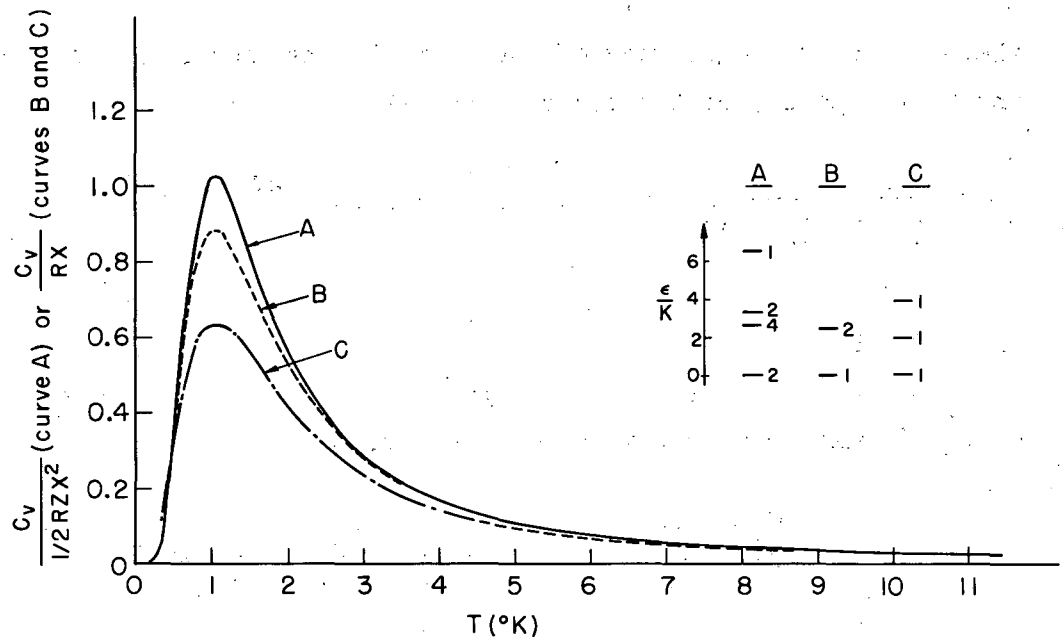

MU-23065

Fig. 40. Comparison of heat-capacity curves: (A) pairwise quadrupole interaction, (B) two-level Schottky model, (C) three-level Schottky model. Energies are per pair for A and per molecule for B and C.

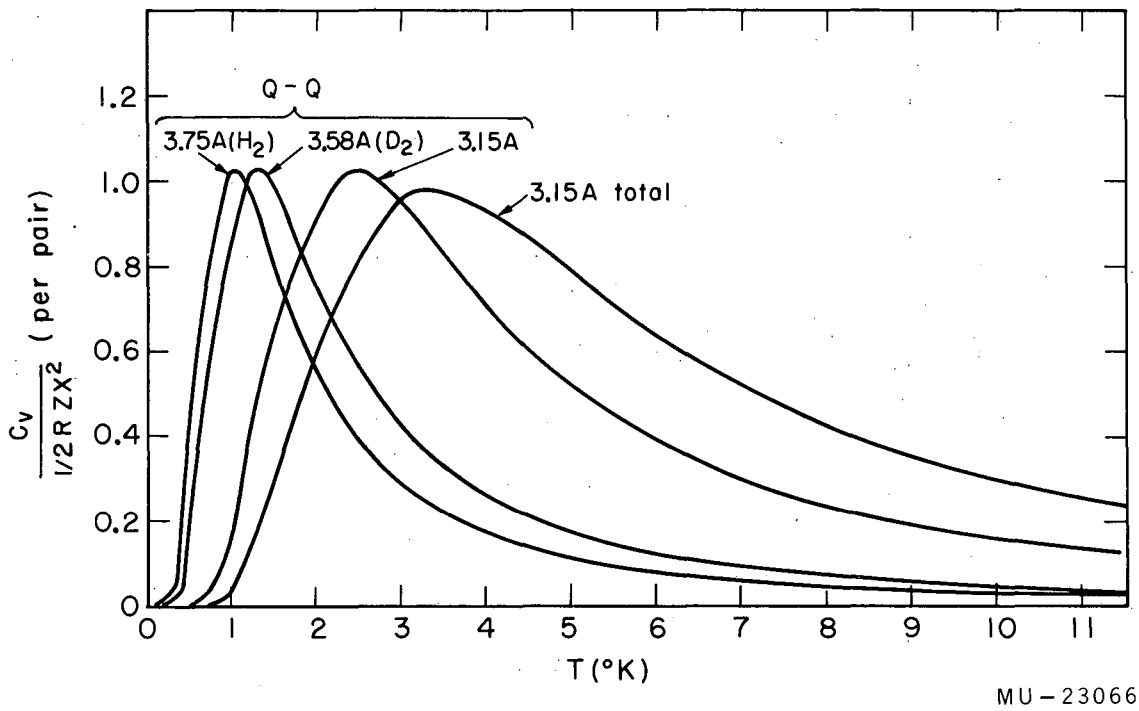

Fig. 41. Predicted anomalous heat capacity for various intermolecular distances.

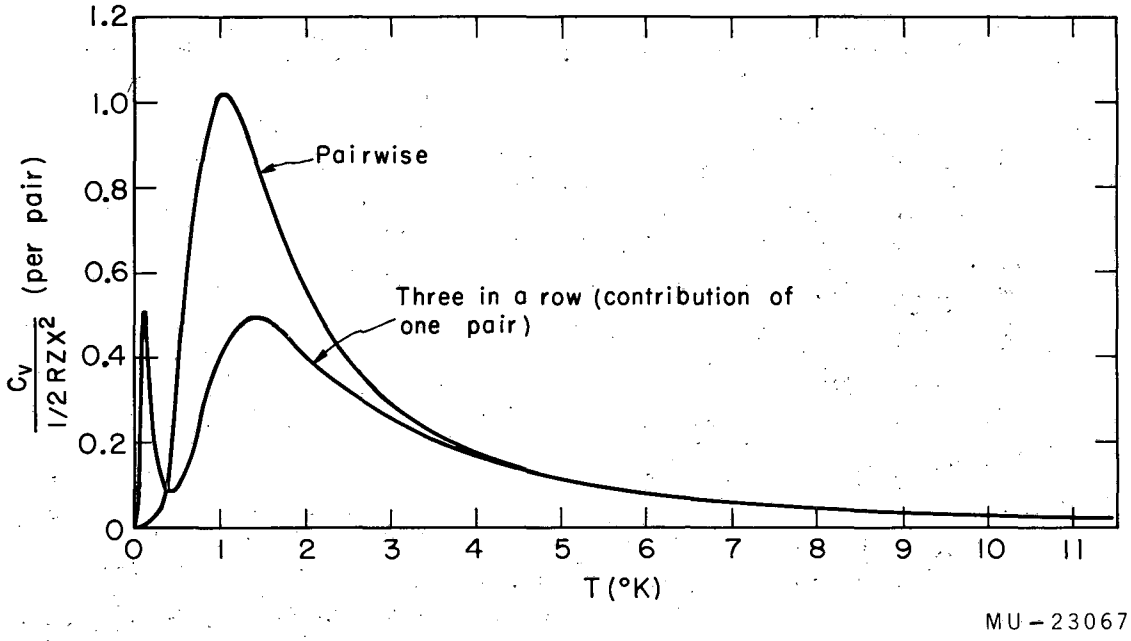

Fig. 42. Comparison of pairwise interaction with "three-in-a-row" model assuming quadrupole interaction at 3.75A.

The shapes of Eqs. (100), (101), and (102) are compared in Fig. 40. The 1-atm separation for solid hydrogen (3.75 A) was used for the calculations based on Eq. (102). In Eqs. (100) and 101), the curves were compressed by multiplying the temperature scales by 2.44 and 1.97, respectively, so that the maxima fell at about the same temperature as for Eq. (102).

In Fig. 41, the heat capacities for the quadrupolar interaction at 3.75, 3.58, and 3.15 A are plotted. The heat capacity resulting from the total interaction at 3.15 A is also plotted. Figure 42 compares the heat capacity of pairwise quadrupolar interaction at 3.75 A with the quadrupolar heat capacity per pair of three ortho molecules in a row at the same separation.

Statistical Considerations at Low Ortho Concentrations

Before the theoretical curves can be compared with the experimental data, the concentration dependence of the various types of interaction must be considered. If the mole fraction of ortho hydrogen is x, that of para 1 - x, and the number of nearest neighbors, z (taken as 12) the total number of ortho-ortho pairs per mole of solid hydrogen is given by N x/2 zx, where zx is the average number of ortho neighbors of an ortho molecule. Similarly, the number of ortho-para and para-para pairs are Nxz(1 - x) and N(1 - x)/2z(1 - x), respectively. The sum of the three terms is Nz/2, the total number of pairwise interactions in one mole of the crystal. This breakdown of the total number of pairs is based on the assumption of a random distribution of ortho and para hydrogen through the lattice.

If the mole fraction of ortho molecules having n neighboring ortho molecules is x_n, then the total number of ortho-ortho pairs is given by $N \frac{1}{2} \sum_{n=0}^{z} n x_n$. The probability of a given ortho molecule having n neighboring ortho molecules is given by the binomial coefficient

$$P_n = \frac{z!}{(z - n)!\, n!} (1 - x)^{z-n} x^n . \qquad (103)$$

The following relationships are also valid:

$$\sum_{n=0}^{z} P_n = 1; \sum_{n=0}^{z} n P_n = zx; \sum_{n=0}^{z} x_n = x; x_n = xP_n \qquad (104)$$

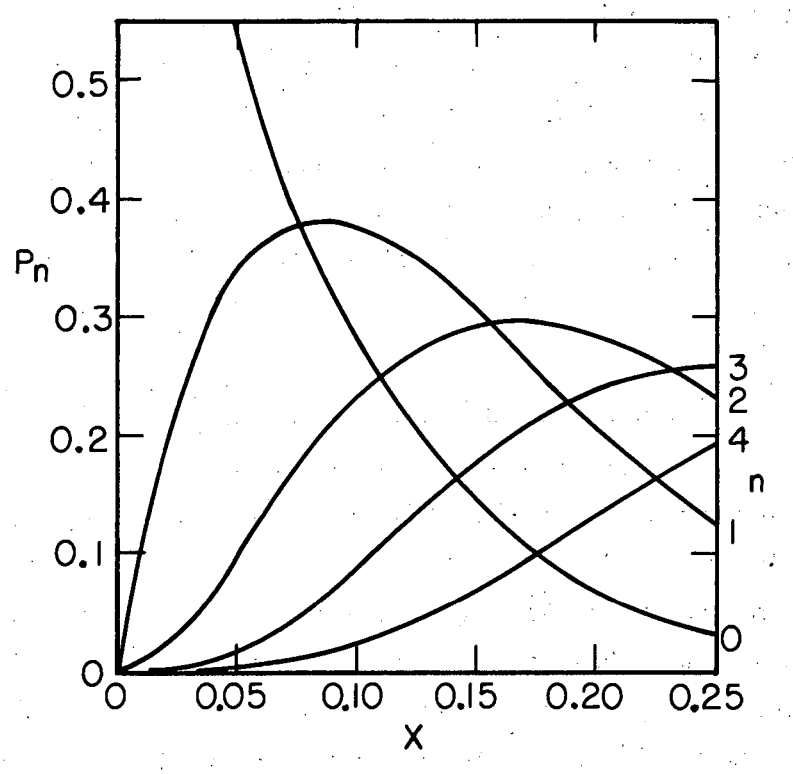

MU-23068

Fig. 43. Probability of n nearest-neighbor ortho molecules versus mole fraction.

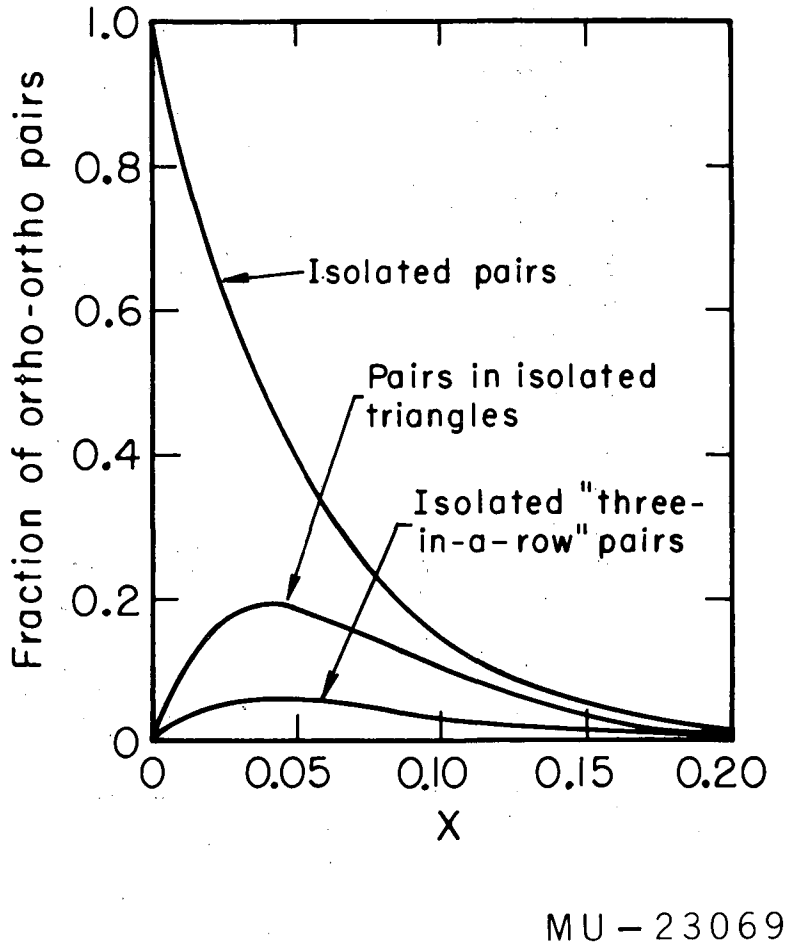

Fig. 44. Fraction of pairs with special configurations.

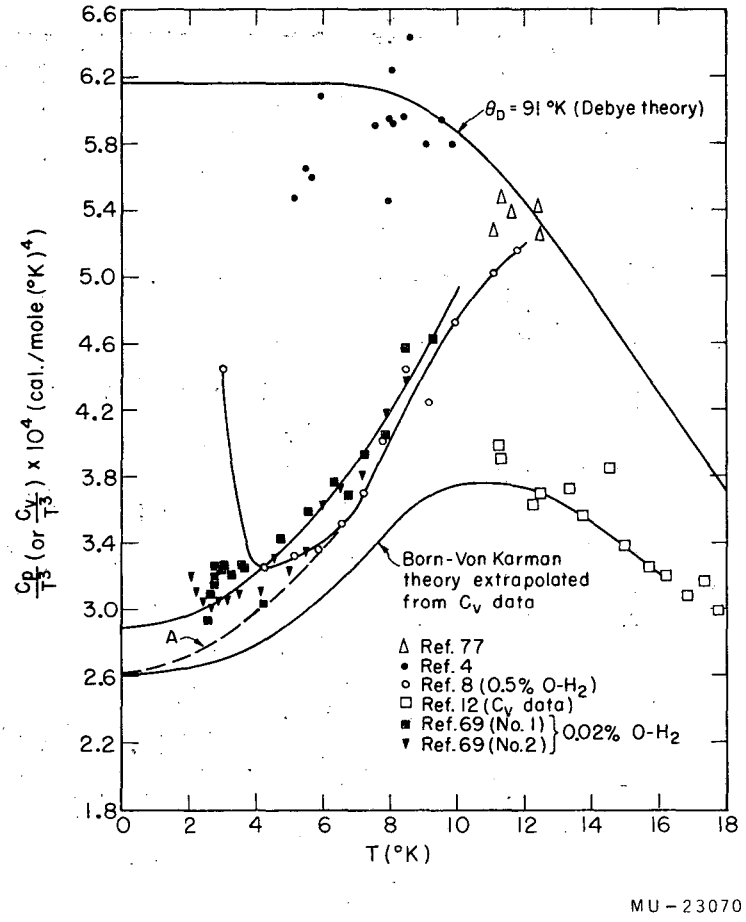

Fig. 45. Available C_p and C_v data for solid p-H_2.

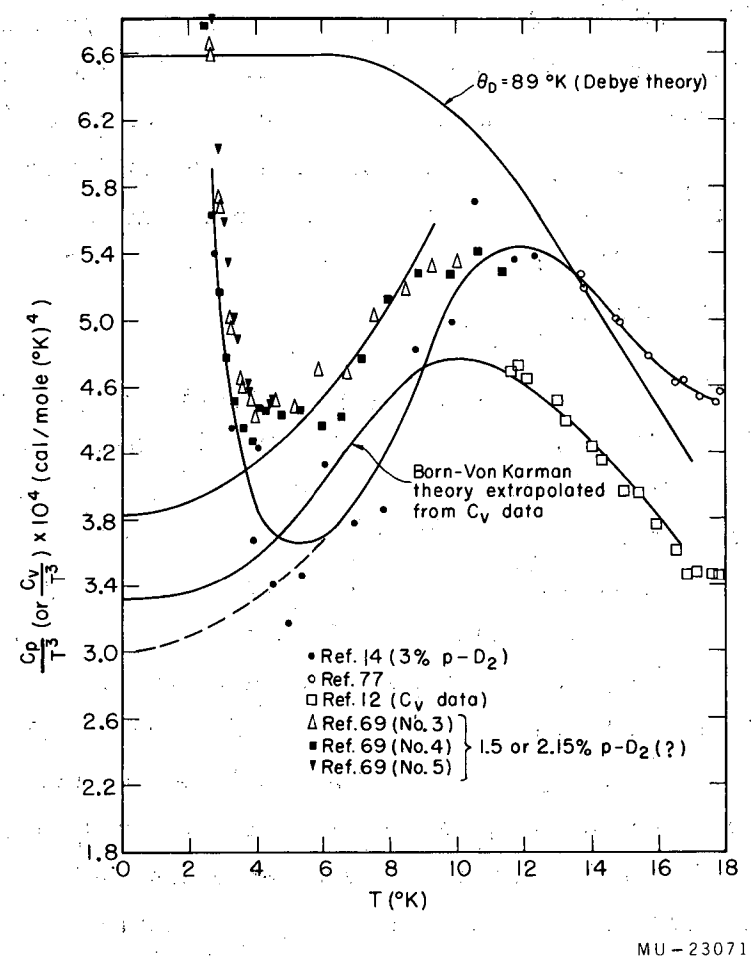

Fig. 46. Available C_p and C_v data for solid o-D_2.

The first few P_n are plotted in Fig. 43.

The above approach does not give the fraction of all ortho-ortho pairs that are isolated. An inspection of the geometry of the situation indicates that the probability of an ortho-ortho pair occurring, in an isolated state, is $zx(1 - x)^{18}$. (There are 18 neighbors of a pair in a close-packed structure.) The total number of such pairs per mole of solid hydrogen is $N\frac{1}{2}xzx(1 - x)^{18}$, and the fraction of all pairs that are isolated is $(1 - x)^{18}$. Similarly, the fraction of all pairs occurring in an isolated three-in-a-row configuration is $4x(1 - x)^{24}$, while the fraction occurring in isolated triangular configurations is $12x(1 - x)^{23}$. These fractions are shown in Fig. 44 as a function of the ortho concentration.

Analysis of Available One-Atmosphere Data

The available C_p and C_v data on solid p-H_2 and o-D_2 have been divided by T^3 and plotted versus T in Figs. 45 and 46, respectively. The theoretical Debye curves for $\Theta_D = 91^\circ K$ and $89^\circ K$ are included for comparison. These values were used originally to fit the C_p data. The high values obtained by Mendelssohn, Ruhemann, and Simon[4] are probably explained by incomplete elimination of exchange gas or by a high ortho hydrogen concentration. The Born-von Karman theory as calculated by Leighton[78] for a face-centered cubic lattice was fitted to the C_v data[12] and plotted to $0^\circ K$. Leighton's curve neglecting second-nearest-neighbor interaction gave the best fit of the C_v data. The curves drawn through Hill and Lounasmaa's data represent their fit,[69] while the curves through Hill and Ricketson's data[8] and Gonzalez, White, and Johnston's data[14] were drawn by the present writer.

Hill and Ricketson reported heat-capacity data for a series of concentrations of o-H_2 down to $2^\circ K$ (in addition to the data below $2^\circ K$ at the higher ortho concentrations).[8] The data were taken from the graph in the publication and the lattice heat capacity was subtracted using the smooth curve shown in Fig. 45 (Curve A). The resulting anomalous C_p is shown in Fig. 47. The units are cal/$^\circ K$ per mole of solid hydrogen (not per mole of ortho hydrogen).

The data have been integrated from the higher temperatures to give the anomalous heat content and entropy per mole of o-H_2 as shown in Figs. 48 and 49. Since the data do not extend through the anomaly, the reference point must be on the high-temperature side, hence the notation "H above T" and "S above T". The anomalous heat content is plotted against the anomalous entropy for each

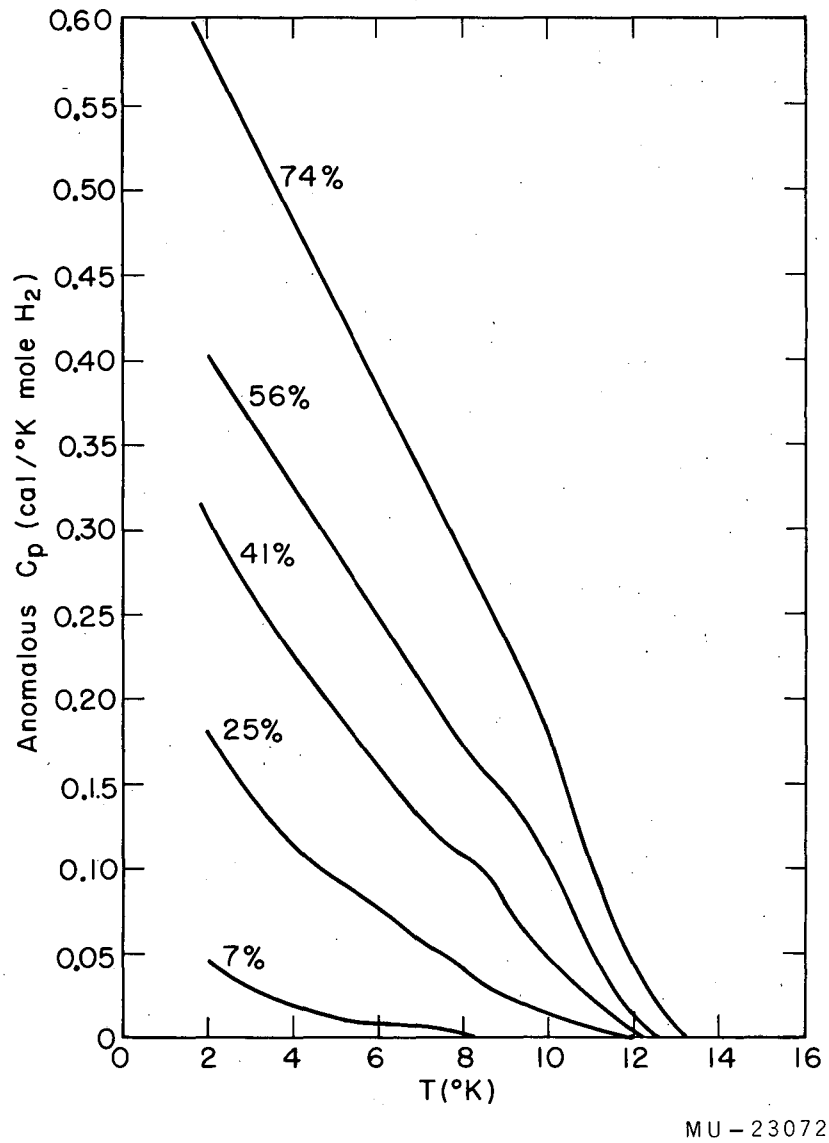

Fig. 47. Anomalous heat capacity data for o-H_2(Ref. 8).

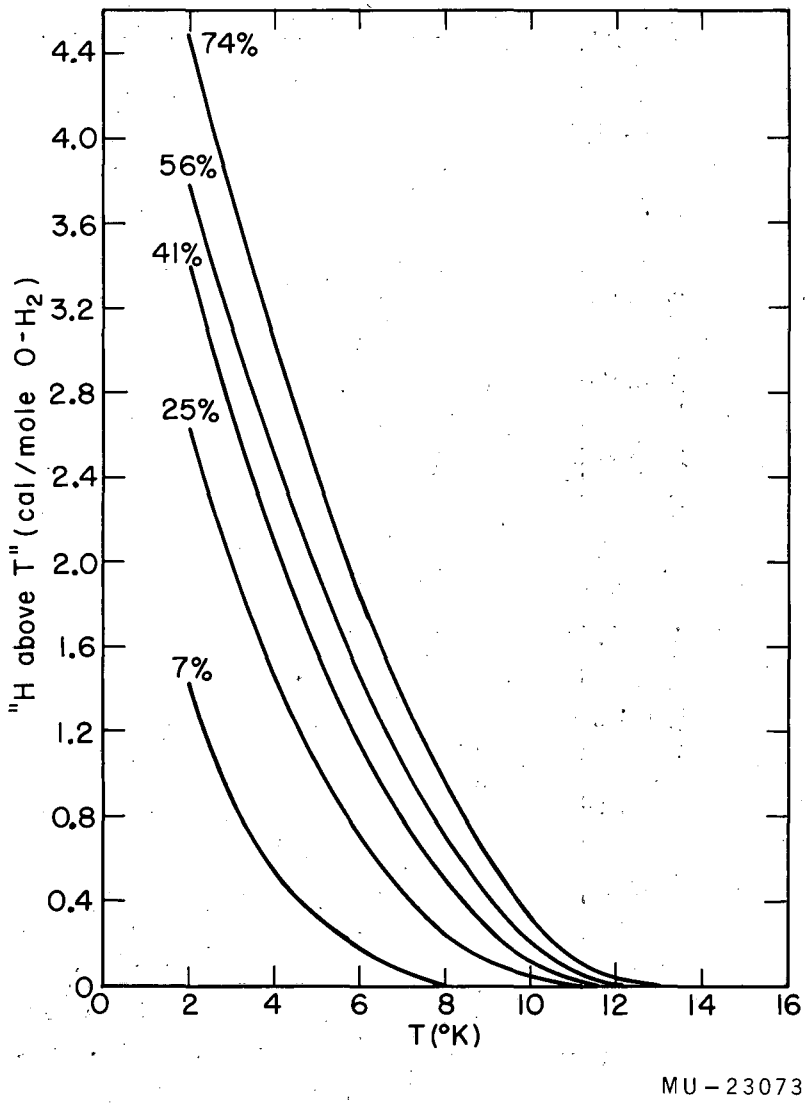

Fig. 48. Anomalous heat content of o-H_2.

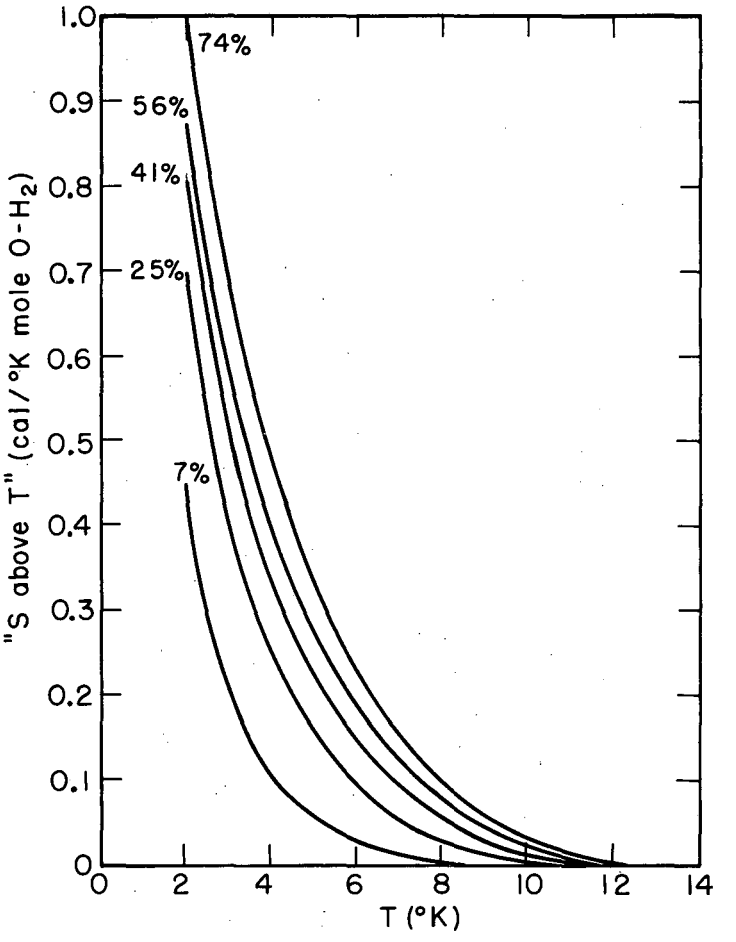

Fig. 49. Anomalous entropy of o-H_2.

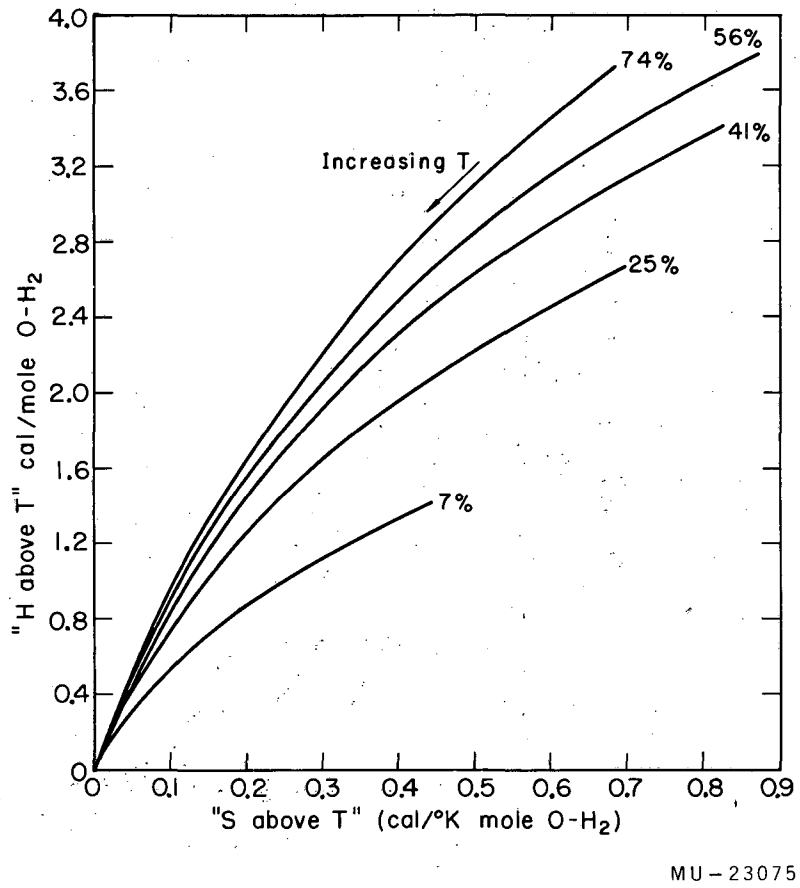

Fig. 50. Anomalous heat content versus anomalous entropy for o-H_2.

concentration of o-H_2 in Fig. 50. Temperature is a parameter on this plot, increasing toward the origin. In order to compare the anomalous contributions to the heat capacity with the theoretical expressions, Hill and Ricketson's 7% and 0.5% data have been plotted in Fig. 51 and 52, respectively.[8] The data of Gonzalez et al on 3% o-D_2 have been plotted in Fig. 53,[14] and Hill and Lounasmaa's data on "nominal" o-D_2 have been plotted in Fig. 54.[69] The nominal p-D_2 concentration of the latter data was 1.5% or 2.15%, depending on whether the sample was equilibrated at the hydrogen boiling point or at the deuterium triple point. Unfortunately, the authors did not report this information.

For the 7% o-H_2 case, it can be seen from Fig. 43 that $(1 - x)^{12}$ or 0.406 of the ortho molecules have all p-H_2 nearest neighbors. Figure 44 indicates that of all the ortho-ortho pairs, $(1 - x)^{18}$ or 0.271 are "isolated," i.e., completely surrounded by p-H_2 nearest neighbors. If the molar heat capacity of isolated o-H_2 molecules is designated by C_a, that of isolated pairs by C_b, and that of pairs in more complicated configurations by C_c, the anomalous heat-capacity expression may be written

$$C_p = x\,(1 - x)^{12}\,C_a + \frac{1}{2}\,(12)\,x^2 \left[(1 - x)^{18}\,C_b + \left\{1 - (1 - x)^{18}\right\} C_c \right] \quad (105)$$

where x is the o-H_2 mole fraction. If one assumes that C_c is given by the "three-in-a-row" calculation, then the pairwise contributions may be calculated. Since many other types of configuration appear besides the "three-in-a-row" type, the above expression leads to some uncertainty in the theoretical expression for C_c. Thus the C_b and C_c contributions have been plotted separately in Fig. 51 for the 7% o-H_2. The values of the theoretical curves were obtained from Fig. 42. As was observed by Nakamura,[70] the theoretical curves account for only one-half of the magnitude of the data. The residual heat capacities were then fitted to the two and three-level anomalies described in Eqs. (100) and (101) and plotted in Fig. 40. (The three-level model was included merely because it was convenient and not for any theoretical reason.) As may be seen from Fig. 51, both models can be fitted to the data by adjusting the temperature scale. One then finds the splitting, ϵ, given by 3.59×10^{-16} ergs for the two-level model and by 2.61×10^{-16} ergs for the three-level model. In order to obtain these numbers, Eq. (105) was used, with the resulting assumption that the effect causing the splitting in the

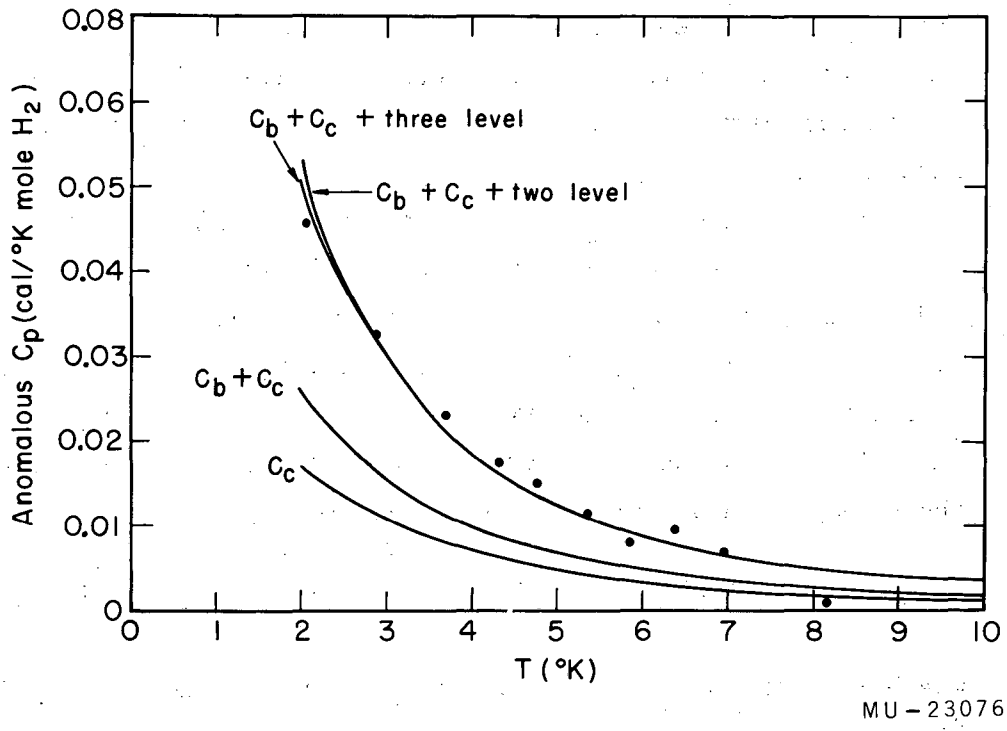

Fig. 51. Comparison of 7% o-H_2 data with theory.

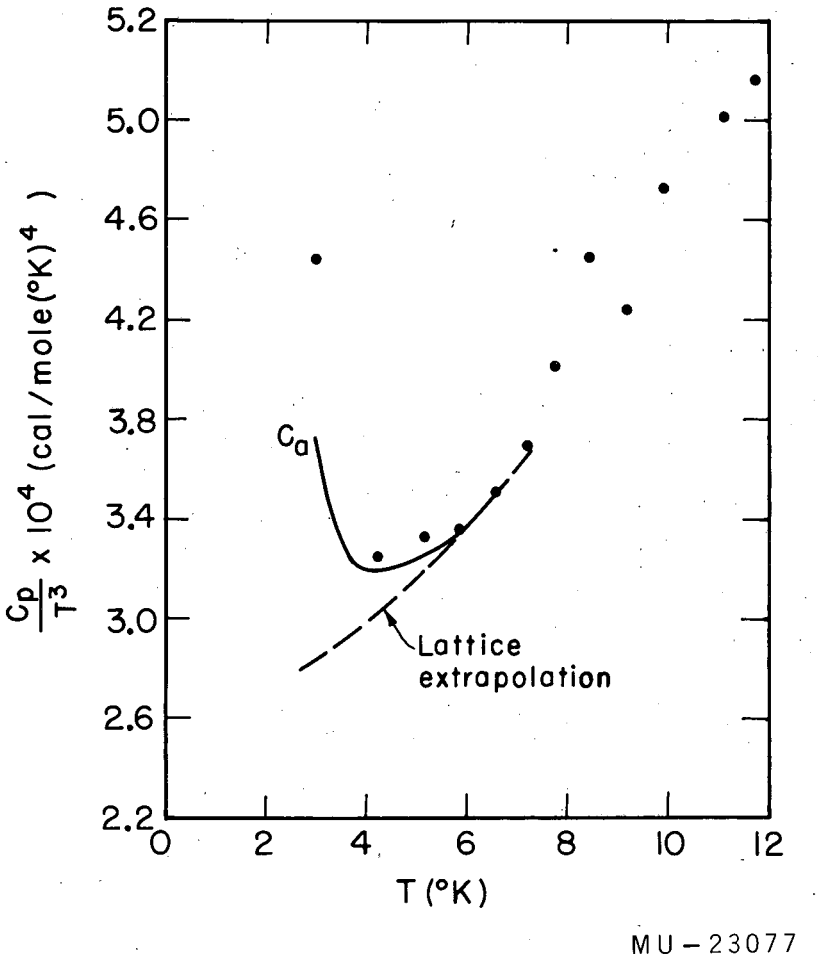

Fig. 52. Comparison of 0.5% o-H_2 data with theory.

isolated ortho molecules does not appreciably change the contribution of the ortho-ortho pairs to the heat capacity. This is a reasonable approximation, since a moderate change in the energy-level diagram for the pairwise interaction should have only a secondary effect on the magnitude of the heat-capacity contribution. Using the two-level model, Nakamura obtained a value of $\epsilon = 2 \times 10^{-16}$ ergs because he did not include the factor $(1 - x)^{12}$ in Eq. (105).

For the 0.5% o-H_2 case, the contributions of C_b and C_c were negligible. The value of C_a obtained from the 7% data was used with Eq. (105) to evaluate this contribution at 0.5%, and the result is shown in Fig. 52. The agreement must be considered satisfactory, and provides a test of the reality of the C_a effect. It is interesting to comment at this point on a different approach in analyzing the data. If it is assumed that C_a is zero, one may calculate what ortho concentration is required to give agreement with the pairwise theory. Values of 9.9% and 3.5 % are obtained for the 7% and 0.5% cases, respectively. It is interesting that a difference of 3% is obtained in each case. Since Hill and Ricketson did not publish an account of their analysis procedure or of the history of their samples,[8] the possibility of a 3% shift in the low end of their concentration scale cannot be definitely ruled out.

The 3% p-D_2 data of Gonzalez et al[14] are shown in Fig. 53. In this case, $(1 - x)^{12}$ or 0.694 of the p-D_2 molecules have all o-D_2 neighbors, while $(1 - x)^{18}$ or 0.578 of the para-para pairs are isolated. The temperature scale of Fig. 42 was divided by $(3.75/3.58)^5 = 1.26$ (the fifth power of the ratio of intermolecular distances in solid hydrogen and deuterium) to expand the theoretical curves of Fig. 42. The C_b and C_c contributions were then plotted in Fig. 53 in the same manner as for the 7% o-H_2. It can be seen that the agreement is very close. However, a rereading of the original paper[14] indicated that the deuterium had been equilibrated in an activated-charcoal trap at 20.4° K, yielding a concentration of 2.2% p-D_2. The liquid was then presumably removed from the trap and warmed to 23° K (equilibrium concentration 3.5%) to speed up the transfer to the calorimeter. Unpublished data of the authors on the homogeneous conversion in liquid D_2 were used to calculate the increase in concentration from 2.2% to 3% during the transfer operation, so that the possibility of a concentration uncertainty also exists for these data. Thus it is possible that the good fit on Fig. 53 is fortuitous, and that a C_a contribution (Eq. (105)) might be required here also.

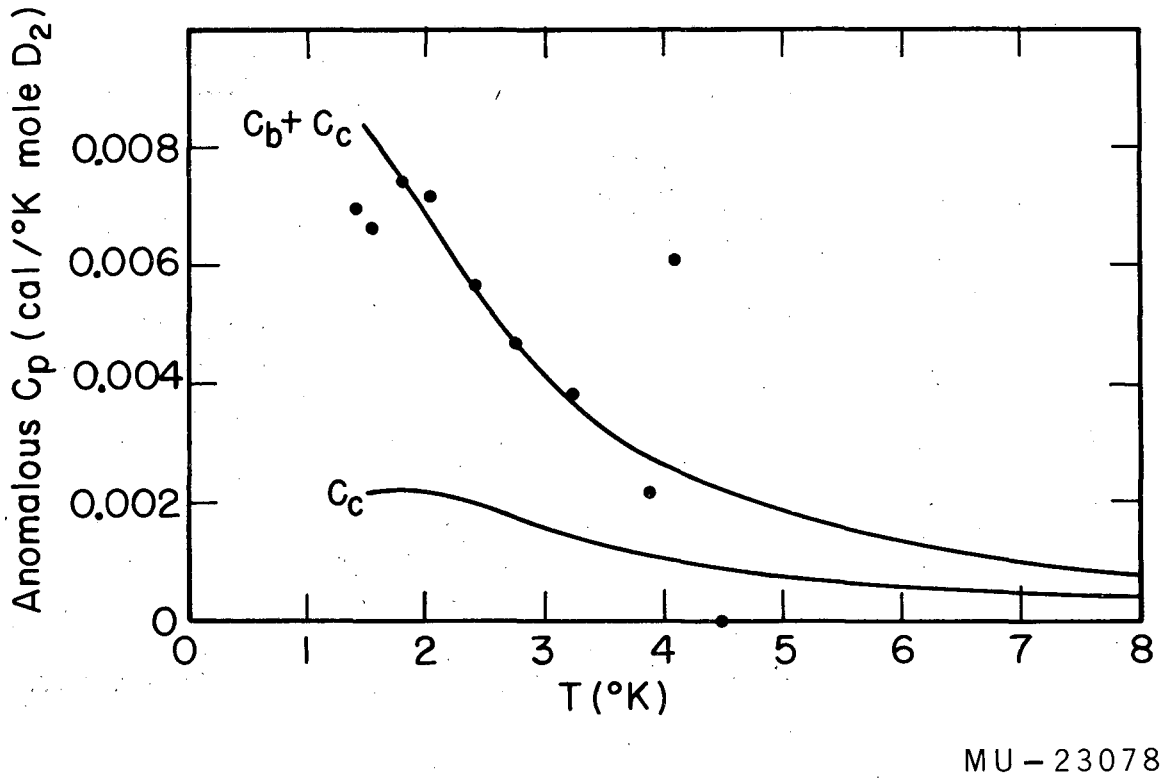

Fig. 53. Comparison of 3% p-D_2 data with theory.

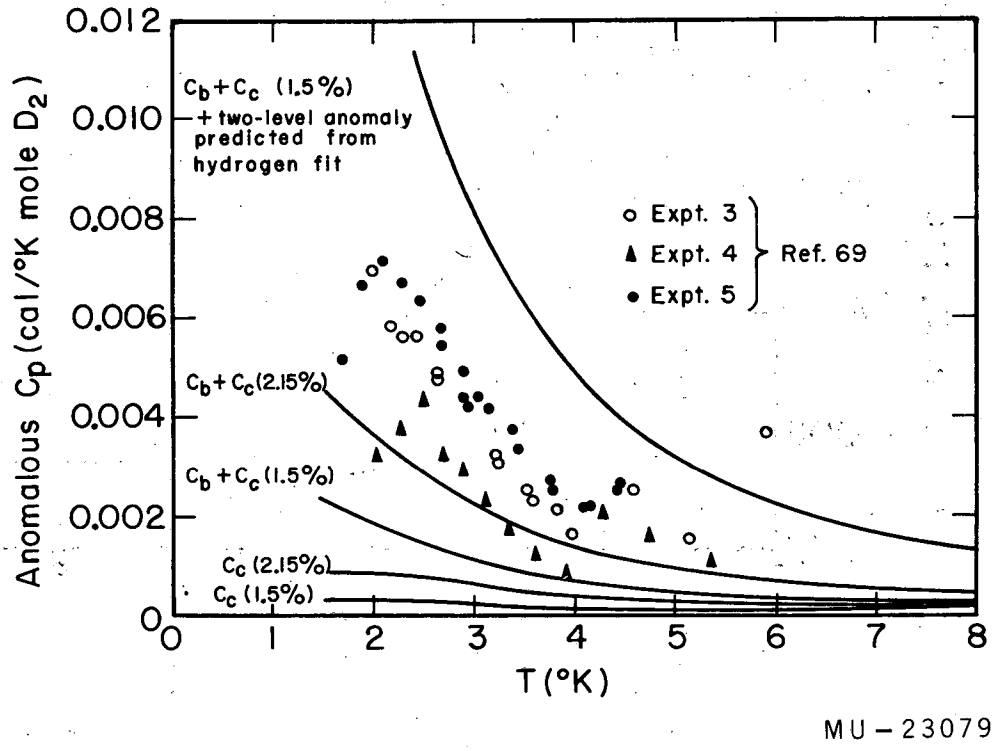

Fig. 54. Comparison of 1.5 or 2.15% p-D_2 with theory.

The data of Hill and Lounasmaa[69] on 1.5% or 2.15% p-D_2 are shown in Fig. 54. The theoretical C_b and C_c contributions are shown for both contributions. The C_a contribution predicted by the hydrogen data is also plotted for 1.5% p-D_2. If the C_a effect is due to translational effects in the lattice as suggested by Nakamura,[70] one might expect the effect to be smaller for deuterium than for hydrogen.

The above analysis of the data on the o-H_2 and p-D_2 anomaly at low concentration indicates that there probably is a term in the heat capacity proportional to the concentration, although more precise and more carefully defined data would make the conclusion more certain. It seems likely that part of the splitting of the levels of isolated ortho molecules is caused by second-nearest-neighbor effects, and this phenomenon should be considered when comparing the data with theories based on translational effects.

Comment on London's Theory

London[29] suggested that "the initial work of compression in solid hydrogen is mainly used to reduce space for the molecules by confining their rotational motion to a smaller angle rather than to drive the molecules deeper into their mutual Van der Waals repulsion field."[29] On this basis he reasoned that "quenching" of the rotational motion should occur when the energy supplied by compression was at least sufficient to raise the ground state ($J = 0$) to the level of the first excited state ($J = 1$). This corresponds to 340 cal/mole for H_2 and 170 cal/mole for D_2. The pressures necessary to supply such an energy of compression were estimated to be 5500 and 4000 kg/cm^2 for H_2 and D_2, respectively.

The above reasoning seems inconsistent with the work of Hobbs[16] on the zero-point energy of H_2, HD, and D_2 (which, incidentally, was suggested by London). A casual observation of the curves in Hobbs paper indicates that between 1 and 5000 kg/cm^2, the potential energy of solid hydrogen decreases about 100 cal/mole, while the zero-point energy rises 400 to 500 cal/mole, giving a net energy increase of about 300 cal/mole. Thus it would be more correct to say that between 1 and 5000 kg/cm^2, the energy of compression only increases the zero-point energy of the lattice. London's estimate of the pressure necessary to "quench" the rotation still seems valid, however, because above 5000 kg/cm^2, the repulsive potential energy rises very steeply.

ACKNOWLEDGMENTS

The author is grateful to Professor Kenneth S. Pitzer for his many timely suggestions and for his understanding and patient guidance during the course of this work.

The author is also indebted to Professor N. E. Phillips for many illuminating discussions on low-temperature calorimetric technique.

It is a pleasure to acknowledge the collaboration of Mr. R. S. Hickman of the Lawrence Radiation Laboratory Mechanical Engineering Department on the design of the high-pressure system and the mechanical design of the calorimeter. The expert and efficient aid of Mr. E. C. Miner of the Radiation Laboratory Mechanical Engineering Department in the design and construction of many of the necessary components of the apparatus greatly expedited the progress of the project.

The enthusiastic cooperation of Mr. J. Beuneman of the Chemistry Department Shop was indispensible in assembling and improving the apparatus. The assistance of Mr. H. Wandesford of the Accelerator Technician Shop is also to be acknowledged. Aid in secretarial matters was excellently provided by Mrs. Jane Waite.

The author also wishes to acknowledge the collaboration of Mr. Gunter Ahlers and a conversation with Mr. L. V. Gregor.

The author is indebted to the Bell Telephone Laboratories and the National Science Foundation for predoctoral fellowships during 1958-59 and 1959-60, respectively, and to the United States Atomic Energy Commission for other support of this project.

APPENDICES

A. Assembly and Disassembly of the Calorimeter

The following comments should be of use in further work on the calorimeter, since there is a certain sequence of operations that should be followed in taking it apart and putting it together if damage is to be avoided. The procedure is as follows:

1. Remove the vacuum can bottom by unbolting the flange at D.
2. Remove the copper radiation baffle at DD and unglue the thermocouple from the bottom of the liquid-nitrogen shield; then unbolt the shield and drop it into the vacuum can.
3. The vacuum can and liquid-nitrogen-shield bottoms may then be lifted out of the pressure shield.
4. Unglue the thermocouple on the outer bath shield, unbolt it at Q, and remove, being careful not to damage the wires underneath it.
5. Unsolder and unbolt the front half of the isothermal shield for access to the cell.
6. To remove the cell from the calorimeter, simply disconnect it and pull it out with the capillaries through flange Y.
7. If it is desired to raise the inner and outer bath, or the liquid-nitrogen reservoir, the cell must be disconnected from these parts and can be clamped to the flange of the vacuum can.
8. Disconnect the vacuum and vapor pressure lines at the top, and using the eyebolts, raise flanges B and C together and hoist several inches so that the top of the liquid-nitrogen shield can be pulled out.
9. Lower the flanges and then raise C by itself. This operation requires two people -- one hoisting and the other guiding the assembly to avoid damaging the wires.
10. Assembling the calorimeter is simply the reverse of the above operations.

B. Summary of Useful Formulas for Thick-Walled Cylinders[44]

Elastic Behavior

The symbols used are:

σ_r	=	radial stress
σ_t	=	tangential stress
ν	=	Poisson's ratio
K	=	r_2/r_1 where r_2 = outer and r_1 = inner radius
P_1, P_2	=	inner, outer pressures, respectively
E	=	Young's modulus.

Stresses

$$\sigma_t = \frac{P_1 - P_2K^2 + (r_2/r)^2 (P_1 - P_2)}{K^2 - 1} \tag{B1}$$

$$\sigma_r = - \frac{P_2K^2 - P_1 + (r_2/r)^2 (P_1 - P_2)}{K^2 - 1} \tag{B2}$$

$$\sigma_z = \frac{P_1}{K^2 - 1} \tag{B3}$$

Strains

$$\frac{\epsilon_r E}{P_1} = - \frac{2\nu - 1 + (1-\nu)K^2 \frac{P_2}{P_1} + (1 + \nu)\left(1 - \frac{P_2}{P_1}\right)\left(\frac{r_2}{r}\right)^2}{K^2 - 1} \tag{B4}$$

$$\frac{\epsilon_t E}{P_1} = \frac{1 - 2\nu + (\nu - 1) \frac{P_2}{P_1} K^2 + (1 + \nu)\left(1 - \frac{P_2}{P_1}\right)\left(\frac{r_2}{r}\right)^2}{K^2 - 1} \tag{B5}$$

$$\frac{\epsilon_z E}{P_1} = \frac{1 - 2\nu + 2\nu K^2 \frac{P_2}{P_1}}{K^2 - 1} \tag{B6}$$

Limits of Elastic Behavior

The limit of elastic behavior determined on a tensile test specimen cannot be applied directly to thick-walled cylinders because these involve stresses in several directions. The simplest criterion seems to come from the maximum-shearing-stress theory: The limit of elastic action occurs when the shearing stress at any point due to any combination of stresses exceeds the shearing proportional limit of the material. The shearing stress at any radius is expressed by

$$\tau = \frac{K^2(P_1-P_2)}{r^2(K^2-1)} \quad . \tag{B8}$$

Inelastic Behavior

When the pressure is released, the parts stretched inelastically behave elastically. If one assumes that the stress-strain curve is flat beyond the yield point (no strain-hardening or work-hardening effects), and if σ_y is the yield strength and r_e is the radius of the outer edge of inelastic action, then one has

$$\sigma_r = \frac{\sigma_y}{\sqrt{3}}\left(\frac{r_2^2 - r_e^2}{r_2^2} + 2 \ln \frac{r_e}{r}\right), \tag{B9}$$

$$\sigma_t = \frac{\sigma_y}{\sqrt{3}}\left(\frac{r_2^2 + r_e^2}{r_2^2} - 2 \ln \frac{r_e}{r}\right), \tag{B10}$$

and

$$\sigma_z = \frac{\sigma_y}{\sqrt{3}}\left(\frac{r_e^2}{r_2^2} - 2 \ln \frac{r_e}{r}\right) \quad . \tag{B11}$$

Inelastic Strains

The inelastic strains may be calculated by recognizing that the volume of an element remains essentially constant as the inelastic strains are increased. Assuming the inelastic region extends throughout the wall to the outer radius, one obtains

$$\sigma_t = (\epsilon_t)_{r_2} \left[\left(\frac{r_2}{r} \right)^2 \left(1 - \frac{\nu}{2} \right) + \frac{\nu}{2} \right] . \tag{B12}$$

The strain at the outer surface is given approximately by

$$(\epsilon_t)_{r_2} = \epsilon_y \frac{\sqrt{3}}{2} \left[\left(\frac{\epsilon_z}{\epsilon_t} \right)^2 + \frac{\epsilon_z}{\epsilon_t} + 1 \right]^{-1/2} . \tag{B13}$$

An expression for the elastic breakdown pressure, P_y, is given by

$$P_y = \frac{\sigma_y}{\sqrt{3}} \frac{K^2-1}{K^2} . \tag{B14}$$

The above agreed with experiment to 15% when residual stresses were allowed for and to 50% otherwise. The overstrain pressure, P_o (the elastic breakdown at the outer radius), is given by

$$P_o = \frac{2\sigma_y}{\sqrt{3}} \ln K . \tag{B15}$$

The strain at the bore at the elastic breakdown pressure is

$$(\epsilon_t)_{y_1} = \frac{P_y}{E(K^2-1)} \left[(K^2+1) + \nu (K^2-2) \right] . \tag{B16}$$

REFERENCES

1. W. H. Keeson, J. DeSmedt, and H. H. Mooy, Communs. Phys. Lab. Univ. Leiden 209d (1930).
2. V. S. Kogan, B. G. Lazarev, and R. F. Bulatova, Soviet Phys. JETP 4, 593 (1957).
3. V. S. Kogan, B. G. Lazarev, and R. F. Bulatova, Soviet Phys. JETP 7, 165 (1958).
4. K. Mendelssohn, M. Ruhemann, and F. Simon, Z. physik. Chem. (Leipzig) B15, 121 (1931).
5. L. Pauling, Phys. Rev. 36, 430 (1930).
6. F. Simon, Ergeb. exakt. Naturw. 9, 260, 269 (1930).
7. K. Schaefer, Z. physik. Chem. (Leipzig) B42, 380 (1939).
8. R. W. Hill and B. W. A. Ricketson, Phil. Mag. 45, 277 (1954).
9. R. W. Hill and B. W. A. Ricketson, and F. Simon, Conf. de Phys. des Basses Temp. (Simon et Cie., Paris 1955), No. 76, p. 317.
10. K. Tomita, Proc. Phys. Soc. (London) A68, 214 (1955).
11. K. Clusius and E. Bartholome, Z. physik. Chem. (Leipzig) B30, 237 (1935).
12. E. Bartholome and A. Eucken, Z. Elektrochem. 42, 547 (1936).
13. H. D. Megaw, Phil. Mag. 28, 129 (1939).
14. O. D. Gonzalez, D. White, and H. L. Johnston, J. Phys. Chem., 61, 773 (1957).
15. F. London, Proc. Roy. Soc. (London) A153, 576 (1936).
16. M. Hobbs, J. Chem. Phys. 7, 318 (1939).
17. E. Cremer and M. Polanyi, Z. physik. Chem. (Leipzig) B21, 459 (1933).
18. E. Cremer, Z. physik. Chem. (Leipzig) B39, 445 (1938).
19. E. Cremer, Z. physik. Chem. (Leipzig) B28, 199 (1935).
20. B. V. Rollin and E. Watson, Conf. de Phys. des Basses Temp. (Simon et Cie., 1955) No. 63.
21. M. Bloom, Physica 23, 767 (1957).
22. G. W. Smith and C. F. Squire, Phys. Rev. 111, 188 (1958).
23. K. Motizuki and T. Nagamiya, J. Phys. Soc. Japan 11, 93 (1956).
24. K. Motizuki, J. Phys. Soc. Japan 12, 163 (1957).
25. F. Reif and E. M. Purcell, Phys. Rev. 91, 631 (1953).
26. F. Simon, Nature 133, 529 (1934).
27. J. A. Stewart, Phys. Rev. 97, 578 (1955).

28. J. A. Stewart, J. Phys. Chem. Solids 1, 146 (1956).

29. F. London, Phys. Rev. 102, 168 (1956).

30. K. S. Pitzer, Quantum Chemistry (Prentice-Hall, Inc., New York 1953) p. 327.

31. J. deBoer, Physica 9, 363 (1942).

32. W. D. McCormick and W. M. Fairbank, Bull. Am. Phys. Soc. [2] 3, 166 (1958).

33. R. Berman, J. Appl. Phys. 27, 318 (1956).

34. J. R. Clement and E. H. Quinnell, Rev. Sci. Instr. 23, 213 (1952).

35. J. R. Clement, E. H. Quinnell, M. C. Steele, R. A. Hein, and R. L. Solecek, Rev. Sci. Instr. 24, 545 (1953).

36. R. Berman, Rev. Sci. Instr. 25, 94 (1954).

37. J. S. Dugdale and F. E. Simon, Proc. Roy. Soc. (London) A218, 291 (1953).

38. P. W. Bridgman, The Physics of High Pressure (G. Bell and Sons, London, 1958), p. 406.

39. O. L. Anderson, Some Safety Problems Associated With High Pressure Equipment. Obtained from Mr. D. H. Newhall of the Harwood Engineering Co., Walpole, Mass.

40. W. Paul and D. M. Warshauer, Rev. Sci. Instr. 27, 418 (1956).

41. W. Paul, G. B. Benedek, and D. M. Warshauer, Rev. Sci. Instr. 30, 874 (1959).

42. K. S. Pitzer, Dept. of Chemistry, University of California, Berkeley, unpublished tables.

43. C. A. Swenson, Phys. Rev. 99, 423 (1955).

44. E. W. Comings, High Pressure Technology, Chapter 6 (McGraw-Hill Book Co., New York, N. Y., 1956).

45. Private communication from Professor G. Benedek of Harvard University August 1960.

46. D. H. Weitzel and O. E. Park, Rev. Sci. Instr. 27, 57 (1956).

47. D. H. Weitzel, W. V. Loebenstein, J. W. Draper, and O. E. Park, J. Research Nat. Bur. Standards 60, 221 (1958).

48. M. Konecnik, Laboratory Note, NBS Cryogenic Engineering Laboratory, Project No. 8123, File No. 59-8, July 2, 1959.

49. C. M. Cunningham , D. S. Chapin, and H. L. Johnston, J. Am. Chem. Soc. 80, 2382 (1958).

50. D. S. Chapin and H. L. Johnston, J. Am. Chem. Soc. 79, 2406 (1957).

51. E. H. Kennard, Kinetic Theory of Gases (McGraw-Hill Book Co., New York, 1938) Chapter IV pp. 162-5, 180-4.

52. J. O. Hirschfelder, C. F. Curtiss, and R. B. Bird, Molecular Theory of Liquids and Gases (John Wiley and Sons, Inc., New York, 1954) Chapters 7 and 8.

53. A. Farkas, Orthohydrogen, Parahydrogen, and Heavy Hydrogen (Cambridge University Press, Cambridge 1935).

54. E. R. Grilly, Rev. Sci. Instr. 24, 72 (1953).

55. H. W. Woolley, R. B. Scott, and F. G. Brickwedde, J. Research Nat. Bur. Standards 41, 379 (1948).

56. H. Van Duk and M. Durieux, Helium Vapor Pressure Scale T_{L55}, K. Onnes Laboratory, Leiden.

57. W. DeSorbo and G. E. Nichols, J. Phys. Chem. Solids 6, 352 (1958).

58. J. R. Clement, presented at 10th Annual Calorimetry Conference, General Electric Research Laboratory, Schenectady, New York (Sept. 1954).

59. Nat. Bur. Standards (U.S.) Ann. Rept. Circ. 556.

60. American Institute of Physics Handbook (McGraw-Hill Book Co., New York 1957).

61. R. B. Scott, Cryogenic Engineering (D. Van Nostrand Co., 1959).

62. F. B. Hildebrand, Advanced Calculus for Engineers (Prentice-Hall, Inc., New York, 1948).

63. M. Michels, W. de Graff, T. Wassenaar, J. M. Levelt, P. Louwerse, Physica 25, 25 (1959).

64. H. L. Johnston and D. White, Trans. ASME, 785 (August 1950).

65. F. E. Simon, M. Ruhemann, and W. A. M. Edwards, Z. physik. Chem. B6, 331 (1930).

66. R. L. Mills and E. R. Grilly, Phys. Rev. 101, 1246 (1956).

67. C. Bartholome, Z. physik. Chem. B33, 387 (1936).

68. Private communication from L. B. Nesbitt and M. D. Fiske, General Electric Co., Schenectady, N. Y., Jan. 17, 1959.

69. R. W. Hill and O. V. Lounasmaa, Phil. Mag. 4, 785 (1959).

70. T. Nakamura, Prog. Theoret. Phys. (Kyoto) 14, 135 (1955).

71. T. Nakamura and N. Uryu, Busseiron Kenku 96, 49 (1956).

72. J. Harrick and N. F. Ramsey, Phys. Rev. 88, 228 (1952).

73. F. London, J. Phys. Chem. 46, 305 (1942).

74. See, for example, L. I. Schiff, Quantum Mechanics (McGraw-Hill Book Co., New York, 1955).

75. J. A. Stratton, Electromagnetic Theory (McGraw-Hill Book Co., New York, 1941.

76. G. S. Rushbrooke, Introduction to Statistical Mechanics (Oxford at the Clarendon Press, London, 1949).

77. K. Clusius and K. Hiller, Z. physik. Chem. (Leipzig) B4, 158 (1929).

78. R. B. Leighton, Revs. Mod. Phys. 20, 165 (1948).

79. E. C. Kerr, E. B. Rifkin, H. L. Johnston, and J. T. Clarke, J. Am. Chem. Soc. 73, 282 (1951).

This report was prepared as an account of Government sponsored work. Neither the United States, nor the Commission, nor any person acting on behalf of the Commission:

A. Makes any warranty or representation, expressed or implied, with respect to the accuracy, completeness, or usefulness of the information contained in this report, or that the use of any information, apparatus, method, or process disclosed in this report may not infringe privately owned rights; or

B. Assumes any liabilities with respect to the use of, or for damages resulting from the use of any information, apparatus, method, or process disclosed in this report.

As used in the above, "person acting on behalf of the Commission" includes any employee or contractor of the Commission, or employee of such contractor, to the extent that such employee or contractor of the Commission, or employee of such contractor prepares, disseminates, or provides access to, any information pursuant to his employment or contract with the Commission, or his employment with such contractor.